Faculty of Science and Engineering
Department of Exploration Geophysics

Theoretical and Numerical Modelling of the Effect of Viscous and Viscoelastic Fluids on Elastic Properties of Saturated Rocks

Dina Makarynska

This thesis is presented for the Degree of
Doctor of Philosophy
of
Curtin University of Technology

April 2010

Declaration

To the best knowledge and belief this thesis contains no material previously published by any other person except where due acknowledgement has been made.

This thesis contains no material which has been accepted for the award of any other degree or diploma in any university.

Signature: 

Date: 14 April 2010

This thesis is dedicated to my family

ACKNOWLEDGEMENTS

It would not be possible for this thesis to have been written without the inspiration I receive from my supervisor Prof Boris Gurevich. I would not have gotten far without his guidance, endless enthusiasm, encouragement and support. His thoughtful ideas and invaluable contributions set this work on a firm basis. I could not have asked for a better supervisor.

I greatly thank my associate supervisor, Dr Marina Pervukhina, for useful discussions and technical input. I also thank Mr Osni De Paula for sharing his codes with me and contributing to this research. I am grateful to Dr Radim Ciz for helping me to get started with the numerical part of this thesis. Much of the work contained in the thesis was carried out in collaboration with other researchers whose contributions are highly appreciated. Individual contributions can be seen on the publication page 5.

I have found that interaction with my fellow colleagues at Curtin has been one of the distinct pleasures during my PhD. The collegiate spirit which exists in the Department of Exploration Geophysics is a major strength. My thanks to all for providing a challenging multicultural and intellectual environment and keeping my spirits alive.

My special thanks go to Ms Deirdre Hollingsworth for her administrative help and to Mr Robert Verstandig for the IT support.

I must also acknowledge the sponsors of the Curtin Reservoir Geophysics Consortium (CRGC), CSIRO Earth Sciences and Resource Engineering, and the Australian Postgraduate Award scholarship for financial support.

Finally, I would like to thank my daughter Alisa and my husband Oleg for their unconditional love, patience and support through the hard times.

TABLE OF CONTENTS

LIST OF FIGURES

ABSTRACT

Rock physics is an essential link connecting seismic data to the properties of rocks and fluids in the subsurface. One of the most fundamental questions of rock physics is how to model the effects of pore fluids on rock velocity and density. Contemporary scientific computing allows geophysicists to conduct extremely complex virtual (computational) experiments on realistic digital representations of complex porous media, and thus directly relate the measurable properties of the media to their microstructure and saturation. Computational (digital) rock physics can also serve as an effective tool in examining new and existing rock physics models. The finite element method (FEM) has been proved effective in simulations of the linear elastic properties of porous rock under static conditions. In this thesis, FEM is used to study the effect of patchy saturation on elastic velocities of digital images of rocks. However, FEM belongs to a group of grid methods, and its accuracy is limited by discretization errors. This can cause errors in rock property predictions and needs to be thoroughly examined. In this thesis, a test scenario based on rigorous theories for grid-based methods such as FEM is developed, which allows establishing optimal computational parameters in terms of accuracy of the results and time cost of computations.

Gassmann's equations are the most widely used relations to predict velocity changes resulting from different pore fluid saturations. This problem is also known as fluid substitution. Despite the popularity of Gassmann's equations and their incorporation in most software packages for seismic reservoir interpretation, important aspects of these equations such as sensitivity to microheterogeneity has not been thoroughly examined. In this thesis, the sensitivity of Gassmann's equations to microheterogeneity is estimated for different quartz/clay porous mixtures using computational (FEM) simulations. The results of this study suggest that the accuracy of Gassmann's fluid substitution remains adequate for a wide variety of highly porous rocks even if the contrast between the elastic properties of mineral constituents is large.

While Gassmann's fluid substitution is robust for rocks saturated with Newtonian fluids (brine, gas, light oil), it breaks down for viscoelastic fluids such as heavy oils. An alternative fluid substitution scheme for rocks saturated with viscoelastic fluids based on self-consistent effective medium theory is proposed in this thesis. Comparison with laboratory measurements shows that the scheme realistically estimates the frequency- and temperature dependent properties of heavy-oil rocks and can be used for practical applications.

A useful tool for modelling and estimation of properties of rocks with arbitrary or unknown microstructure are rigorous bounds on elastic moduli. The common elastic bounding methods such as Hashin-Shtrikman bounds are not applicable for heavy-oil rocks because of viscoelastic rheology of heavy oils. In this work, it is demonstrated that the viscoelastic bounding method of Milton and Berryman for the effective shear modulus of a two phase three-dimensional isotropic composite provides rigorous bounds for dispersion and attenuation of elastic waves in heavy-oil rocks. In particular, computation of these bounds shows that dispersion and attenuation in a rock saturated with a fluid (viscous or viscoelastic) can be much stronger than in the free fluid. This phenomenon is caused by wave-induced fluid flow relative to the solid. At sonic and ultrasonic frequencies, dispersion and attenuation appears to be dominated by the local (pore-scale) flow between pores of different shapes and orientations. The Mavko and Jizba expressions for the so-called unrelaxed frame bulk and shear moduli are one of the most popular quantitative models of squirt dispersion. However, these expressions are limited to liquid-saturated rocks and high frequency. In this thesis, The Mavko-Jizba relations are generalized to gas-saturated rocks. Furthermore, dispersion and attenuation is computed using a new squirt flow model, presented in this thesis. All the parameters in this model can be independently measured or estimated from measurements. The model gives complex frequency- and pressure-dependent effective bulk and shear moduli of a rock consistent with laboratory measurements.

Variation of elastic properties of rocks with pressure is often modelled using penny-shaped or spheroidal cracks as idealization of real crack/pore geometry. In this doctorate, the validity of this approach is analysed by extracting the ratios of shear to

bulk stress sensitivity coefficients, and normal to tangential compliances from ultrasonic measurements on a number of dry sandstone samples. The ratios show large scatter and, for a large number of dry sandstone samples, are not consistent with spheroidal crack theory. This inconsistency results in significantly different estimates of crack density from bulk and shear moduli, and in deviation of predicted pressure variation of Poisson's ratio from the measured data.

INTRODUCTION

RESEARCH BACKGROUND

Maximizing the recovery of existing hydrocarbon reserves and exploration of new reserves is one of the biggest challenges facing the petroleum industry today. Identification of pore fluids at depth and mapping of hydrocarbon deposits are the primary goals of seismic exploration. Seismic reflection methods provide spatially continuous data about the mechanical properties of the subsurface rocks. Those data implicitly contain information about the presence of hydrocarbons and permeability of reservoir rocks. Rock physics is an essential link connecting seismic observables such as velocity or reflectivity to the presence of in situ hydrocarbons and to reservoir characteristics. The most fundamental question of rock physics is how to model the effects of pore fluids on rock velocity and density. This problem is central to quantitative interpreting of seismic attributes for hydrocarbon detection, analysing 4D seismic, and understanding seismic signatures of lithology and porosity.

The fluids within sedimentary rocks have properties that vary substantially with composition, pressure, and temperature. Pore fluids can be multiphase mixtures as a result of a multitude of geological settings. Partial fluid saturation arises when two or more immiscible fluids occupy the pores. For instance, gas, oil and brine can commonly share the available pore space in the upper part of gas capped reservoirs. This can have a substantial effect on seismic waves propagating through the rock, resulting in attenuation and dispersion of propagating waves. Oil and brine properties can be dramatically altered if significant amounts of gas are absorbed. The variable compositions and ability to absorb gases produce wide variations in the seismic properties of oils. These variations are categorized in terms of API (American Petroleum Institute) gravity. Depending on API gravity, hydrocarbons form a continuum ranging from ultra-heavy to light oils. Viscosity is a function of API gravity and one of the most important properties of hydrocarbons, which determines how easily oil flows at reservoir temperature. Highly viscous oil can exhibit

viscoelastic behaviour resulting in the ability of the material to have an effective shear modulus and propagate a shear wave. Velocities and moduli of the oil become strongly temperature- and frequency-dependent.

Production from oil reservoirs changes pressure and fluid saturation. Therefore, it is important to understand how changes in fluid properties contribute to those changes in the seismic response, for different stress and production scenarios. Optimal production strategies require accurate monitoring of production-induced changes of reservoir saturation and pressure over the life of the field. Time-lapse seismic technology is increasingly used to map these changes in space and time. To this end, rock-physics relationships are required to link seismic parameters (velocities and attenuation coefficients) to the properties of reservoir fluids as function of frequency and pressure, volume and temperature conditions.

The overall objective of this thesis is to combine theoretical and computational rock physics to model the effect of viscous and viscoelastic fluids on effective elastic properties of porous rocks. In particular, research aspects covered in the thesis include (1) numerical modelling of the effect of partial saturation on serismic velocities and developing a test scenario for grid-based numerical methods, (2) investigating the sensitivity of Gassmann's equations to microheterogeneity, (3) developing an alternative fluid substitution scheme for rocks saturated with viscoelastic fluids, (4) examining rigorous viscoelastic bounds for heavy-oil rocks, (5) theoretical modelling of squirt dispersion of elastic wave velocity, (6) analysing the validity of using spheroids as idealization of real crack geometry to model pressure dependencies of rock properties.

I refer to work presented in this thesis in first person plural (we) because each chapter is the result of multiple discussions and close collaboration between several people involved in this research. The results of the research reported in this dissertation have been published as journal and conference papers. Publications arising from this thesis can be seen on pages 5-6.

THESIS LAYOUT

The following describes motivation for each chapter of this dissertation and briefly outlines the chapters content.

Chapter 1. The elastic properties of rocks are affected in complex ways by saturation and fluid type and primarily depend on the morphology of the pore space and solid phase/phases. The progress in computer architecture and parallel computing makes it possible to conduct extremely complex and realistic numerical simulations of physical phenomena on realistic 3D digital images of core materials. Computational (digital) rock physics allows one to directly relate elastic properties of porous rocks to their microstructural information and saturation. A finite–element method or FEM has been proven to be effective in simulations of the linear elastic properties of dry and saturated rocks (Arns et al., 2002; Garboczi, 1998). FEM can be used as a tool for examining new and existing theoretical rock physics models. However, the accuracy of numerical simulations can be limited by the resolution of digital images and computational errors. In Chapter 1, a test scenario based on rigorous theories for grid-based methods such as FEM is developed, and FEM is used to calculate elastic properties of rocks under partially saturated conditions. The established optimal computational parameters enable more efficient use of FEM in terms of accuracy of the results and time cost of computations. This allows using of FEM as a tool to test the accuracy of theoretical models.

Chapter 2. For over half a century, Gassmann's theory (Gassmann, 1951) has been used for modelling the effects of pore fluids on seismic data. This problem is also known as fluid substitution. Fluid substitution refers to prediction of seismic velocities in rocks saturated with one fluid from properties of dry rocks or rocks saturated with another fluid. Gassmann fluid substitution is remarkably robust and general. When used under the appropriate conditions, it is usually as accurate as the measurements of saturation, velocity, and porosity that are input parameters to the Gassmann's equations (e.g. Plona, 1980; Wang, 2000; Artola and Alvarado, 2006). However, a number of assumptions underlie Gassmann's theory: the rock has to be statistically isotropic and monomineralic with fully connected pores that the pore

fluid is in hydraulic equilibrium. These assumptions may not be appropriate for microheterogeneous rocks such as shaley sediments due to a high contrast in elastic properties of the host mineral and shale, and due to the ability of clay to inhibit the movement of fluids. Although generalization of Gassmann's equations to multimineral rocks has been given by Brown and Korringa (1975), their result has not yet found use in practical applications as it contains two new compressibilities which are difficult to measure. Investigating sensitivity of Gassmann's equations to microheterogeneity can improve understanding of the operation and application of Gassmann's equations. In Chapter 2, the accuracy of Gassmann fluid substitution is tested for different quartz/clay mixtures using computational (FEM) simulations.

Chapter 3. One important result of Gassmann's theory and its extension to finite frequencies (Biot's theory) is that the effective (wet) shear modulus is identical to the frame (dry) shear modulus. In other words, the existence of a fluid has no effect on the effective shear modulus of a rock. This lack of shear dependence on saturating fluid is often contradicted when pore fluid is viscoelastic such as heavy oil. Viscoelastic rheology of heavy oils makes Gassmann's theory inapplicable to heavy-oil rocks. In Chapter 3, we propose an alternative fluid substitution scheme based on self-consistent effective medium theory for rocks saturated with viscoelastic fluids.

Chapter 4. A useful tool for modelling and estimation of properties of rocks with arbitrary or unknown microstructure are rigorous bounds on elastic moduli. Rigorous bounding methods such as Hashin-Shtrikman (HS) bounds cannot be used for testing laboratory measurements and results of modelling if rock is saturated with viscoelastic fluid. The HS bounds are no longer rigorous if the rock moduli are complex. In Chapter 4, appropriate rigorous bounding methods especially designed for viscoelastic composites are examined. In particular, computation of these bounds shows that dispersion and attenuation in a rock saturated with a fluid (viscous or viscoelastic) can be much stronger than in the free fluid. This phenomenon is caused by wave-induced fluid flow relative to the solid.

Chapter 5. At sonic and ultrasonic frequencies, dispersion and attenuation appears to be dominated by the local (pore-scale) flow between pores of different

shapes and orientations. The Mavko and Jizba expressions for the so-called unrelaxed frame bulk and shear moduli (Mavko and Jizba, 1991) are one of the most popular quantitative models of squirt dispersion. However, these expressions are limited to liquid-saturated rocks and high frequency. There is a need for a more comprehensive frequency-dependent model, which can describe dispersion and attenuation of elastic waves due to squirt flow. In Chapter 5, we present a generalization of the Mavko-Jizba model to gas-saturated rocks as well as a new model of squirt-flow dispersion and attenuation for a wide range of frequencies in granular fluid-saturated media.

Chapter 6. Understanding and modelling of the effect of stress on elastic properties of rocks is important for interpreting a variety of seismic data. Variation of the elastic properties with pressure is often modelled using penny-shaped or spheroidal cracks as idealization of real crack/pore geometry. In Chapter 6, we investigate the validity of this approach using real rock laboratory data.

PUBLICATIONS ARISING FROM THE THESIS

- Makarynska, D., B. Gurevich, and R. Ciz, 2007, Finite element modelling of Gassmann fluid substitution of heterogeneous rocks, 69th EAGE Conference & Exhibition in London, UK.
- Makarynska, D., B. Gurevich, R. Ciz, C. Arns, and M. Knackstedt, 2008, Finite element modelling of the effective elastic properties of partially saturated rocks, Computers & Geosciences, 34, 647-657.
- Makarynska, D., B. Gurevich, R. Ciz, and K. Osypov, 2008, Fluid substitution in rocks saturated with heavy oil, 70th EAGE Conference & Exhibition, 9 - 12 June 2008, Rome, Italy (extended abstract).
- Makarynska, D., B. Gurevich, R. Ciz, and C. Arns, 2008, Rock physics modelling of elastic properties of rocks saturated with heavy oils, SEG Summer Research Workshop, 20-24 July, Galway, Ireland (abstract).

- Makarynska, D., and B. Gurevich, 2008, Fluid substitution in heavy oil rocks, SEG International Exposition and 78th Annual Meeting, Las Vegas, USA (extended abstract).
- Gurevich, B., D. Makarynska, and M. Pervukhina, 2009, Mavko-Jizba relations for ultrasonic moduli of saturated rocks rederived and generalized, Geophysics, 74, no.4, N25-N30.
- Gurevich, B., D. Makarynska, M. Pervukhina, and O. De Paula, 2009, A new model for squirt-flow attenuation and dispersion in fluid-saturated rocks, 71st EAGE Conference & Exhibition, Amsterdam, the Netherlands (extended abstract).
- Gurevich, B., D. Makarynska, and M. Pervukhina, 2009, Are penny-shaped cracks a good model for compliant porosity? SEG International Exposition and 80th Annual Meeting, Houston, USA, (extended abstract).
- Makarynska, D., B. Gurevich, J. Behura, and M. Batzle, 2010, Fluid substitution in rocks saturated with heavy oil, Geophysics, 75, no.2, E115-E122.
- Gurevich, B., D. Makarynska, M. Pervukhina, and O. De Paula, 2010, A simple model for squirt-flow dispersion and attenuation in fluid-saturated granular rocks, Geophysics, 75, no.6, N109-N120.
- Makarynska, D., and B. Gurevich, 2010, Bounds for viscoelastic properties of heavy-oil rocks, 72nd EAGE Conference & Exhibition Barcelona, Spain (extended abstract).

Appendix 1 contains permission statements from the copyright owners of the material presented in this thesis which was published as journal articles or conference extended abstracts.

CHAPTER 1 – FINITE ELEMENT MODELLING OF THE EFFECTIVE ELASTIC PROPERTIES OF PARTIALLY SATURATED ROCKS

1.1 BACKGROUND

Quantitative interpretation of geophysical data requires the knowledge of relationships between physical properties of rocks and their microstructure. With the advances in computer technology, it has become feasible to compute macroscopic physical properties of porous rock from its microstructural information using rigorous numerical simulations of physical experiments in realistic pore space geometries. This approach, which has become known as digital (or computational) rock physics, has been used to model the effect of pores, fractures and fluids on the effective acoustic properties (Arns et al., 2002; Grechka, 2003; Gurevich et al., 2005; Roberts and Garboczi, 2000; Saenger et al., 2004;) as well as geometrical, hydraulic and electric properties of rocks (Arns et al., 2001, 2004; Auzerais et al., 1996; Keehm et. al., 2004; Schwartz et al., 1994; Spanne et al., 1994). The computational rock physics technology relies on digitalized microstructural information which can be obtained either through X-ray microtomography (Dunsmuir et al., 1991; Flannery et al., 1987; Spanne et al., 1994), laser confocal microscopy (Fredrich et al., 1995), or stochastic models (Adler et al., 1992; Arns, 2002; Roberts and Garboczi, 2002; Yeong and Torquato, 1998). The numerical approach allows one to study properties of complex multi-phase materials with physically realistic phase distributions. However, computer simulations are not exact and their accuracy is limited by the simulation algorithm and by computational parameters such as spatial discretization. Therefore, in order to optimize the computational parameters, it is important to test the results of such simulations against known rigorous solutions.

One algorithm that has proved effective in simulations of the linear elastic properties of rocks is a numerical model based on a finite element method (FEM)

developed by Garboczi (1998) and Arns et al. (2002) for linear elastic problems. There is a difficulty in testing such algorithms as values of the elastic properties are not known exactly for a porous material of any particular 3-D pore geometry. However, one rigorous theory applicable to the elastic properties in such a case is the Gassmann's theory (1951), which is exact for a monomineralic macroscopically homogeneous porous medium with fully connected statistically isotropic pore space and no chemical/physical interaction between rock and pore fluid. In this chapter, we propose a test scenario for static numerical simulations for a medium saturated with a fluid mixture. This test scenario is based on application of the Gassmann's theory. When the Gassmann's theory is applied to a medium saturated with a fluid mixture, the effective bulk modulus of the fluid mixture is computed with Wood's equation (Wood, 1955), which is an exact isostress formula for a mixture of Newtonian fluids. Wood's equation implies that fluid pressure is spatially uniform throughout the pore space. Since all the assumptions of the Gassmann's theory could be simulated by FEM, a comparison of the numerically predicted parameters with the theory provides a natural test of the accuracy of numerical results. Arns et al. (2002) have shown that FEM simulations on media saturated with one fluid agree with the Gassmann predictions for a variety of porous structures. Here we extend those simulations to porous rocks saturated by a mixture of two fluids and test the predictions against Gassmann solutions. The goal is to determine computational parameters that ensure accurate and robust simulations.

1.2 NUMERICAL METHOD

FEM code for linear elastic problems developed by Garboczi (1998) and Arns et al. (2002) is specifically designed to be applied to images of materials/rocks that have been generated either using microstructure models, or by an experimental techniques like X-ray tomography. The code operates directly on digital images by treating each voxel as a linear finite element.

Given bulk and shear moduli of material solid constituents and fluid phases, FEM can simulate the macroscopic physical properties, such as the effective elastic

moduli, on 3D images of porous rocks at the pore scale. The method uses a variational formulation of the static linear elastic equations, and finds the solution by minimising the elastic energy using a fast conjugate-gradient relaxation algorithm. A macroscopic strain is applied, with the resultant average stress or the average elastic energy giving the effective elastic moduli. The images are assumed to have periodic constant-strain boundary conditions. Further details of the theory and the code can be found elsewhere (Arns, 2002; Garboczi, 1998).

There are several sources of errors in using this algorithm on a specific rock digital image (Arns et al., 2002; Roberts and Garboczi, 2000). The first error is related to finite size effects. The digital image must contain enough of the microstructure to provide good averaging of the elastic properties. The image should also be representative of the rock microstructure in such a way that different realizations of the same microstructure do not significantly differ from each other.

The second source of error is how well the minimum energy state is approximated in the solution algorithm. Usually this type of errors is on the order of the round-off error of the computer, and so is negligible (Garboczi and Day, 1995).

The third source of error is associated with the resolution of microstructural features of the rock. This error is due to the use of discrete voxels to represent continuum objects. In practice, the accuracy of the results can be significantly limited by discretization errors. As mentioned above, FEM discretizes digital images that each voxel in 3-D is taken to be a 3-linear finite element. Increasing the system (digital model) size in terms of the number of voxels per unit length improves the resolution. However, the number of voxels depends on computer memory and speed (230 bytes for a voxel). Since the numerical simulations are computationally expensive, there is always a trade-off between number of voxels and computational speed.

In this work, we use digital images at a scale from $(180)^3$ up to $(400)^3$ voxels to investigate the effect of spatial resolution on the accuracy of the FEM predictions for partially saturated rocks.

1.3 NUMERICAL TEST SCENARIO

To examine the accuracy of FEM simulations we apply them to a rock saturated with a mixture of two fluids. Because FEM predicts static effective properties, they can be compared with the exact solution based on the Gassmann's theory.

Gassmann's equation (Gassmann, 1951) for an effective bulk modulus of a fluid-saturated porous material can be written in the form

$$K = K_{dry} + \sigma^2 M \,, \tag{1.1}$$

where

$$M = \left[\frac{\sigma - \phi}{K_g} + \frac{\phi}{K_f} \right]^{-1} , \tag{1.2}$$

is called the pore space modulus and

$$\sigma = 1 - \frac{K_{dry}}{K_g} , \tag{1.3}$$

is the Biot-Willis effective stress coefficient (Biot and Willis, 1957; Gurevich, 2004), ϕ is porosity, K_{dry}, K_g, and K_f are the bulk moduli of the dry frame, the solid grain material and the fluid, respectively.

If the frequency is low enough, then during each half cycle of oscillation the fluid in the pore space is able to equilibrate at a common value. If the pore space is filled with a mixture of n fluids with different fluid bulk moduli, where the heterogeneities are small compared with a wavelength, the bulk modulus K_f of the fluid mixture is given exactly by Wood's formula (Wood, 1955)

$$\frac{1}{K_f} = \sum_{i=1}^{n} \frac{x_i}{K_i} , \tag{1.4}$$

where x_i and K_i are the volume fractions and bulk moduli of the individual fluid phases, respectively. Wood's formula is often called the isostress average because it gives the ratio of stress to average strain when all phases are assumed to have the same stress (pressure). This situation occurs when the phases are mixed at the finest scales, and pore pressure increments of each fluid equilibrate with each other to a single average value. The collection of phases in such case could be replaced with a single "effective fluid".

A critical assumption in the effective fluid model represented by the Wood's formula is that differences in wave-induced pore pressure have time to flow and equilibrate among the various phases. The characteristic relaxation time or diffusion time for heterogeneous pore pressures of scale L is $\tau \approx L^2 / D$, where $D = kK_f / \eta$ is the diffusivity, k is the permeability, and η is the viscosity (Mavko et al., 1998). At a seismic frequency $f = 1/\tau$, pore pressure heterogeneities will have time to relax and reach a local isostress state over scales smaller than $L_c \approx \sqrt{D/f}$. On scale larger than L_c, spatial fluctuations cannot be accurately described by the effective fluid model.

For a mixture of two fluids, say, gas and water, equation 1.4 reads

$$\frac{1}{K_f} = \frac{S_w}{K_w} + \frac{1 - S_w}{K_{gas}}, \tag{1.5}$$

where S_w is water saturation, K_w is the bulk modulus of water and K_{gas} is the bulk modulus of gas. Substitution of the fluid modulus as given by equation 1.5 into Gassmann's equation 1.1 yields so-called Gassmann-Wood (GW) formula (Johnson, 2001; White, 1983) or the low-frequency limit

$$K_{GW} = K_{dry} + \sigma^2 \left[\frac{\sigma - \phi}{K_g} + \frac{\phi S_w}{K_w} + \frac{\phi (1 - S_w)}{K_{gas}} \right]^{-1} \tag{1.6}$$

Equation 1.6 gives the static elastic modulus K_{GW} of a rock, where all fluid phases in the pore space are immiscible, and there are no hydraulically isolated pores. The low-frequency limit holds only if the frequency is so low that the pore pressure has time to equilibrate between the fluid phases regardless of the spatial distribution of the fluids. This is the situation easily simulated by FEM or other static algorithm, and therefore comparison of the simulation results with the predictions of equation 1.6 gives a measure of validity of the simulations.

To check how well the simulations predict this particular limit, we also compare them with the high-frequency limit. In the high-frequency limit or when there is the greatest separation of fluid phases, the pore pressure in the fluid phases does not have enough time to equilibrate within one half wave cycle. Therefore, the regions of the porous medium saturated with different fluids will behave as if they were hydraulically isolated (Bear, 1988; Dvorkin et al., 1999; Johnson, 2001; Toms et al., 2006). However, each patch at scale $\approx L_c$ will have fluid phases equilibrated within the patch at scales smaller than L_c, whilst neighboring patches at scales $> L_c$ will not be equilibrated with each other. Consequently, the rock in each patch will have a different bulk modulus, whilst the shear modulus will remain unchanged and spatially uniform. Thus within each patch the bulk modulus is given by the Gassmann equation evaluated with respect to the saturating fluid within that patch. The effective elastic bulk modulus of the rock with spatially varying bulk modulus but uniform shear modulus is given by Hill's (1961) average:

$$K_{GH} = \left[\sum_{i=1}^{n} \frac{x_i}{K_i + 4/3\mu} \right]^{-1} - 4/3\mu , \tag{1.7}$$

where K_{GH} is the effective bulk modulus of the rock, *n* is the number of fluid phases, x_i is the volume fraction of the *i* th fluid, μ is the shear modulus of the rock, and K_i is the bulk modulus of the rock completely saturated with *i* th fluid. Specifically, for two fluids, water and gas, we have:

$$K_{GH} = \left[\frac{S_w}{K_w^{sat} + 4/3\mu} + \frac{1 - S_w}{K_{gas}^{sat} + 4/3\mu} \right]^{-1} - 4/3\mu, \tag{1.8}$$

where saturated moduli K_w^{sat} and K_{gas}^{sat} are given by Gassmann's equations 1.1 – 1.3 with the fluid modulus K_f equal to K_w and K_{gas}. The modulus given by equation 1.7 is known as the Gassmann-Hill (GH) or high-frequency limit (Johnson, 2001).

A number of authors have shown experimentally that it is possible to see either GW, GH or in between the limits behavior, depending upon the saturation protocol and the measurement frequency (e.g. Knight et al., 1998; Lebedev et al., 2009; Mavko and Mukerji, 1998). The difference between GW and GH limits yields the magnitude of frequency dispersion of the bulk modulus of a rock saturated with a fluid mixture. In the numerical experiments that follow, we compare any deviation of the numerical results from the GW limit against this difference.

1.4 NUMERICAL EXPERIMENTS

1.4.1 FEM SIMULATION OF EFFECTIVE ELASTIC PROPERTIES FOR BOOLEAN RANDOM MODELS

To test the performance of FEM simulations against the theory, we predict linear effective elastic properties of two types of three-dimensional (180x180x180) digital models of partially saturated rocks (Figure 1.1). We assume that this size provides good averaging of the elastic properties (Arns, 2002). The models have different distribution of fluid patches but similar porosity and saturation. The locally patchy model (Figure 1.1a) has uniformly distributed fluid patches, whereas the macro-patchy model (Figure 1.1b) contains a single spherical inclusion in the middle of the porous system. Because FEM is a static code, we expect the numerical estimates of the effective elastic properties be identical for both models regardless of their geometry.

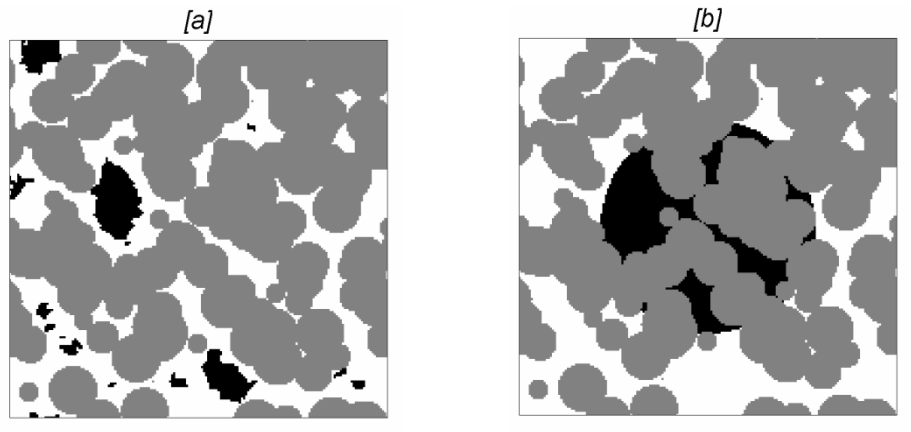

Figure 1.1. Central slices of 3D Boolean models: local patchy model (a) and macro patchy model (b) consisting of three phases (quartz - grey, water – white, gas - black).

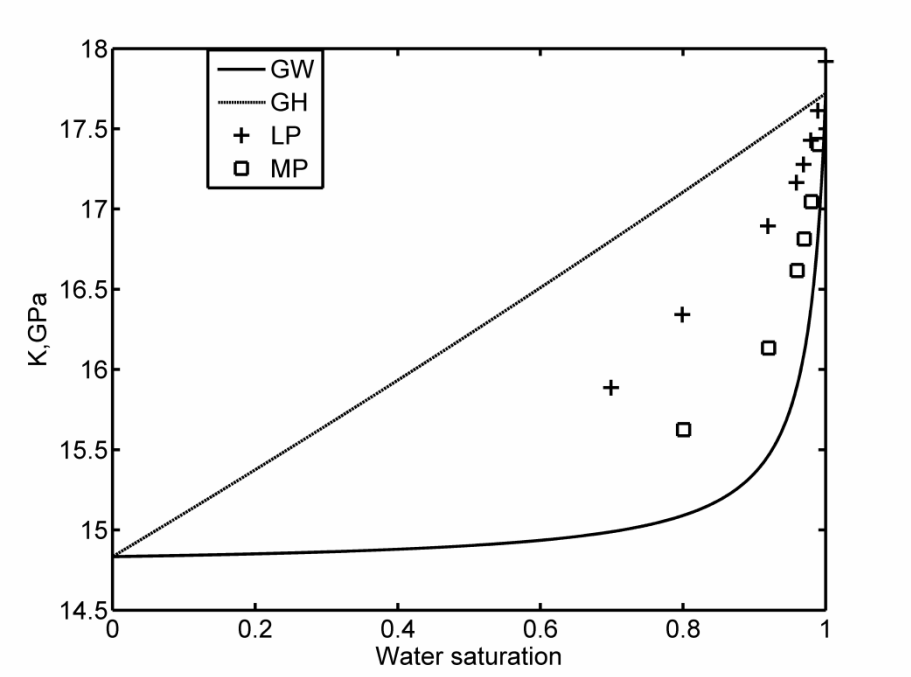

Figure 1.2. Comparison of numerical estimates of the effective bulk moduli (K) to Gassmann-Wood (GW) and Gassmann-Hill (GH) limits for two Boolean models: local patchy (LP) and macro patchy (MP).

The model morphologies were generated using a simple Boolean overlapping spheres method (Arns, 2002; Knackstedt et al., 2003) for various degrees of saturation ranging from dry to fully saturated conditions with porosity approximately equal to 0.25. The Boolean models are often used to represent irregular spatial structures generated by gradual build up of a phase via the overlap of permeable particles such as spheres, each with arbitrary location and orientation.

A three-dimensional digitized model or image is a collection of discrete voxels in which each voxel can, in principle, be a different phase of material. We use images in a binary form with "1" and "3" assigned to the voxels that fall into the fully connected pore space and represent gas and water accordingly, "2" is assigned to the voxels standing for the solid phase (quartz). We assign the same elastic properties of each constituent to both models. The elastic properties for quartz skeleton are taken to be $K_g = 37$ GPa, $\mu = 44$ GPa. The properties of pore fluids are taken to be $K_w = 2.22$ GPa and $\mu = 0$ GPa for water, and $K_{gas} = 0.05$ GPa, $\mu = 0$ GPa for gas (Mavko et al., 1998). FEM allows the fluids to be modelled as solids with zero shear modulus. To ensure full equilibrium of fluid flow, pore fluids are treated by FEM as frictionless with zero viscosity. The results of numerical simulations performed for the Boolean models are demonstrated in Figure 1.2. The Gassmann's theory described above stipulates that the effective elastic properties of rocks represented by such models should be independent of the geometry and size of fluid patches. Hence, the predicted effective elastic moduli should be the same for both models and agree with the GW theory. However, the numerical estimates show significant differences between the models, and both disagree with the GW limit.

To investigate this discrepancy, we output the central slices illustrating the pressure field at the end of the relaxation process for both models (Figure 1.3). According to Pascal's law, when fluid is at rest in the absence of body forces the pressure is the same throughout all fluid points. However, we can observe significant variation in the pressure field over the pore space.

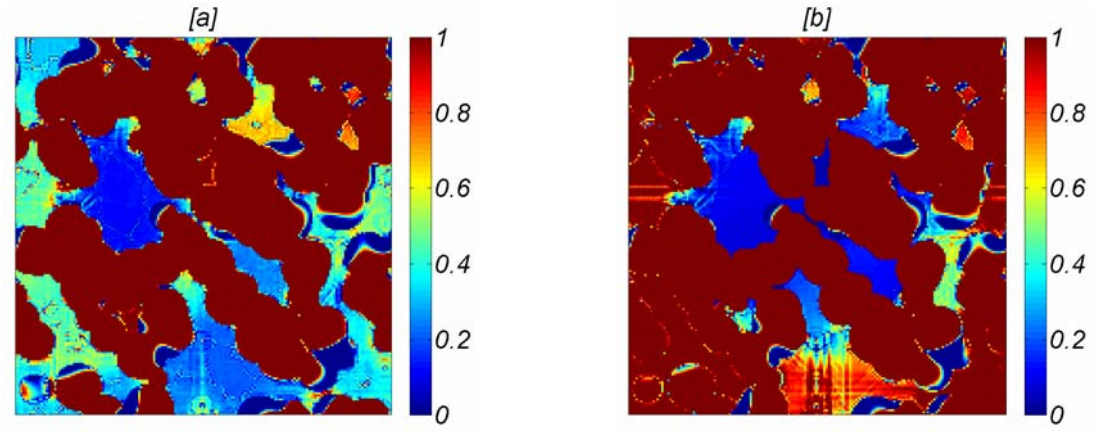

Figure 1.3. Variation of pore fluid pressure in central slices of local patchy model (a) and macro patchy model (b).

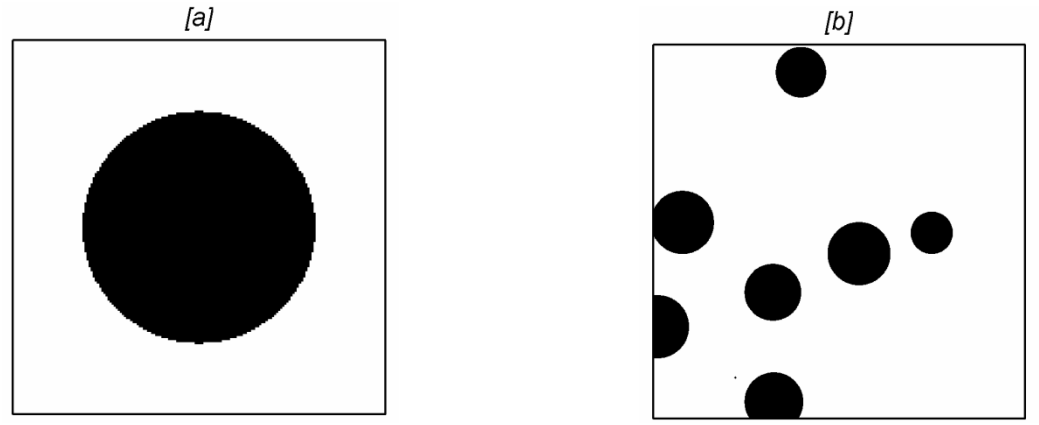

Figure 1.4. Central slices of digital models with fluid constituents (no solid phase). Gas depicted in black, water in white.

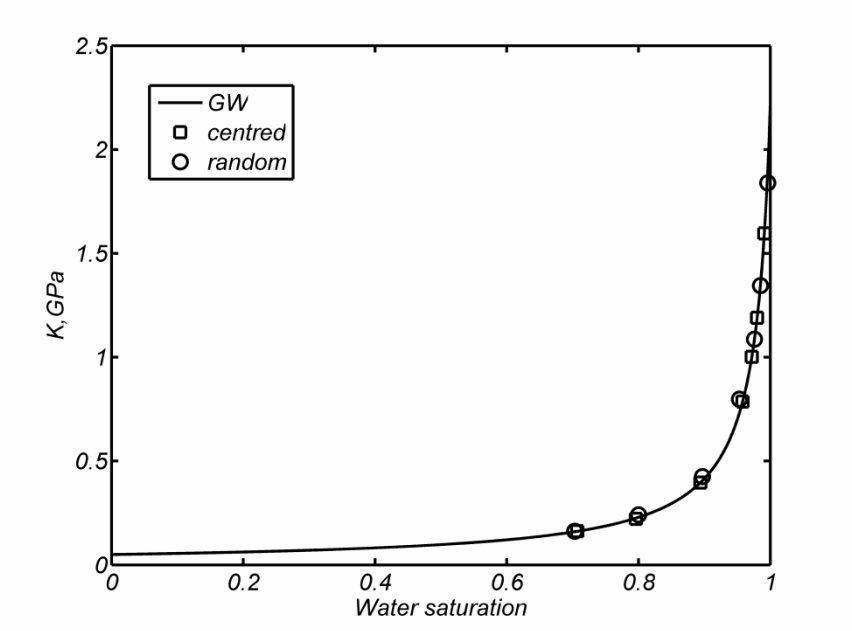

Figure 1.5. Comparison of numerical estimates of effective bulk moduli (K) to GW limit for two models with fluid constituents (no solid phase). Centred model contains a single gas inclusion in centre of a liquid cube, and random model has randomly distributed gas inclusions within liquid.

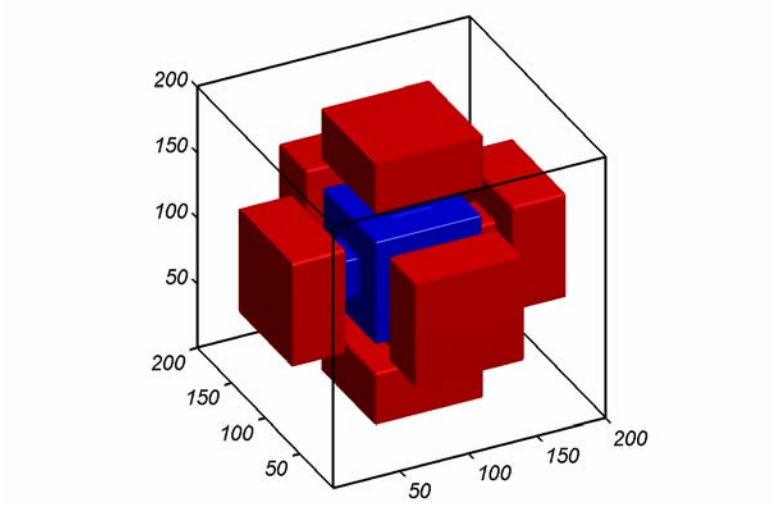

Figure 1.6. Pore space image of an idealized poroelastic material with six channels. Blue volume represents gas-filled pore space, red volume represents water-filled pore space. Transparent part is rock frame.

To check if FEM can properly handle pressure relaxation in fluids, we perform simulations for models of media containing two free fluid phases (water and gas) with different distribution of gas patches as in the models described above. The models geometries are shown in Figure 1.4. The first model contains a single spherical gas inclusion in the centre of a liquid cube, while the second one has several randomly distributed gas bubbles of different size. We test the numerical estimates of the effective elastic bulk modulus against Wood's formula (equation 1.4).

Wood's formula uses a concept of a compressible homogeneous pore fluid to treat a fluid mixture, each component of which is assumed to have the same stress. Hence, the numerical results should be the same for both models regardless of their geometries. A comparison of the predicted moduli for different levels of saturation (0.7-1) in Figure 1.5 demonstrates excellent agreement of both models with Wood's formula. This proves the capability of the FEM code to predict the effective elastic moduli of a fluid mixture.

These results suggest that in the presence of solid particles the FEM simulations fail to equilibrate fluid pressure throughout the pore space, even if the pore space is fully interconnected. One possible explanation for this is an insufficient number of finite elements across thin fluid channels (i.e., insufficient density of FEM grid in channels), which can lead to a hydraulic separation of pore fluids. It is difficult to explore this effect using random packs of spheres (or any other random model) as all pores and pore channels have different sizes. Therefore, below we investigate this effect using models with idealized regular pore and channel geometry.

1.4.2 EFFECT OF PORE CHANNEL SIZE

To explore the extent to which small (in voxels) pore connections can be resolved properly by the FEM code, we conduct numerical experiments on the images of the idealized partially saturated rocks with regular pore geometry. In contrast to random Boolean models with variable size of interconnections between pores, we generate a simple three dimensional model of poroelastic material

(200x200x200), where a cubic inclusion ('pore') in the centre of a solid (quartz) cube is connected with other 'pores' by channels of adjustable cross-section (Figure 1.6).

To test pressure equilibration between liquid and gas (the 'worst' case), we assume that the inner pore is filled with gas while the outer pores are water-filled, the gas/water interface crosses the channels. Since the fluid-fluid interface separates the fluids within the channels, we could control the area of the interface by changing the cross-sectional area of the channels. The numerical simulations are carried out for the images with 0.25 porosity considering three levels of saturation: dry, 0.75, and fully saturated.

In Figure 1.7, we compare the results of three sets of experiments with different cross-sectional area of the channels, ranging from 4 elements (voxels) to 900. For the model with the widest channels and, consequently, the largest total contact area between the fluids, the FEM code yields results which are in excellent agreement with the GW limit, demonstrating that the pressure field is fully equilibrated. In contrast, the predicted effective moduli for the image with the thinnest channels are close to the GH limit. We observe significant pressure variation over the pore space with extreme values in the channels. For the model with cross-sectional area of 100 voxels, the predicted moduli tend to the GW limit, but still show relatively big deviation from it. The mismatch between GW theory and numerical results for the images with relatively small pore fluid interface area, could be due to the fact that, the FEM algorithm treats the fluids in such cases as segregated phases violating the "effective fluid" assumption.

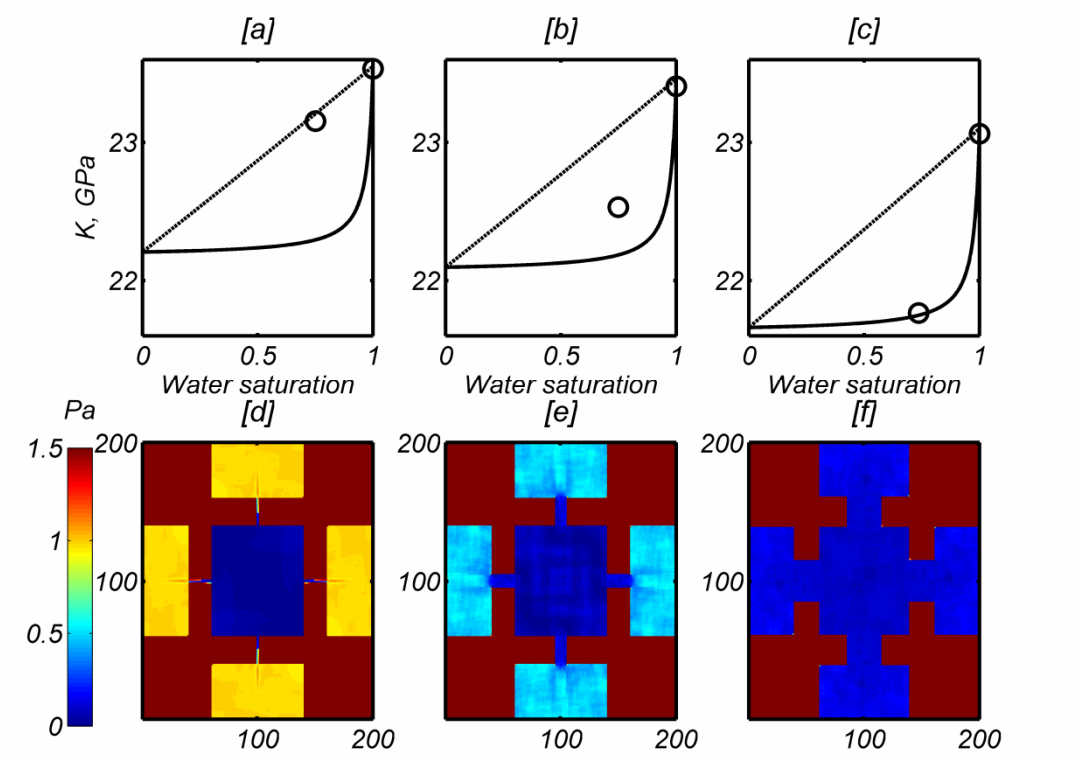

Figure 1.7. Comparison of results of numerical simulations for images with different width of channels: 2 voxels (a, d), 10 voxels (b, e), and 30 voxels (c, f). Plots (a, b, c) show FEM estimates of effective bulk moduli (black circles) versus GW (solid line) and GH (dashed line) limits. Panels (d, e, f) show central slices of fluid pressure (in Pa) at end of relaxation process.

To further investigate this numerical effect we increase the contact area between the pore fluids by increasing the total number of pore channels and varying the individual channel size. Specifically, we carry out simulations for three different models of the same porosity and water saturation, but with variable numbers of channels: 2166, 600 and 150 channels with each channel having cross-sectional area of 4, 16 and 64 voxels, respectively. An example of the model with 600 channels is shown in Figure 1.8. The corresponding FEM simulations are shown in Figure 1.9. The models with 600 and 150 channels have exactly the same total area of fluid interface. Despite this, the results are in better agreement with the GW for the 150

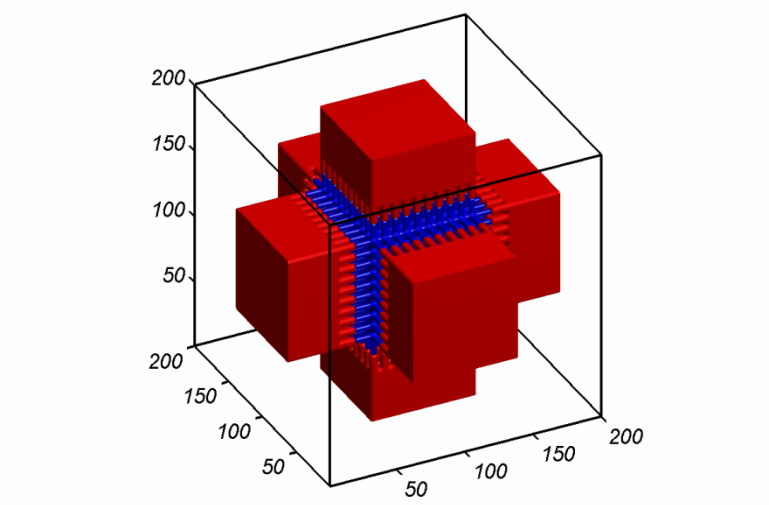

Figure 1.8. Pore space image of an idealized poroelastic material with six hundred channels. Blue volume represents gas-filled pore space, red volume represents water-filled pore space. Transparent part is rock frame.

channel model having wider channels. At the same time, the substantially increased number of channels and, as a result, the increased area of the fluid interface for the model with 4 voxel cross-sectional area considerably improves the numerical estimates (see Figure 1.7 a for a comparison). However, the deviation from the GW bound is still significant, and the pressure varies significantly over the pore space.

The results demonstrate that in the numerically simulated process of pressure equilibration, both the total area of the water-gas interface in pore connecting channels and channel size play a key role. That is, for a given area of the water-gas interface, the size of the individual channels needs to be relatively large (>4 voxels in diameter) to ensure adequate pressure relaxation.

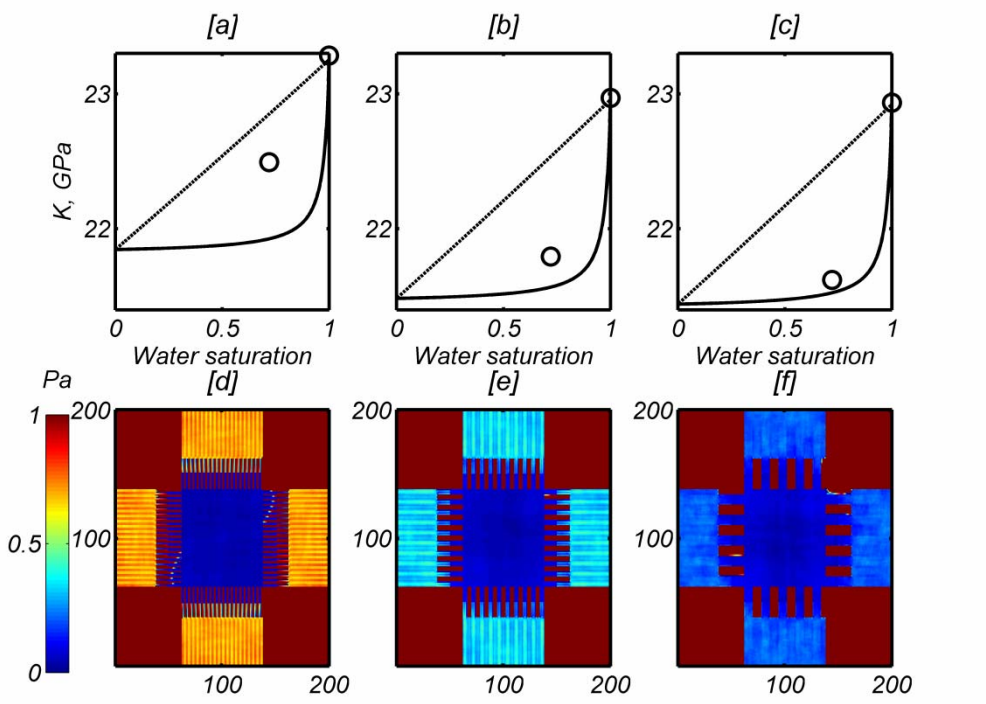

Figure 1.9. Comparison of numerical results for models with different number and width of channels: 2166 channels (a, d), 600 channels (b, e), 150 channels (c, f) with 4, 16, 64 voxels cross-sectional areas respectively. Plots a, b, and c show FEM estimates of effective bulk moduli (K) (black circles) versus GW (solid line) and GH (dashed line) limits. Panels (d, e, f) show central slices of fluid pressure (in Pa) at end of relaxation process.

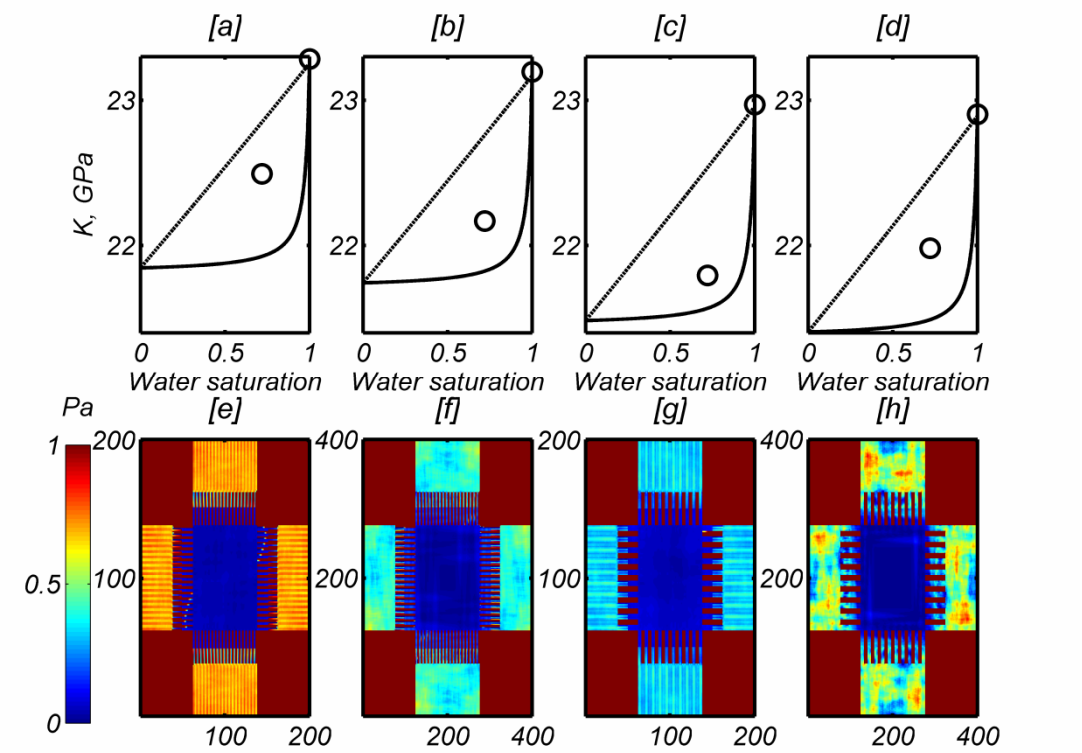

Figure 1.10. Comparison of numerical results for images with increased spatial resolution (b, f) and (d, h) to original models (a, e) and (c, g) respectively. Panels (a, e), (b, f) show results for the 2166 channel model and panels (c, g), (d, h) for the 600 channel model. Plots (a, b, c, d) show FEM estimates of effective bulk moduli (K) (black circles) versus GW (solid line) and GH (dashed line) limits. Panels (e, f, g, h) show central slices of fluid pressure (in Pa) at end of relaxation process.

1.4.3 EFFECT OF SPATIAL RESOLUTION

Our results described above suggest that in order to obtain reliable numerical estimates of the effective elastic parameters we need to control the total area of the fluid-fluid interface and the channel size (in voxels). When dealing with actual images or synthetic models of real materials with complex morphology, it is realistic to control the size of pore interconnections only by varying the spatial resolution of the digital models. In order to verify the effect of spatial resolution, we extend the models with 2166 and 600 channels to the size of 400x400x400 by doubling the

number of individual elements. Figure 1.10 shows that the higher-resolution numerical estimates calculated for the 2166 channel model provide better agreement with the GW theory.

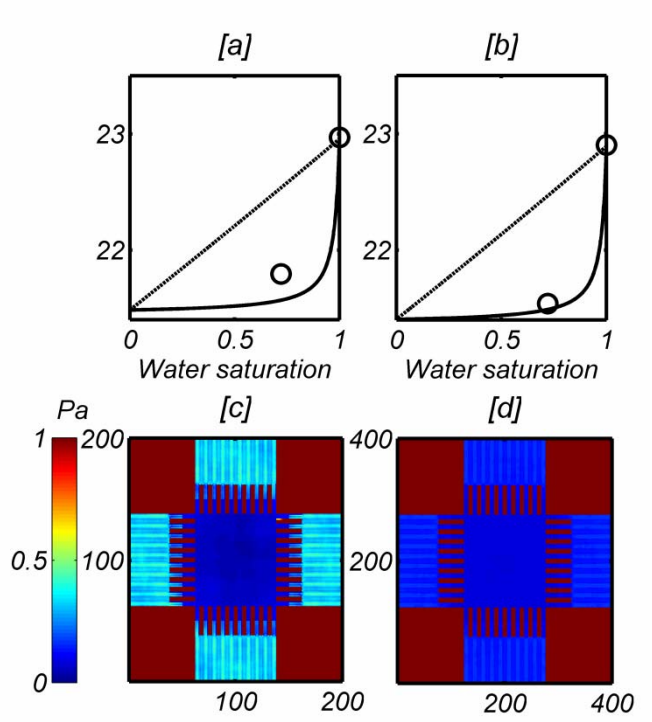

Figure 1.11. Comparison of numerically obtained results for the 600 channel model with increased spatial resolution (b, d) to original model (a, c). The computations for upscaled model were done using the tolerance parameter of 10-5. Plots (a, b) show FEM estimates of effective bulk moduli (K) (black circles) versus GW (solid line) and GH (dashed line) limits. Panels (c, d) show central slices of fluid pressure (in Pa) at end of relaxation process.

The output of the fluid pressure slices demonstrates better pressure equilibration for this case. However, the increased spatial resolution for the model with 600 channels does not provide an expected improvement. Instead, the results become worse, which is reflected in significant pressure variation over the pore space. We find this unexpected result to be caused by the insufficient magnitude of the tolerance parameter (relative error) used in the FEM code for this case. The tolerance on the relative changes of all stress and strain components is the stopping criterion in the process of energy relaxation. To investigate this effect, the tolerance

was changed from 10^{-4} to 10^{-5}, this drastically increased the number of iterations and the time of computations, when the effective elastic properties were calculated for the 600 channel model. Figure 1.11 shows a significant improvement in the equilibration of the pressure field, this improves estimates of the effective bulk moduli, which now comply very well with the GW limit. At the same time, computations for 200x200x200 models with a tolerance parameter lower than 10^{-4} fail to converge. We found that the optimal tolerance parameter depends on the size and geometry of the model, and the smallest admissible tolerance parameter for 200x200x200 models is 10^{-4}. Thus we conclude that the results shown in Figures 1.7, 1.9 yield the best pressure equilibration that can be achieved with this algorithm without improving the spatial resolution of the models.

1.5 CHAPTER CONCLUSIONS

We have used, for the first time, a static finite element approach to predict the linear effective elastic properties of three-dimensional materials saturated with a mixture of gas and water. We have developed a scenario to test the FEM simulations against an analytical solution based on Gassmann's theory to determine computational parameters that ensure accurate and robust simulations. According to the theory, the effective elastic properties of rock saturated with a mixture of fluids should be independent of distribution and size of gas patches.

On the contrary, the numerical simulations have shown that the computed effective moduli depend significantly upon geometry and the size of fluid patches. This discrepancy is a numerical artefact caused by the un-equilibrated pressure field in the pore-filling mixture of gas and water due to the poorly resolved tiny pore channels. We have also shown that the pressure relaxation process is dependent upon the area of an interface between pore fluids as well as the size of pore channels (in voxels). That is, for a given area of the water-gas interface, the size of the individual pore channels needs to be relatively large (>4 voxels in diameter) to ensure pressure equilibration.

We have also shown that the increased spatial resolution of digital images improves the numerical results. On the other hand, the numerical simulations are computationally expensive, and the number of voxels determines memory requirements and the CPU time. It is important to note that the tolerance parameter should be chosen with care as it can significantly affect the results and speed of computations.

The results of the numerical simulations confirm that the FEM code is capable of accurately predicting the effective elastic properties of 3-D digitised images of rock microstructure providing the resolution of the images is adequate.

CHAPTER 2 – FINITE ELEMENT MODELLING OF GASSMANN'S FLUID SUBSTITUTION IN HETEROGENEOUS ROCKS

2.1 BACKGROUND

One of the most common problems in rock physics is the prediction of seismic velocities in rocks saturated with one fluid from the velocities in rocks saturated with another fluid. This problem known as fluid substitution is routinely performed using Gassmann's equations 1.1-1.3, which provide a powerful framework for evaluating various fluid scenarios. Rigorous application of Gassmann's equations is limited by the assumption that the porous frame is microhomogeneous (composed of only one mineral). This assumption seldom applies to natural materials like rocks that are usually composites of minerals with varied elastic properties.

Brown and Korringa (1975) generalized Gassmann's result to account for multiple minerals in the rock frame. The parameter M in their results is equivalent to

$$M = \left[\frac{\phi}{K_f} + \frac{\sigma}{K_m} - \frac{\phi}{K_\phi} \right]^{-1} \tag{2.1}$$

and

$$\sigma = 1 - \frac{K_{dry}}{K_m} \tag{2.2}$$

where ϕ is porosity, K_{dry} is the bulk modulus of the dry frame, K_f is the bulk modulus of the pore fluid, and K_m and K_ϕ are material constants. These constants are defined as

$$\frac{1}{K_m} = -\frac{1}{V}\left(\frac{\partial V}{\partial P_p}\right)\Bigg|_{P_d=constant}, \qquad \frac{1}{K_\phi} = -\frac{1}{V_\phi}\left(\frac{\partial V_\phi}{\partial P_p}\right)\Bigg|_{P_d=constant},$$

where V is the total volume of a sample of rock, V_ϕ is the volume of pore space within the sample, P_c is the confining pressure, $P_d = P_c - P_p$ is the differential pressure, and P_p is the pore pressure. These special moduli describe the effect on sample volume and pore volume of equally incrementing confining pressure and pore pressure.

If the rock frame is microhomogeneous, $K_m = K_\phi = K_g$ and equations 2.1-2.2 reduce to Gassmann's equations 1.1-1.3. However, if the rock frame is composed of two or more constituents (inhomogeneous case), the constants K_m and K_ϕ have a complicated dependence on the material properties and are difficult to estimate (Berryman and Milton, 1991; Berryman, 1992b). For that reason, the equations of Brown and Korringa have not yet found use in practical applications.

Fortunately, the accuracy of Gassmann's fluid substitution for rocks composed of multiple minerals with elastic constants of the same order of magnitude has been proven adequate. This has been confirmed by numerical tests (Knackstedt et al., 2005; Ciz et al., 2006). However, the use of Gassmann's equations for shale-rich rocks may present some particular problems especially in the case of elastic properties of the host mineral and shale being of a large contrast.

Elastic properties of clay minerals are poorly known, mainly because of the difficulty of direct measurements. The values of the bulk modulus of clay being reported in the literature vary from 1.5 up to 50 GPa (Katahara, 1996; Prasad et al., 2002; Vanorio et al., 2003; Bayuk et al., 2007) depending on mineralogy, water content, etc. In practice, when applying Gassmann's equations for multimineral rocks, one must choose the appropriate mixing scheme among the various theoretical effective-medium theories and empirical relationships (Mavko et al., 1998). The most common approach is to use a simple mixing law, such as Voigt-Reuss-Hill average (VRH) (Hill, 1952; Mavko et al., 1998). However, such scheme might introduce some errors in the presence of large amounts of clay in the rock frame,

especially when the elastic moduli of clay are much smaller than those of quartz, feldspar, dolomite etc. Furthermore, the textural distribution of clay minerals has a significant effect on the elastic properties of composites (Katahara, 2004). For instance, pore-filling clay and structural clay impact the fluid effects differently, thus the lithology-dependent mineral-mixing scheme might be more adequate in such situations.

Another problem associated with fluid substitution in shaley sediment is that the low permeability of clay can result in immobility of water inside it. Hence, the assumption of Gassmann's theory that the fluid can easily flow and relax wave-induced pore pressure increments during the seismic period may not be appropriate (Gurevich and Carcione, 2000). When clay is water-saturated, the surfaces of clay crystals can be separated by fluid sheets, which may be bound to the surfaces due to the small distance between the clay platelets (Bayuk et al., 2007). Hence, the clay mass can be considered as a clay-water composite where water is immobile. Dvorkin et al. (2007) introduce an alternative fluid substitution scheme for shaley sediments, where a clay-water composite is treated as part of the solid grain material. Therefore, the porosity within the shale is excluded from the total porosity so that only the effective porosity is used in the scheme. Parameters required by the alternative method include the elastic properties of a clay-water composite, which can be estimated by rock physics models. However, the choice of the model and the parameters of porosity and mineralogy of clay may be somewhat arbitrary.

The purpose of this chapter is to investigate the microheterogeneity effect on the accuracy of Gassmann's fluid substitution for different isotropic quartz/clay mixtures. As follows from the work of Arns et al. (2002) and Knackstedt et al. (2005) and as it has been shown in the first chapter, a finite element method or FEM can be successfully applied to accurately predict the effective elastic properties of complex multiphase materials with physically realistic phase distribution if the sources of numerical error are minimised. Since the low frequency limit of Gassmann's equation coincide with static conditions modelled by FEM, we combine FEM simulations with the theory to test the accuracy of Gassmann's fluid substitution for microheterogeneous materials.

2.2 METHODOLOGY

Given the bulk and shear moduli of the material solid constituents and a fluid phase, FEM can simulate the macroscopic physical properties, such as the effective elastic modulus, on 3D images of porous rocks at the pore scale. In this chapter, we use digital images with well resolved pore space at the scale of (200x200x200) voxels. We assume that this size provides good averaging of the elastic properties (Arns, 2002).

To test the accuracy of Gassmann's equations, we use a methodology which combines a numerical approach with the traditional and generalized Gassmann's equations. The main idea of the methodology is to test sensitivity of Gassmann fluid substitution to K_g estimated by common techniques against Gassmann predictions with K_g estimated by accurate numerical approach. Figure 2.1 shows the workflow used to implement the methodology. First, we use FEM to calculate the effective bulk moduli of dry rock K_{dry}, μ_{dry} by simply setting the properties of a saturating fluid to zero. Then we perform several FEM runs using the properties of different saturating fluids. We estimate the bulk modulus of a mineral mixture K_g by substituting the numerically estimated effective bulk modulus K for the rock saturated with the first fluid into Gassmann's equations 1.1-1.3 and solving them for K_g. Second, using the estimated K_g and equations 1.1-1.3 we predict the effective bulk modulus K for the same rock saturated with the 3rd fluid (oil). We also perform fluid substitution with K_g obtained by two different mixing rules, namely the VRH average and self-consistent effective medium theory known as CPA (Berryman, 1980a; Berryman, 1980b; Berryman, 1992b).

Using the output of two FEM runs (with different saturating fluids: fluid 1 and fluid 2) and substituting K into Brown-Korringa generalized Gassmann's equations 1.1 and 2.1-2.2 we also calculate K_m and K_ϕ. Then we predict the

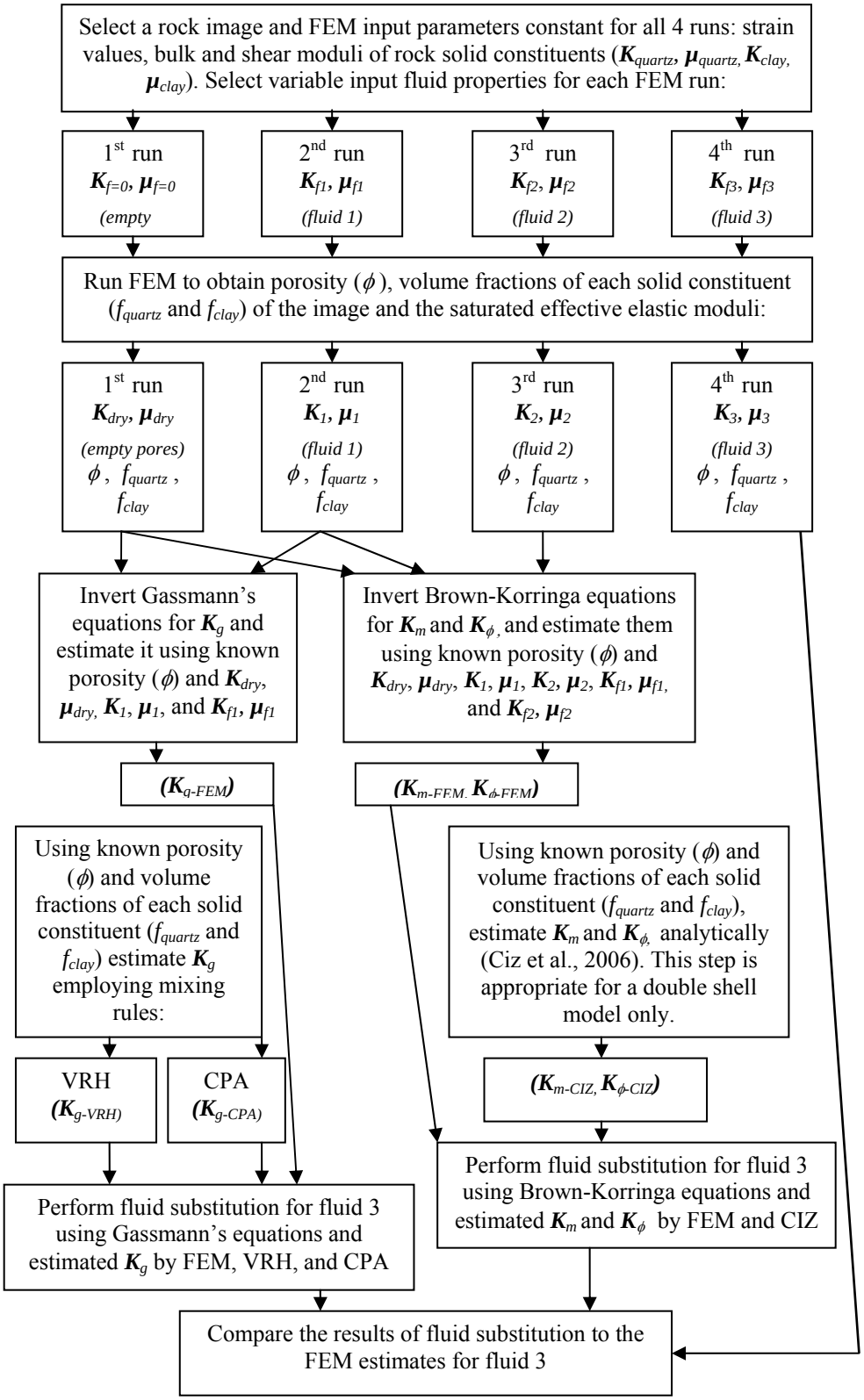

Figure 2.1. Workflow for testing the accuracy of Gassmann's equations.

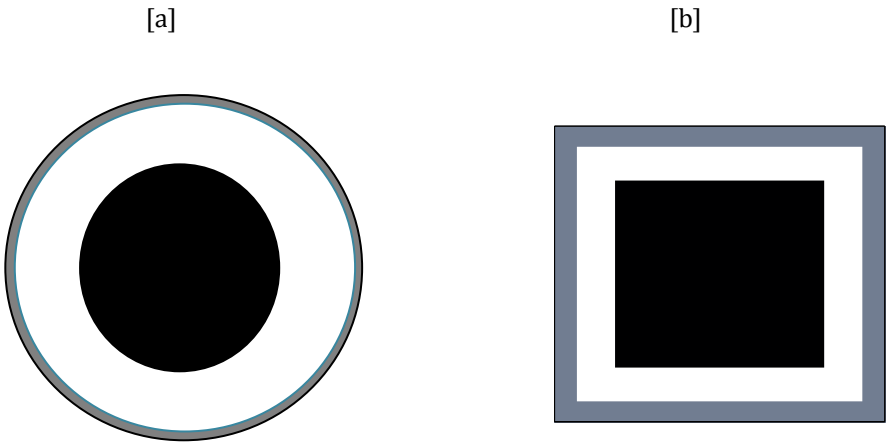

Figure 2.2. Double shell model used for analytical analysis (a) and in numerical simulations (b) consisting of three phases (quartz-white, clay-grey, fluid-black).

effective bulk modulus K for a rock saturated with the 3rd fluid using the estimated matrix properties K_m and K_ϕ and equations 1.1 and 2.1-2.2. Finally, we estimate the error of Gassmann's predictions against the FEM data.

2.3 DOUBLE SHELL MODEL

To investigate the microheterogeneity effect on the accuracy of Gassmann's fluid substitution we use a very simple geometrical configuration of a porous quartz/clay mixture. Ciz et al. (2006) analytically derived solid effective parameters K_m and K_ϕ for a double shell spherical model (Figure 2.2a). In our numerical experiments, we use a similar double shell model with cubic geometry (Figure 2.2b). This allows us to compare numerically derived material properties with the analytical ones. We generate different realizations of the model for a wide range of mineral moduli ratios with constant porosity (0.25). We perform numerical simulations for different contrasts between the elastic properties of the material constituents.

Specifically, we keep the bulk and shear moduli of quartz ($K_{g1} = 37$ GPa, $\mu_{g1} = 44$ GPa) constant and vary the bulk modulus K_{g2} of a soft phase (wet clay) from 2.09 to 20.5 GPa and the shear modulus μ_{g2} from 0.69 to 6.85 GPa. These ranges are intended to cover all possible properties of wet clay packs.

Figure 2.3a shows the results of predictions of the difference between the bulk moduli of water-saturated and dry quartz/clay porous mixture with relatively low contrast between the elastic properties of the matrix constituents ($K_{g1} / K_{g2} = 1.8$ and $\mu_{g1} / \mu_{g2} = 6.4$). We can see a good agreement between the Gassmann, Brown-Korringa and numerical estimates for all mineral ratios, with the maximum error of 0.05 GPa. However, for a large contrast between the mineral moduli $K_{g1} / K_{g2} = 17.8$ and $\mu_{g1} / \mu_{g2} = 63.8$ (Figure 2.3b), we can see significant deviations of the Gassmann estimates obtained with VRH and CPA mixing rules from the FEM results (error >1 GPa). At the same time, the estimates produced by both the traditional Gassmann's equations with numerically derived K_g and by Brown-Korringa equations with numerically estimated K_m, K_ϕ are in an excellent agreement with the analytical estimates and the FEM data.

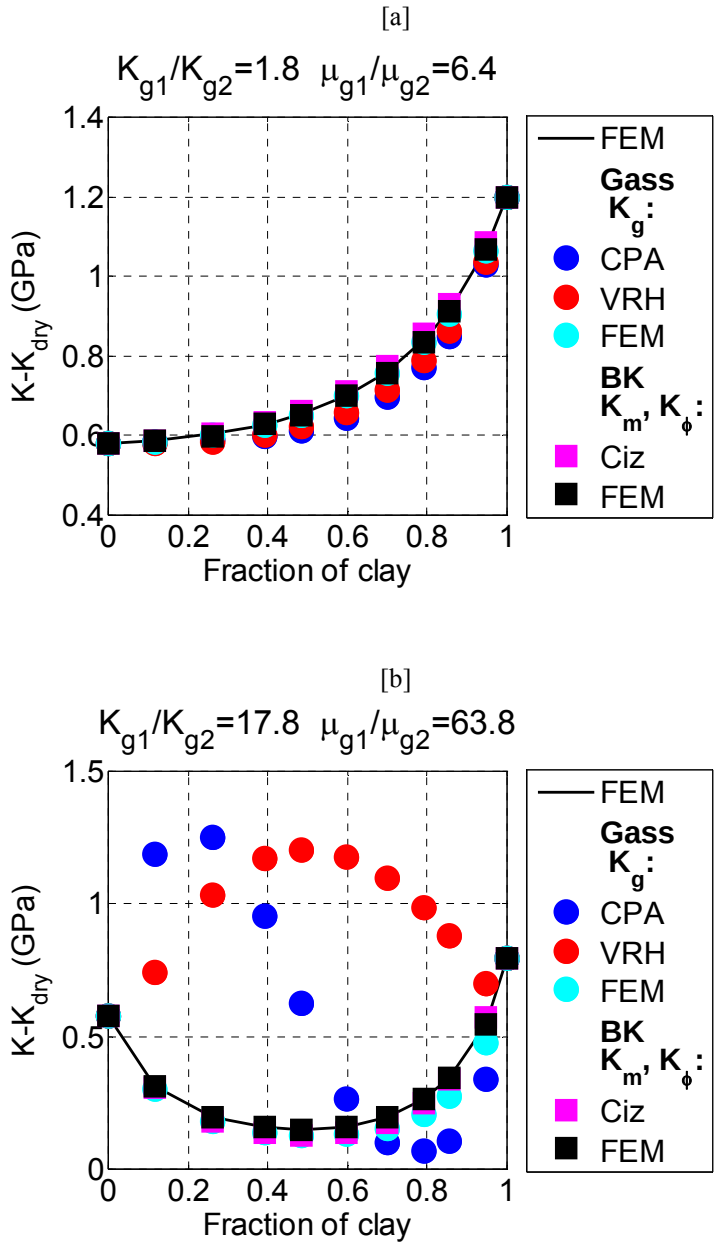

Figure 2.3. Difference between the wet (K) and dry (K_{dry}) bulk moduli of a double shell model as a function of clay fraction for (a) low and (b) high contrasts between the constituents of a composite solid phase. Black line is FEM estimates. Colour circles show Gassmann predictions (Gass) with K_g obtained by different mixing schemes: CPA, Voigt-Reuss-Hill (VRH), and FEM. Colour squares show Brown-Korringa estimates (BK) with material properties K_m and K_ϕ estimated analytically (Ciz) and numerically (FEM).

2.4 MODELS WITH DIFFERENT CLAY DISTRIBUTIONS

Clay minerals have a low-to-moderate effect on elastic properties of sandstones depending on where the clay is located (Anstey, 1991). The distribution of clay depends on the conditions at deposition, on compaction, bioturbation and diagenesis. To investigate the effect of different clay distributions on Gassmann's fluid substitution, we generate four idealized model morphologies of porous quartz/clay mixtures with different shape and location of clay (Figure 2.4). The "dispersed clay" model shown in Figure 2.4a consists of quartz grains covered by clay isolating the contacts between the grains. The "structural" or "framework"

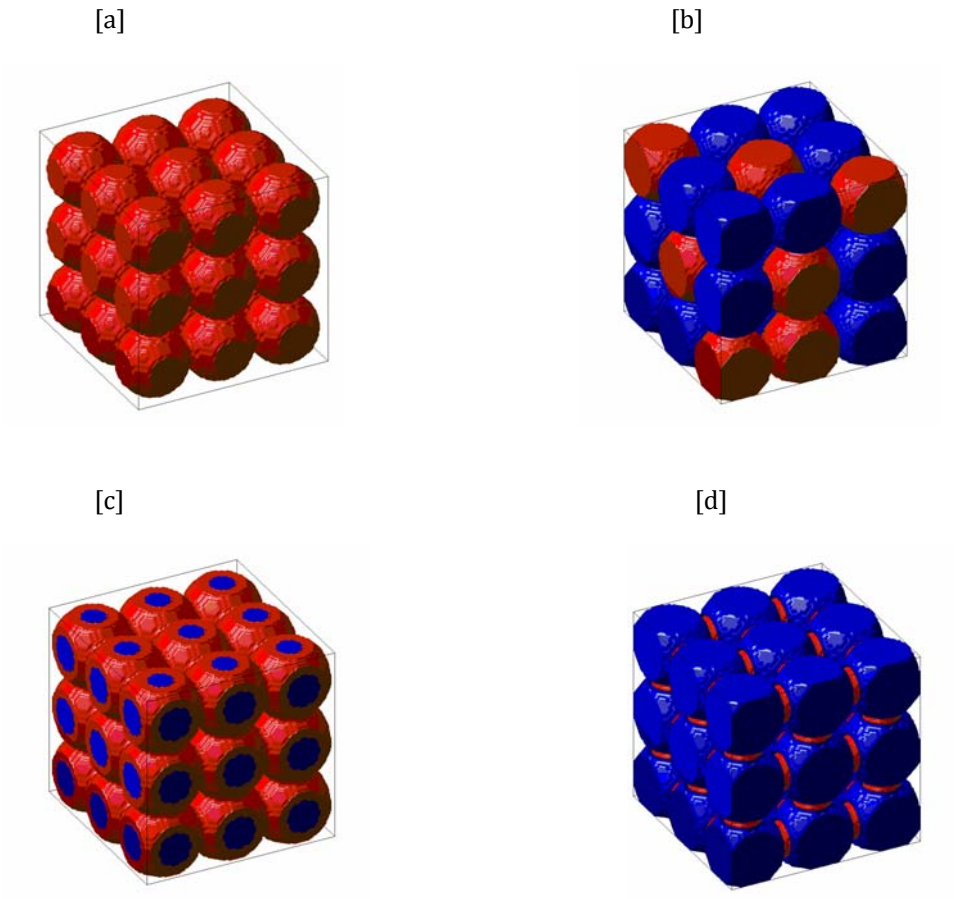

Figure 2.4. Models of sandstones with different clay distributions: (a) dispersed clay (no contacts between quartz grains), (b) framework clay, (c) coating clay (quartz grains in contact), (d) interstitial clay. $K_{g1} / K_{g2} = 5$, $\mu_{g1} / \mu_{g2} = 38$ for all models. Quartz grains are depicted in blue, clay in red.

model (Figure 2.4b) contains clay of the same shape as quartz grains. Quartz grains are in the full contact in the "coating" clay model (Figure 2.4c), which can represent a situation when clay particles are being squeezed out into the pore space by compaction. Clay bridges the grain contacts in the "interstitial" clay model, where the clay can be also considered as structural (Figure 2.4d).

We generate our models with approximately the same porosity $\phi \approx 0.35$. We use the elastic properties of clay determined from well log data from offshore West Africa (Halbert, 2006) by inversion of the lower Hashin-Shtrikman bound (Hashin and Shtrikman, 1963). The use of the lower Hashin-Shtrikman bounds is appropriate to compute the effective elastic properties of clay-sand mixtures when the clay is the primary load-bearing material, and this is generally assumed in shales and shaly sands (Goldberg and Gurevich, 1997). In the calculations of the clay properties, the clay was assumed as being wet and porous and the concept of the effective porosity (pore space available to free-flowing fluids) was used (Dvorkin et al., 2007). This means that bound water associated with clay porosity was treated as the part of the solid clay fraction. Further details of the inversion of the lower Hashin-Shtrikman bound and the description of the log data used in the inversion can be found in Halbert (2006).

The properties of wet clay are taken to be: bulk modulus $K_{g2} = 7.35$ GPa and shear modulus $\mu_{g2} = 1.16$ GPa. We assume that quartz grains have the same properties as mentioned above, so the contrasts between the elastic constants of minerals composing the rock frame are $K_{g1} / K_{g2} = 5$ for the bulk moduli and $\mu_{g1} / \mu_{g2} = 38$ for the shear moduli. For all the models, we consider similar mineral ratios when clay fraction is approximately equal to 0.12 and 0.35. These very high contrasts are used deliberately to assess the maximum deviations from Gassmann predictions.

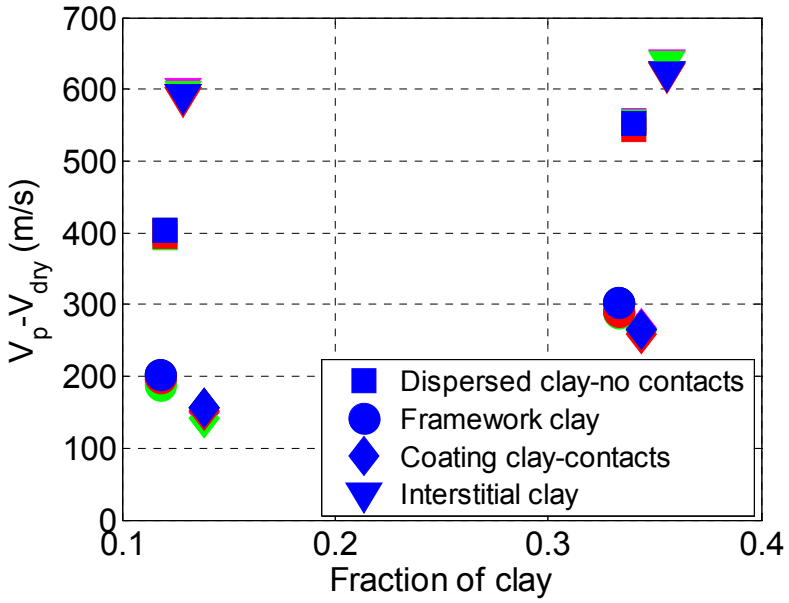

Figure 2.5. Gassmann predictions versus numerical estimates as a function of clay fraction for periodic spheres models with different clay distributions. Black symbols are FEM estimates. Magenta, green and red symbols show Gassmann predictions (Gass) with K_g obtained by CPA, Voight-Reuss-Hill and FEM, respectively. Blue symbols show Brown-Korringa estimates with material properties K_m and K_ϕ estimated by FEM. Black and blue symbols coincide.

We apply FEM to the images with different clay distribution to estimate the dry and water saturated moduli. Following the workflow shown in Figure 2.1 we perform fluid substitution with K_g estimated by CPA, VRH, and FEM. We also calculate the dry and saturated P-wave velocity. As can be seen from Figure 2.5, different clay distributions have significant effect on the P-wave velocity of the conglomerates. The highest velocities $V_p - V_{dry} \approx 630$ m/s are observed for the "interstitial" clay model and the lowest $V_p - V_{dry} \approx 150$ m/s for the "coating" clay model with grains in contacts. However, we can see that Gassmann predictions produced using different mixing laws as well as Brown-Korringa estimates are in a good agreement with the numerical data for all considered microstructures. The maximum deviation of the Gassmann predictions of $V_p - V_{dry}$ from the FEM estimates is about 16 m/s. This suggests that the accuracy of Gassmann's fluid substitution is more than adequate for these idealised morphologies.

These numerical results may appear to contradict the results of Berryman (1992a), who showed that for certain geometrical configurations of heterogeneous rocks, the moduli K_m and K_ϕ in Brown-Korringa equations may be very different from each other, and K_ϕ can even be negative. However we note that for rocks with $K_g >> K_{dry}$ and $K_g >> K_f$, we also have $K_m >> K_{dry}$, $K_m >> K_f$, $|K_\phi| >> K_{dry}$, $|K_\phi| >> K_f$. Thus, moduli K_g, K_m and K_ϕ have a relatively minor influence on the effective bulk modulus of a saturated rock K (see equation 2.1), and therefore the effect of spatial variation of K_g is also insignificant.

2.5 CHAPTER CONCLUSIONS

We have analysed the effect of microheterogeneity on Gassmann's fluid substitution in its traditional and generalized forms for different idealized porous quartz/clay structures. We utilize a scheme combining numerical simulations with Gassmann's equations to estimate the material properties of a rock frame. For a simple double shell model, the accuracy of Gassmann predictions significantly

depends on contrasts between the elastic moduli of minerals composing the rock frame. The common mixing laws such as VRH and self-consistent effective-medium theory introduce significant errors into the predictions of K for digital models with large contrasts between the properties of solid phases (factor 18 for K_g, and 64 for μ_g, error>1GPa).

For more realistic highly porous structures ($\phi \approx 0.35$) such as periodic spheres models with different clay distributions, the accuracy of Gassmann predictions of the P-wave velocity remains relatively high (error 16 m/s) despite the large contrasts between the moduli of solid phases (factor 5 for K_g, and 38 for μ_g). This suggests that simple lithology-independent mixing laws provide robust estimates of elastic properties of multiphase minerals. This further suggests that Gassmann's equations are adequate for highly porous granular rocks composed of multiple minerals with elastic constants of relatively high contrast.

CHAPTER 3 – FLUID SUBSTITUTION IN ROCKS SATURATED WITH VISCOELASTIC FLUIDS

3.1 BACKGROUND

Continuously growing demand for hydrocarbon energy sources has renewed interest in production from bituminous and heavy-oil reservoirs. Heavy oil reserves account for more than 6 trillion barrels- in- place worldwide-triple the world's reserves of conventional oil and gas (Batzle et al., 2006). However, the high viscosity of heavy oils makes them difficult or impossible to produce using conventional technology. A variety of methods, currently used by the industry, aim at lowering the viscosity by injecting heat or chemical solvents. Thermal recovery methods have been the most efficient in heavy-oil production with recovery rates as high as 80%. Injected heat alters the already complex physical properties of the heavy-oil reservoirs such as seismic velocity, density, and attenuation. Tracking these changes with time-lapse seismic techniques can considerably improve recovery efficiency. Appropriate rock physics modelling is important for quantitative interpretation of the changes in seismic response due to alterations in reservoir and fluid properties during production.

As mentioned in previous chapters, seismic fluid substitution modelling using Gassmann's equations is routine in the analysis and interpretation of seismic velocities and amplitudes (Smith et al., 2003). Given pore, frame, and fluid properties of a rock, the Gassmann's equations can be used to predict the bulk modulus of a rock under quasi-static conditions. The corresponding dynamic moduli can be obtained from Biot's theory of poroelasticity (Biot, 1956a; Biot,1956b), an extension of Gassmann's theory to finite frequencies. One important result of the Gassmann/Biot's theory is that the effective shear modulus is identical to the frame shear modulus. In other words, the existence of the fluid has no effect on the effective shear modulus of the rock.

As known from laboratory measurements (Nur et al., 1984; Eastwood, 1993; Schmitt, 1999; Batzle et al., 2006; Behura et al., 2007; Han et al., 2007a), heavy oils exhibit viscoelastic behaviour such that their moduli are frequency- and temperature-dependent. Oil that behaves like a Newtonian liquid at low frequencies can act as a nearly elastic solid at high frequencies. In between these extreme cases, wave propagation in heavy oil is dispersive and exhibits strong attenuation. Indeed, the heavier the oil, the more long-chain or high-carbon-number molecules are present, resulting in higher viscosity. Although viscosity is influenced by pressure and gas content, it is primarily a function of oil gravity and temperature. Depending on temperature conditions, heavy oil can have a finite shear modulus even at seismic frequencies making Gassmann/Biot's poroelastic constitutive equations inapplicable to heavy-oil rocks.

When a rock is saturated with heavy oil, its behaviour also becomes viscoelastic (Behura et al., 2007). A dramatic decrease of compressional velocities in heavy-oil sands with increasing temperature has been observed in laboratory experiments (Tosaya et al., 1987). Despite the fact that this decrease was in part caused by the abnormally high pressure in the experimental setup, the main factor responsible for the velocity decrease is the change in fluid properties with temperature. The latest laboratory experiments provide evidence of the complex properties of heavy-oil rocks. In particular, Han et al. (2007a, 2007b, 2008) study various effects on the compressional- and shear-wave velocities of heavy-oil sands, such as rock texture, pore-fluid properties, pressure, and interaction between pore fluids and rock-frame properties at different temperatures. Han et al. (2007b) also test Gassmann predictions against experimental data for a range of temperatures. They indicate that as temperature decreases below 60°C, heavy oil becomes dispersive and Gassmann estimates no longer match the data. Viscoelastic behaviour of the oil violates Gassmann's theory. Indeed, Gassmann's theory is based on the Pascal's Law, which states that, in the absence of body forces, fluid pressure exerted anywhere in a confined incompressible fluid is transmitted equally in all the directions. This means that pressure is the same throughout the pore space. This law is not applicable to viscoelastic media. Biot's theory is not applicable to heavy oils

either because it ignores the viscoelastic phenomenon by neglecting the fluid shear stress in the microscopic (pore-scale) constitutive equations (Pride et al., 1992; Gurevich, 2002).

Several approaches to modelling effective elastic properties of rocks saturated with heavy oil have been proposed (Marion and Nur, 1991; Eastwood, 1993; Tsiklauri and Beresnev, 2003; Leurer and Dvorkin, 2006; Ciz and Shapiro, 2007; Das and Batzle, 2008; Gurevich et al., 2008). However, until recently, verification of these models using controlled laboratory experiments was not possible.

In this chapter, we propose an alternative modelling scheme based on equivalent-medium theory for rocks saturated with viscoelastic fluids. Comparison with laboratory data allows us to refine the scheme using the concept of dual porosity to obtain reasonable agreement between theory and experiment. Our approach can be used for practical applications to produce reliable estimates of effective frequency- and temperature-dependent properties of heavy-oil rocks.

3.2 METHODOLOGY

3.2.1 EFFECTIVE-MEDIUM MODEL

Fluid saturation is an important parameter influencing the seismic properties of rocks. As mentioned the effect of a Newtonian pore fluid on the elastic moduli of a rock can be predicted from the properties of dry rock and fluid compressibility using the Gassmann/Biot's theory. An alternative approach, which addresses the problem of estimating elastic moduli from knowledge of rock constituents and microstructure, is based on effective-medium theories (e. g., Hashin and Shtrikman, 1963; Budiansky, 1965; Hill, 1965; Mukerji et al., 1995). These theories allow one to compute equivalent elastic properties of a mixture of two or more elastic constituents. Unlike the Gassmann/Biot's theory, effective-medium theories require characterization of matrix and pore space geometry. Furthermore, at sufficiently low frequencies, these theories (schemes) can be applied to mixtures of viscoelastic constituents by considering them as solids with frequency-dependent moduli. This is

known as elastic-viscoelastic analogy or the correspondence principle (Hashin, 1970; Haddad, 1995). Hence, effective-medium theories can be applied to heavy-oil rocks.

To gauge the effect of viscoelasticity of the pore-filling material on the overall rock properties, we use a scheme based on a self-consistent theory of Berryman (1980a,b; 1992b). This scheme is a self-consistent version of the average T-matrix approximation of Küster and Töksöz (1974) and is also known as the coherent potential approximation (CPA). CPA is a versatile mixing law of the theory of composites. It is known to provide reliable estimates of frame moduli of heterogeneous materials (Ogushwitz, 1985). CPA uses the concepts of elastic-wave scattering theory for the deformation of isotropic inclusions and approximates the interaction of the inclusions by replacing the background medium with an as-yet-unknown effective medium. This means that the effect of many pores of a particular shape is given by solving the canonical problem of a single pore surrounded by a uniform medium with yet-unknown elastic properties of the porous composite. It has been proved rigorously that CPA is a realizable effective medium scheme, i.e. there exists a particular geometrical arrangement of the constituents for which this scheme is exact (Milton, 1985).

A key property of CPA is that it is symmetrical with respect to the constituents. Each constituent is treated equally in the scheme, meaning that no single constituent acts as a host to the others but that a more abundant constituent is the load-bearing one. Thus, a solid-fluid mixture is modelled as a solid with fluid inclusions of a particular shape when fluid concentration is small, and as a suspension of solid particles in the fluid when the solid concentration is small. This property is consistent with the concepts of percolation and critical porosity (Nur et al., 1995) and allows one to model situations when heavy oil is a pore-filling fluid and when it is part of the rock matrix.

CPA calculates the effective properties of a porous rock using known properties of the solid matrix, the pore fluid, and the pore aspect ratio. The implicit CPA formulas for bulk K and shear G moduli of a two-component rock (one solid phase, one fluid phase) are:

$$\phi\left(K_f - K\right)P^f + \left(1-\phi\right)\left(K_s - K\right)P^s = 0\,, \tag{3.1}$$

$$\phi\left(G_f - G\right)Q^f + \left(1-\phi\right)\left(G_s - G\right)Q^s = 0\,, \tag{3.2}$$

where ϕ is the porosity; K_f and G_f are bulk and shear moduli of the pore fill, respectively; K_s and G_s are bulk and shear moduli of the matrix (grain) material, respectively; and P and Q are invariants of the so-called Wu tensor (Wu, 1966). The components of this tensor depend on the aspect ratio of the pores and on the bulk and shear moduli of the pore-fill, matrix material, and as-yet-unknown effective moduli K and G of the composite. We use the expressions of the Wu tensor for spheroidal inclusions of arbitrary aspect ratio α to describe the pore/grains geometry of typical sandstones. These expressions are cumbersome and can be found in Berryman (1980b) or Mavko et al. (1998).

Equations 3.1 and 3.2 are coupled and can be solved by iteration:

$$K_{n+1} = \frac{\phi K_f P_n^f + \left(1-\phi\right)K_s P_n^s}{\phi P_n^f + (1-\phi)P_n^s} \tag{3.3}$$

$$G_{n+1} = \frac{\phi G_f Q_n^f + \left(1-\phi\right)G_s Q_n^s}{\phi Q_n^f + (1-\phi)Q_n^s}\,. \tag{3.4}$$

Equations 3.3 and 3.4 can be used to estimate the effective elastic moduli of a saturated rock. The iteration process requires a first guess of K_1 and G_1, which can be calculated using the Voigt-Reuss-Hill average. The scheme can also be used to calculate the dry frame properties (K_{dry}, G_{dry}) by setting the bulk and shear moduli of the saturating fluid to zero (rock with empty pores).

3.2.2 *COMPLEX SHEAR MODULUS OF HEAVY OIL*

To apply CPA to calculate the effective properties of a rock saturated with heavy oil, we need to know its complex temperature- and frequency-dependent shear modulus. For viscoelastic materials, the shear modulus G is complex and represents

the ability of a material to store energy elastically and to dissipate it as a viscous fluid:

$$G = G' + iG'', \tag{3.5}$$

where G', in theory of viscoelasticity, is a storage modulus and G'' is a loss modulus (Ferry, 1980).

The frequency dependency of the complex shear modulus of heavy oil can be approximated by Cole-Cole type empirical dispersion equations (Cole-Cole, 1941; Gurevich et al., 2008), which relate complex shear modulus with the shear moduli at the low- and high-frequency limits, angular frequency, and relaxation time. The relaxation time depends on fluid viscosity which is a function of temperature. According to Han et al. (2008), the temperature dependency of heavy oils can be described by three main stages, depending on the oil liquid point: liquid state, quasi-solid state, and solid state. This dependency can also be approximated by empirical relationships (e. g., Beggs and Robinson, 1975).

The dependency of properties of linear viscoelastic materials on frequency and temperature can be simplified by using so-called temperature-frequency superposition principle, which states that the dispersion curves for different temperatures are the same if the frequency is normalized by some temperature-dependent parameter (Williams, et al., 1955). This means, for instance, that the Cole-Cole dispersion equation can be used for all temperatures using the Beggs and Robinson (Beggs and Robinson, 1975) viscosity-temperature relationship.

To perform fluid substitution for heavy-oil rocks, frequency- and temperature-dependent complex modulus must be used in equations 3.3 and 3.4 instead of G_f.

3.2.3 *COMPARISON WITH KNOWN SOLUTIONS FOR DRY AND -SATURATED ROCKS*

Before applying CPA to heavy-oil rocks we test its applicability to the limiting case of Newtonian liquid/solid mixtures. Figure 3.1 shows CPA predictions for dry and water-saturated rocks with a quartz matrix for a range of porosities and

aspect ratios. The predicted bulk moduli are compared with the empirical model of Krief et al. (1990) and the Hashin-Shtrikman (HS) bounds (Hashin and Shtrikman,

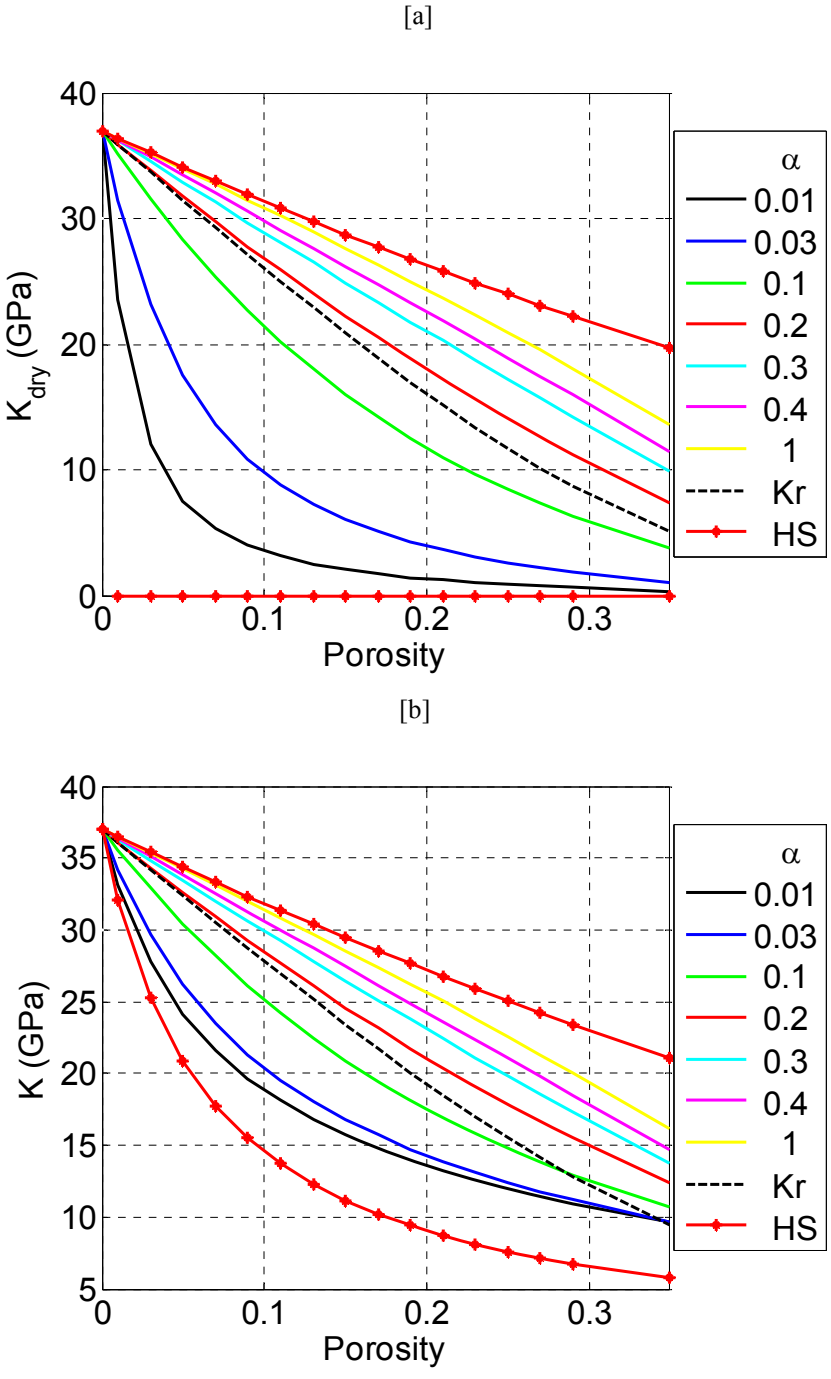

Figure 3.1. Bulk moduli of dry (a) and saturated (b) quartz sandstone versus porosity. CPA estimates for different aspect ratios α (solid lines), Hashin-Shtrikman bounds (symbols) and Krief et al. model (dashed lines).

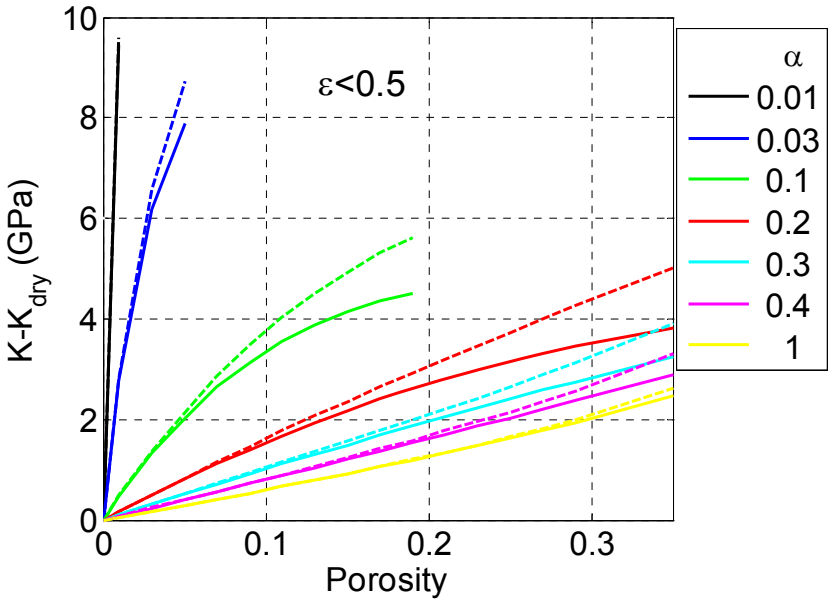

Figure 3.2. Difference between water-saturated and dry moduli of a rock with quartz matrix as a function of porosity and aspect ratio α for crack densities $\varepsilon < 0.5$: CPA (dashed lines) versus Gassmann estimates (solid lines).

1963). The Krief at al. (1990) estimates of K_{dry} correspond more closely to the CPA estimates with $\alpha \simeq 0.2$, which are consistent with values of aspect ratios for sand-related pores reported in literature (e. g., Xu and White, 1995). As expected, all CPA estimates lie within HS bounds.

In Figure 3.2, we compare the difference between CPA estimates of saturated and dry moduli $(K - K_{dry})$ with Gassmann predictions for quartz/water mixtures for realistic crack densities $\varepsilon < 0.5$ (the crack density is related to porosity ϕ and aspect ratio α of the spheroidal crack by $\varepsilon = 3\phi/4\pi\alpha$). This comparison is important because any mixture model for rock saturated with a viscoelastic substance must be consistent with Gassmann's equations when the pore-filling substance is a Newtonian fluid. At the same time, models based on isolated ellipsoidal pores are not exactly Gassmann-consistent because fluid pressure in the pores varies with their orientations (Thomsen, 1985; Mavko and Jizba, 1991). As can be seen from Figure

3.2, the CPA results are in the best agreement with Gassmann predictions for spherical pores and show the maximum deviation from Gassmann estimates for relatively flat pores. For aspect ratios $\alpha = 0.2 - 0.4$ and typical porosities of up to $\phi = 0.25$ we observe satisfactory agreement with Gassmann predictions. The discrepancy is less than 1 GPa. We thus conclude that CPA is approximately Gassmann-consistent within typical measurement errors.

3.3 FLUID SUBSTITUTION SCHEME USING CPA

If the effective pore aspect ratio α is known, the effective elastic properties of a rock can be computed by iterating equations 3.3 and 3.4. Here we assume that the rock structure can be approximated by ellipsoids with the same effective aspect ratio. Of course, pore geometry of real rocks is more complicated and consists of pores of different sizes and shapes. However, ellipsoids often are used to capture some essential properties of subsurface voids, providing simple parameterization of the enormous complexity of the real pore space.

For a given rock sample, the effective pore aspect ratio α can be estimated from dry moduli (note that in Gassmann's fluid substitution K_{dry} is the key input parameter as well). Given K_{dry}, the effective aspect ratio α can be estimated by the inverse CPA scheme (equations 3.3 and 3.4) with fluid moduli set to zero. The aspect ratio α can also be derived using the inverse CPA scheme if we know the bulk modulus K of the rock saturated with a fluid with known bulk modulus (e.g. water). Alternatively, the aspect ratio can be estimated from shear moduli.

Once α is estimated, we can calculate the effective moduli of a saturated rock for any desired pore-filling material using the forward CPA scheme.

We can summarize the CPA fluid substitution workflow in the following steps:

1. Employ inverse CPA to estimate the effective aspect ratio α using known dry or saturated bulk or shear modulus.

2. Obtain the frequency- and temperature-dependent complex shear modulus of the pore fill G_f from laboratory measurements. If such measurements are not available in the range of temperatures and frequencies required, they can be interpolated using known empirical relationships (Beggs and Robinson, 1975; Cole-Cole, 1941) and the frequency-temperature superposition principle (Williams et al., 1955, Ferry, 1980).
3. Calculate the effective elastic moduli of a rock saturated with viscoelastic fluid employing forward CPA scheme (equations 3.3 and 3.4) with complex shear modulus of a pore-fill G_f.

3.4 COMPARISON WITH LABORATORY MEASUREMENTS

3.4.1 UVALDE HEAVY-OIL ROCK

We apply our CPA fluid substitution scheme to Uvalde heavy-oil rock from Texas, U.S.A. The laboratory measurements carried out on this rock have been reported in the literature (Batzle et al., 2006; Behura et al., 2007; Das and Batzle, 2008).

The Uvalde rock is a carbonate saturated with extremely viscous heavy oil with an API density of 5 (1.12 g/cm^3). It has porosity of approximately 25%, and permeability of 550 mD. A shear rheometer was used to measure the complex shear modulus of the rock at temperatures ranging from $30°\,\mathrm{C}$ to $350°\,\mathrm{C}$ and frequencies ranging from 0.01 to 80 Hz. Then the oil was extracted and its complex shear modulus was measured in the same frequency range and temperatures from $30°\,\mathrm{C}$ to $250°\,\mathrm{C}$.

The measured storage modulus of the Uvalde rock and the extracted oil for the whole range of frequencies and temperatures ranging from $30°\,\mathrm{C}$ to $200°\,\mathrm{C}$ are shown in Figure 3.3. The missing data points have been interpolated. The modulus of the heavy-oil-saturated rock shows a moderate dependency on frequency and is strongly influenced by temperature. The storage modulus G' of the rock increases

[a]

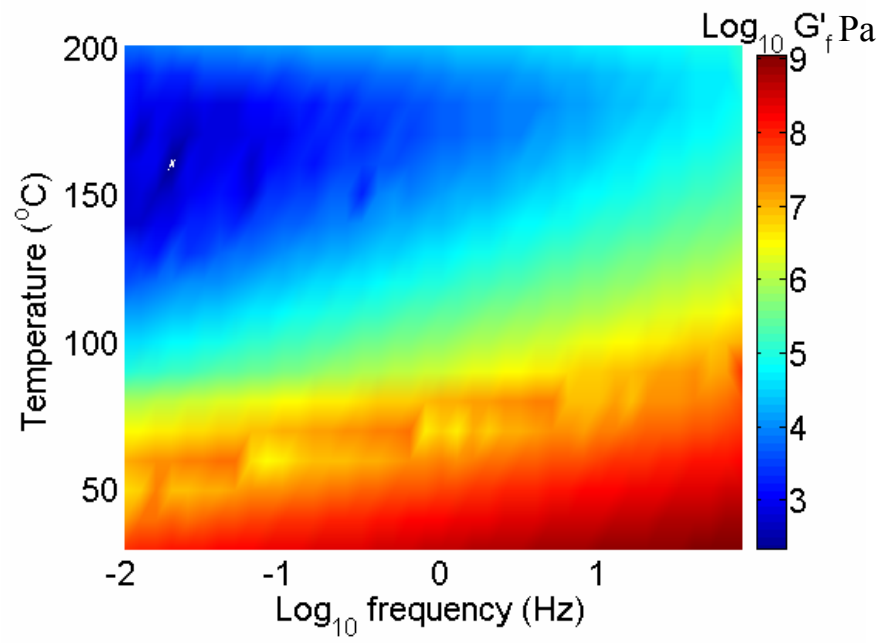

[b]

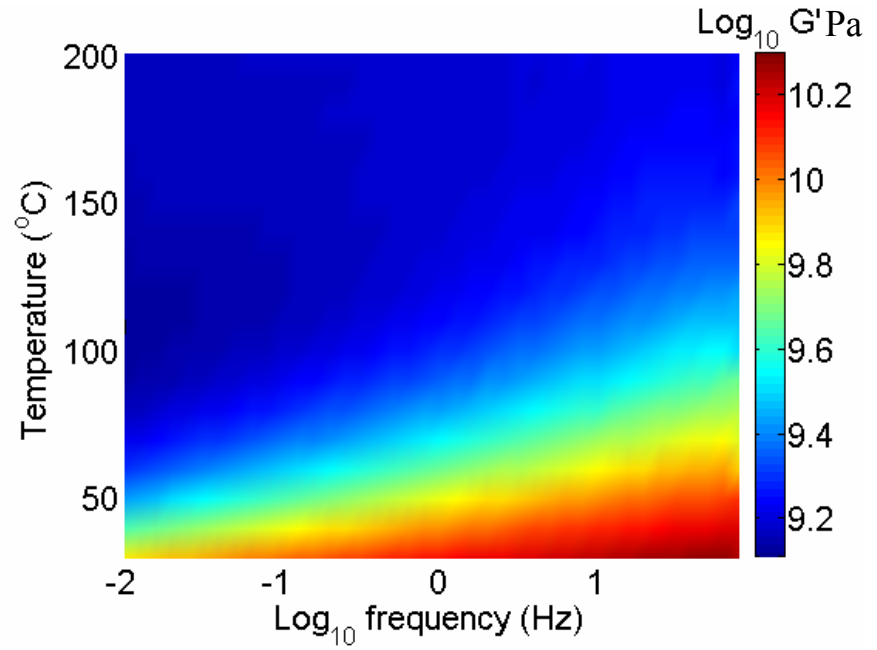

Figure 3.3. Variation of (a) storage modulus $G_f^{'}$ of Uvalde heavy oil and (b) storage modulus $G^{'}$ of Uvalde heavy-oil rock with frequency and temperature as measured by Behura et al. (2007).

with frequency for temperatures less than $150°\,\mathrm{C}$. At higher temperatures, the behaviour of the storage modulus G' is weakly dependent on frequency.

The trends observed for the rock shear properties look similar to those for the extracted oil. The Uvalde oil shows noticeable dispersion for temperatures less than $180°\,\mathrm{C}$. At low temperatures, the extracted heavy oil supports a shear wave, but with increasing temperature, its storage modulus decreases rapidly, similar to what is observed for the rock shear modulus. As in the case with the rock, we can see that at higher temperatures the storage modulus of the oil G_f' is nearly independent of frequency. In general, G_f' increases with increasing frequency for all temperatures.

Therefore, we can conclude that the mechanical response of a heavy-oil rock with changing temperature and frequency is strongly influenced by the behaviour of the pore-filling oil.

3.4.2 *MODELLING WITH A SINGLE ASPECT RATIO*

Given that the measurements of the shear properties of the Uvalde oil and Uvalde rock are available, we use the fluid substitution workflow as described above. First we predict the effective elastic properties of the Uvalde rock saturated with the Uvalde oil using CPA. Then we compare the predicted storage modulus of the rock with laboratory data. We perform our modelling for the full range of frequencies and the temperatures ranging from $30°\,\mathrm{C}$ to $200°\,\mathrm{C}$. We take the physical properties of the grain material as those of calcite ($K_s = 60\,\mathrm{GPa}$, $G_s = 30\,\mathrm{GPa}$, density $\rho_s = 2.71\,\mathrm{g/cm^3}$). The dry shear modulus G_{dry} of the Uvalde rock has not been measured, so we perform an analysis of the available values of the temperature- and frequency-dependent shear properties of the oil and rock to obtain G_{dry}. In our analysis, we assume that at high temperatures and low frequencies, the pore fluid behaves as a Newtonian fluid and has no effect on the effective shear properties of the rock. Indeed, careful analysis of laboratory data (Figure 3.3) shows that for temperatures over $120°$ the shear modulus of the Uvalde rock is a real constant

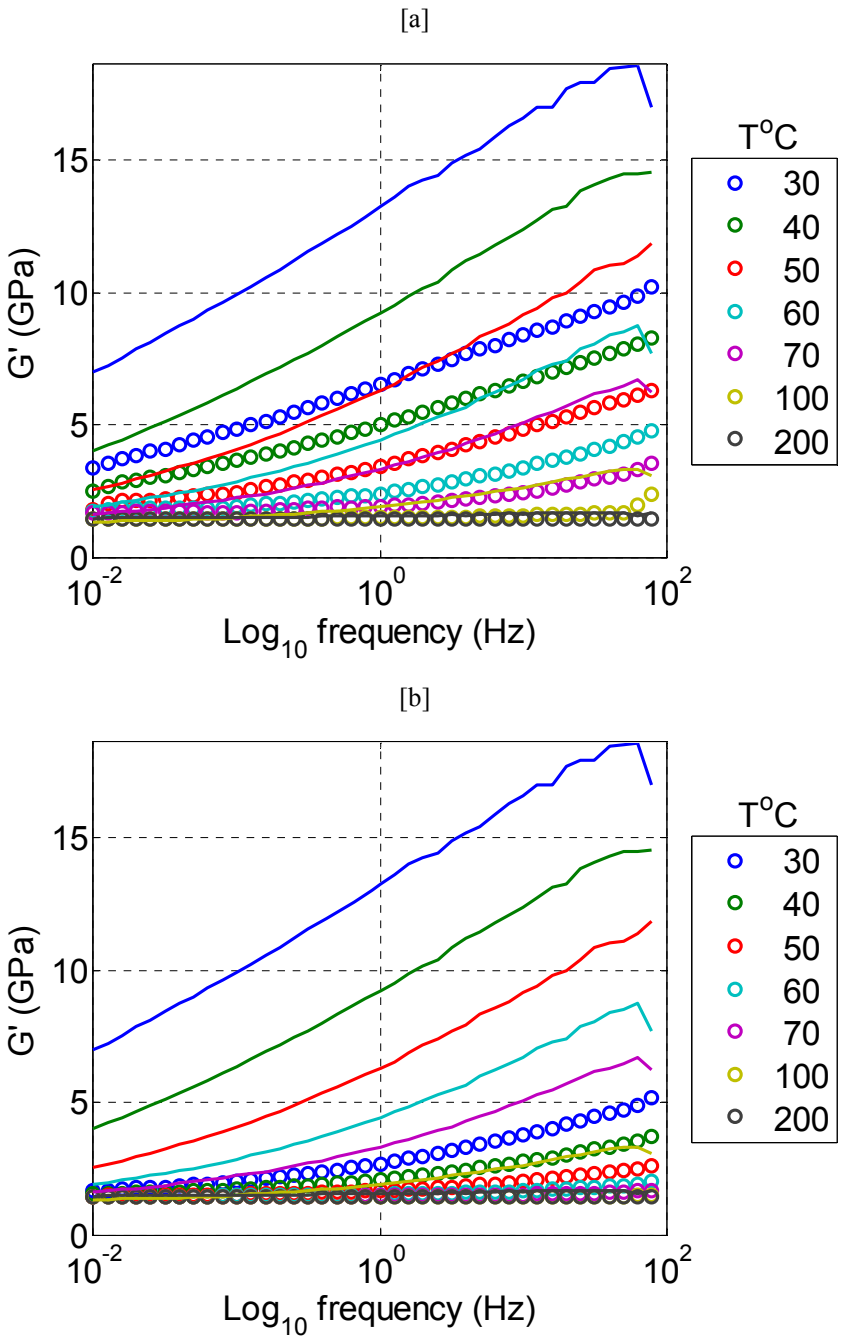

Figure 3.4. Comparison of frequency- and temperature-dependent storage modulus G' predicted by (a) CPA with a single aspect ratio (symbols) and by (b) extended Gassmann (symbols) with laboratory measurements conducted on an Uvalde heavy-oil rock sample (lines). T is temperature.

$G = 1.45$ GPa. This means that the effective shear modulus G becomes identical to the dry shear modulus G_{dry}.

Next, we solve equations 3.3 and 3.4 to obtain the aspect ratio α using the estimated G_{dry}. Then we use the forward CPA to compute the frequency- and temperature-dependent effective shear modulus of the Uvalde rock saturated with the Uvalde oil. In Figure 3.4a, we compare the calculated effective shear moduli of the rock (symbols) with the laboratory-measured moduli (lines). We can see that CPA is unable to capture the trend of the frequency- and temperature-dependency of the rock shear properties, especially for low temperatures. The estimated moduli are significantly lower than the measured ones. In Figure 3.4b, we compare the predictions of the effective storage modulus computed by the viscoelastic extension of Gassmann's theory (EG) (Ciz and Shapiro, 2007) with laboratory data. We can see that the EG predictions (symbols) deviate from the laboratory data (lines) even more than the CPA estimates (Figure 3.4a).

3.4.3 COMPLIANT POROSITY

For additional insight into frequency- and temperature-dependent behaviour of the Uvalde rock, we compare storage moduli of the rock and oil as a function of temperature for different frequencies (Figure 3.5). We observe a substantial variation of the rock storage modulus G' (symbols) with temperature for different frequencies, contrary to the relatively moderate variation of the oil storage modulus G_f' (lines). For instance, G' (80 Hz frequency) varies from approximately 2 GPa up to 17 GPa, whereas G_f', varies from almost 0 to 1.2 GPa. This suggests that a simple mixing law, such as CPA with a single aspect ratio, cannot account for those observations.

The effect of porosity and fluids on elastic properties of rocks is often modelled using the binary structure of the pore space-relatively stiff pores that occupy most of the pore space, and relatively compliant (soft) pores that are present at grain contacts and responsible for the pressure dependency of the elastic moduli.

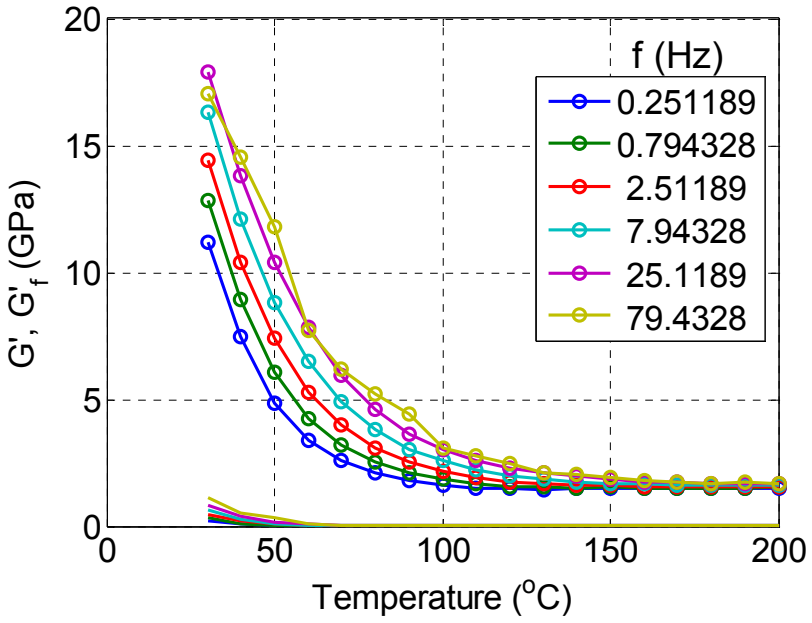

Figure 3.5. Laboratory measurements of storage moduli G_f' of Uvalde heavy oil (lines) and G' of Uvalde heavy-oil rock (symbols) for a range of frequencies and temperatures.

At high frequencies, fluid flow does not have enough time to equilibrate pore-pressure gradients between the two pore types, effectively isolating compliant pores from stiff pores and from each other. If a rock is saturated with viscoelastic fluid, this effect may occur even at relatively low frequencies, as considered in this study. When heavy oil is in a near-elastic state, it cannot flow out of soft pores, stiffening the compliant grain contacts. The presence of compliant pores may lead to additional dispersion of both compressional and shear waves in heavy-oil rocks due to the dependency of the normal stiffness of these contacts on the storage modulus of the pore fill (Mavko and Jizba, 1991). Poor performance of both CPA with a single aspect ratio and EG, may be explained by the presence of compliant pores in the rock matrix.

3.4.4 MODELLING WITH TWO ASPECT RATIOS

To account for the effect of double porosity, we introduce the compliant porosity terms to equations 3.3 and 3.4:

$$K_{n+1} = \frac{\phi_s K_f P_n^{fs} + \phi_c K_f P_n^{fc} + (1-\phi) K_s P_n^s}{\phi_s P_n^{fs} + \phi_c P_n^{fc} + (1-\phi) P_n^s} \tag{3.6}$$

$$G_{n+1} = \frac{\phi_s G_f Q_n^{fs} + \phi_c G_f Q_n^{fc} + (1-\phi) G_s Q_n^s}{\phi_s Q_n^{fs} + \phi_c Q_n^{fc} + (1-\phi) Q_n^s}, \tag{3.7}$$

where ϕ_s is stiff porosity that occupies most of the pore space, ϕ_c is compliant porosity present within the grains and at grain contacts, and $\phi = \phi_s + \phi_c$.

Now the problem becomes more complicated because equations 3.6 and 3.7 must be inverted to estimate three unknown parameters: compliant porosity ϕ_c, and aspect ratios of compliant and stiff pores α_c .and α_s respectively. For the fitting

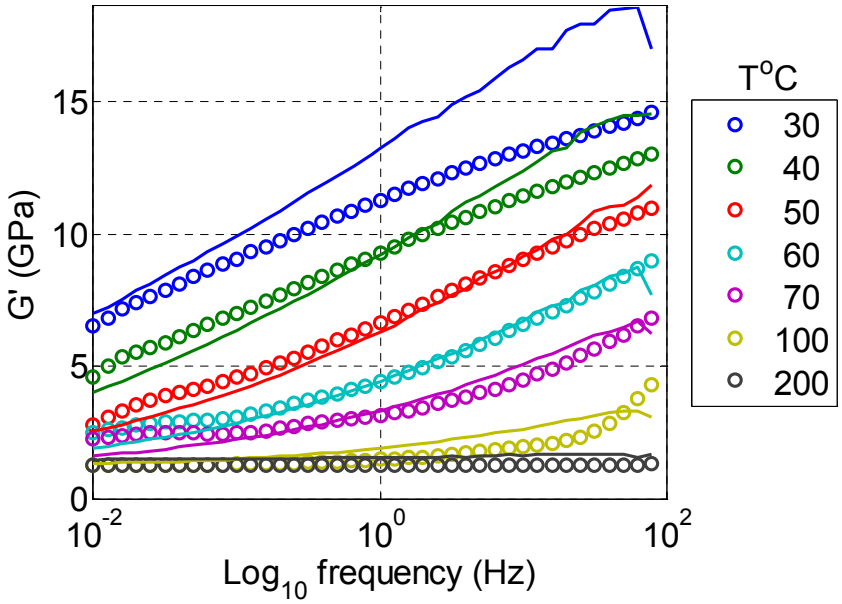

Figure 3.6. Comparison of frequency- and temperature-dependent storage modulus G' predicted by CPA with two aspect ratios (symbols) with laboratory measurements carried out on an Uvalde heavy-oil rock sample (lines).

[a]

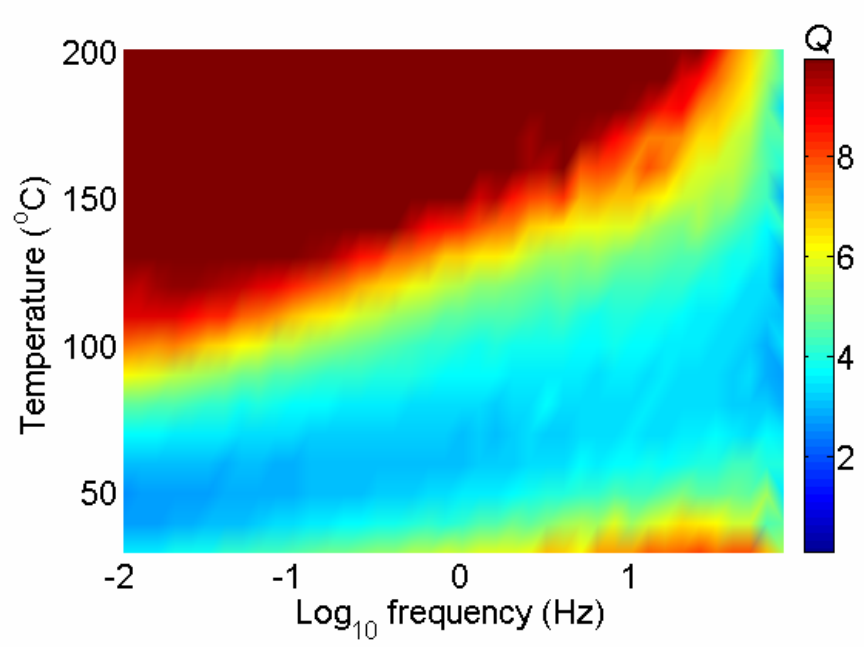

[b]

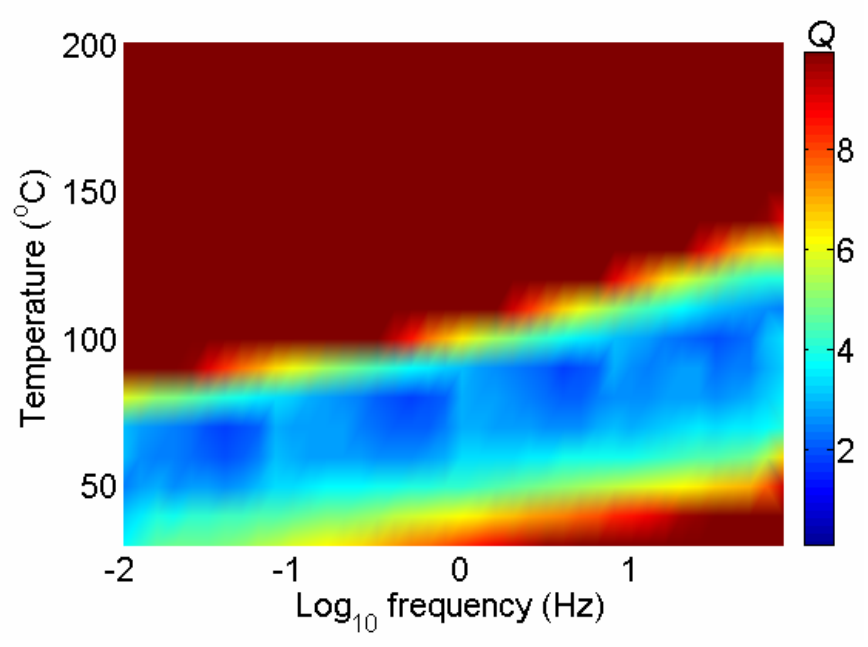

Figure 3.7. Variation of quality factor Q of Uvalde heavy-oil rock with frequency and temperature (a) as measured by Behura et al. (2007) and (b) as predicted by CPA with two aspect ratios.

procedure, we use dry shear modulus G_{dry} and saturated shear modulus G measured at temperature $50°\,\mathrm{C}$ and two frequencies, 0.08 Hz and 15.85 Hz. We assume the grains can be described by the aspect ratio $\alpha_g = 0.8$ and keep it constant. The results of the fitting or the inverse CPA are $\phi_c = 0.1$, $\alpha_s = 1$, and $\alpha_c = 0.004$.

Next, we use the estimated parameters in the forward CPA scheme to predict the frequency- and temperature-dependent shear modulus G of the Uvalde rock. The results are compared with measurements in Figure 3.6. We observe very good agreement between the CPA predictions (symbols) and the laboratory data (lines). The only deviation larger than the measurement error (approximately ± 2.09 GPa; see Behura et al., 2007) is observed at high frequencies for $30°\,\mathrm{C}$.

We also compute the shear quality factor Q (inversely proportional to the attenuation coefficient) from the predicted complex effective shear modulus of the rock. Figure 3.7b shows Q predicted by CPA. The general trend of estimated attenuation is similar to the measured one (Figure 3.7a). However, the measured Q exhibits more significant variation with frequency.

3.5 DISCUSSION

The method described in this chapter as well as other methods based on effective-medium theories are based on analogy between elasticity and viscoelasticity. This analogy is limited to sufficiently low frequencies such that the inertial terms in the equations of viscoelasticity are small and can be neglected (Hashin, 1970). This limitation is expected to be satisfied at seismic frequencies but may no longer be valid at higher frequencies where effects of squirt may become important (Leurer and Dvorkin, 2006).

In this chapter, we have described the CPA fluid substitution workflow assuming a single aspect ratio. One can use a single aspect ratio when the range of pore shapes does not vary significantly. This might be the case when compliant grain-to-grain contacts or intragranular porosity does not significantly contribute to overall rock stiffness-for instance, well consolidated rocks with welded grains or at

high effective pressure when compliant pores are closed. However in most sedimentary rocks, compliant pores (grain-to-grain contacts) with low aspect ratio contribute to the total porosity and are responsible for the stress dependency of elastic properties. When compliant pores are present in the rock matrix, introducing a second pore aspect ratio into the scheme becomes important.

The present work assumes that the porosity and geometry of the pore space of the rock matrix are the same for dry and oil-saturated rock, regardless of the oil rheology. We also assume that oil composition does not vary with temperature. These conditions may be violated in field and laboratory studies (Behura et al., 2007; Han et al., 2007a). Note that we do not examine the pressure and gas effect on moduli/velocities, which might be important in the recovery process.

3.6 CHAPTER CONCLUSIONS

We have used a self-consistent mixing method known as coherent potential approximation (CPA) as an alternative fluid substitution scheme for rocks saturated with viscoelastic fluids. First, CPA equations were inverted to obtain the effective aspect ratio of a rock from dry modulus. Then forward CPA with a temperature- and frequency-dependent shear modulus of viscoelastic pore fill was used to obtain saturated moduli.

We tested CPA estimates of effective bulk moduli of a dry and a Newtonian fluid saturated rock against analytical solutions. CPA predictions satisfy the Hashin-Shtrikman bounds and are approximately consistent with Gassmann's equations and the Krief et al. (1990) model.

A comparison with laboratory measurements revealed that CPA with a single aspect ratio is not adequate in predicting the frequency and temperature dependency of the effective shear modulus of the Uvalde heavy-oil rock.

We modified the scheme to account for the binary structure of the pore space. Inverted CPA was used to estimate three unknown parameters: compliant porosity and aspect ratios of stiff and compliant pores from the laboratory measured effective dry and saturated shear moduli at a single temperature and at two frequencies. In this

case, CPA reproduced frequency- and temperature-dependent behaviour of the shear modulus and attenuation of Uvalde heavy-oil rock, proven by good agreement with laboratory data. This confirms that the proposed scheme provides realistic estimates of the properties of heavy-oil rocks and can be used as an approximate fluid substitution approach for rocks saturated with viscoelastic fluids.

CHAPTER 4 – BOUNDS FOR VISCOELASTIC PROPERTIES OF HEAVY-OIL ROCKS

4.1 BACKGROUND

As mentioned in Chapter 3, heavy oils exhibit viscoelastic behaviour which is strongly frequency- and temperature- dependent. One result of viscoelastic rheology of heavy oils is that shear velocity in rocks in the seismic frequency band would significantly differ from that in the sonic logging-frequency range and the ultrasonic band. Therefore, the most common poroelastic theories of Gassmann (1951) and Biot (1956) cannot be applied to heavy-oil rocks.

Accurate laboratory data are important for establishing the right model. However, laboratory measurements of velocity dispersion are rather difficult and require development of special measurement techniques (Han, 2007a; Han, 2007b). To date, few laboratory studies have been published in the literature (Nur et al., 1984; Batzle et al., 2006; Behura et al., 2007; Han et al., 2008). While the measurements provide physical understanding of complex properties of heavy oil, their accuracy can be affected by different sources of errors such as poor quality of P- and especially S-wave signals, inadequate temperature and pore pressure control, difficulties in preserving integrity of a heavy oil sample, etc.

Rigorous bounding methods could provide a benchmark for testing laboratory measurements and results of modelling. They can also be used as an indicator as to whether the viscoelastic response of a given composite is extreme in the sense of being close to the edge of the bound. The best elastic bounds giving the narrowest range without specifying anything about the geometries of the constituents are Hashin-Shtrikman (HS) bounds (Hashin and Shtrikman, 1963). These bounds are constrained by requirement of isotropy, and thus correspond to realistic geometrical structures of rocks. It is known that the correspondence principle between elasticity and viscoelasticity can be used to describe the linear response of viscoelastic

composites at sufficiently low frequencies of oscillation. This means that HS bounds can be applied to solid/viscoelastic fluid mixtures. However in this case, the HS bounds become complex and are not longer rigorous as the notion of a value lying between two bounds is unidentified for complex numbers. HS bounds could provide rigorous realizable estimates only for the limiting cases of low temperature (elastic solid pore fill) and high temperature (Newtonian fluid pore fill). For the viscoelasticity problem, the set of possible effective moduli should fill a region in the complex plane and bounds should be represented as closed curves.

In this chapter, we apply rigorous bounds (Milton and Berryman, 1997) specifically designed for two-phase viscoelastic composites to the complex shear modulus measured on Uvalde heavy-oil rock sample (Behura et al., 2007). We also apply the bounds to the results of CPA modelling of elastic properties described in the previous chapter. We restrict our analysis to shear properties only because they are more sensitive to temperature changes in reservoirs than bulk properties.

4.2 RIGOROUS VISCOELASTIC BOUNDS

Milton and Berryman (1997) extended HS bounds for the effective shear-modulus to viscoelasticity using variational principles (for derivation details and the algorithm see Milton and Berryman, 1997; Gibiansky and Milton, 1993). They considered the dynamic response of statistically isotropic three dimensional composites with two viscoelastic isotropic phases mixed in fixed proportions in the quasi-static regime or at frequencies where the wavelength of a passing wave is much larger than the inhomogeneities (inclusions). The bounding regions in a complex plane are composed by arcs of circles containing four points related to the bulk and shear moduli of the constituents. The resulting bounds form a lens-shaped region obtained by taking the intersection of all such arcs.

Similarly to HS bounds, the viscoelastic bounds are independent of rock microstructure. The only input parameters needed to construct the bounding curves are the constituent bulk and shear moduli and the volume fractions of the constituents. The method is relatively easy to apply in practice due to simplified

parameterization used in the derivation. On the other hand, these simplifications could make the resulting bounds less tight than if extracted from the more general theory. Importantly, the points which correspond to HS bounds on the shear modulus always lie inside or on the boundary of the bounding region. In the limiting case, when all the constituent moduli are real the viscoelastic bounds reduce precisely to HS bounds.

4.3 APPLICATION OF VISCOELASTIC BOUNDS

We apply the viscoelastic bounds to the shear properties of Uvalde heavy-oil rock. Measurements carried on an Uvalde heavy-oil rock sample and the extracted oil were made in the linear viscoelastic regime. As it was pointed out by Behura et al. (2007), strain amplitude lying within this linear region was selected for conducting all temperature-frequency measurements. It is important to note that the strain limit for the linear behaviour varies from one rock or material to another. The same strains ($6\cdot10^{-5}$ - $8\cdot10^{-5}$) were used for testing heavy-oil rocks and the extracted oil. Note that the used strains are more than one order larger than the strains encountered in exploration seismology. This might result in laboratory measured properties different from seismic ones at the same frequency range.

In chapter 3, we use self-consistent effective medium theory CPA (Berryman, 1980b) as an alternative fluid substitution technique to predict the shear properties of Uvalde heavy-oil rock. The results of modelling are compared with measurements in Figure 3.6. CPA predictions and laboratory data are in a very good agreement with the only deviation larger than the measurement error (approximately ± 2.09 GPa) observed at high frequencies for $30°$ C. In order to understand this discrepancy, we use the viscoelastic bounds for testing the results of modelling and laboratory data.

We calculate the bounds for the range of frequencies and temperatures. As input parameters we use the properties of calcite (see chapter 3) and frequency- and temperature-dependent shear properties of heavy oil. Unfortunately, measurements of the bulk modulus of heavy oil K_f are not available. Therefore, we keep K_f constant

[a]

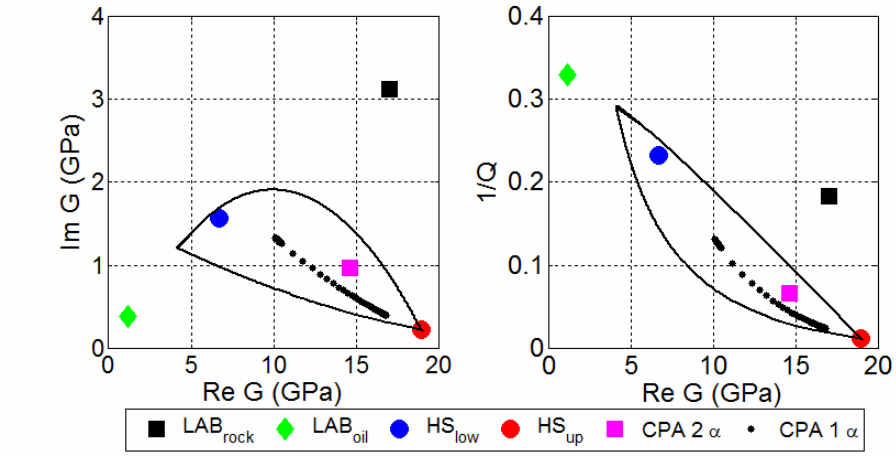

[b]

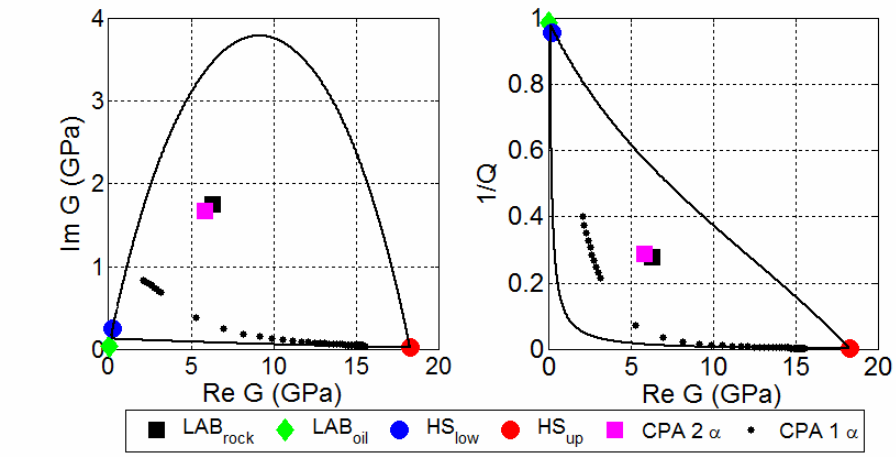

Figure 4.1 Viscoelastic bounds (black lines) for the effective shear modulus G (left panels) and inverse quality factor $1/Q$ (right panels) of Uvalde heavy-oil rock: (a) $T = 30°$ C and $f = 79$ Hz, (b) $T = 70°$ C and $f = 40$ Hz. CPA predictions of G (magenta squares) are compared to laboratory data (black squares). Also shown: CPA estimates of G for a range of aspect ratios (black dots), HS lower (blue circles) and upper (red circles) bounds, and measured G_f of heavy oil (green diamonds).

($K_f = 3$ GPa). We believe that this will not significantly affect the results because K_f is less sensitive to frequency and temperature changes than G_f. Figure 4.1a shows the bounding curves calculated for the saturated rock shear modulus G and inverse quality factor Q^{-1} at the temperature ($T = 30°\,\mathrm{C}$) and frequency ($f = 79\,\mathrm{Hz}$) of the largest mismatch between CPA estimates and laboratory data, when the oil inside the rock is close to a solid state ($G_f = 1.1 + 0.4\mathrm{i}$ GPa). Note that the bounds are quite narrow for the imaginary part of G (loss modulus) responsible for the energy dissipation. This also applies to the inverse quality factor. This behaviour of bounds is physically plausible as the heavy oil in these temperature and frequency conditions is nearly a solid. We can see that CPA estimates lie within the bounds, whereas measured G lies outside. This suggests that the mismatch between the predictions and laboratory data is caused by measurement errors.

When temperature increases ($T = 70°\,\mathrm{C}$) and frequency becomes lower ($f = 40\,\mathrm{Hz}$), the bounding curves become wider (Figure 4.1b). To construct the bounds for this case, we use the measured oil shear modulus $G_f = 0.03 + 0.03\mathrm{i}$ GPa. We can see that CPA estimates and laboratory data agree very well and are contained within the bounds.

As a test, we also plot CPA estimates for aspect ratios ranging from 0 to 1 (black dots), which represent different pore geometries. As expected, all CPA estimates lie within the bounds.

4.4 CHAPTER CONCLUSIONS

We have demonstrated that viscoelastic bounds of Milton and Berryman (1997) for the effective shear modulus of a two phase three-dimensional isotropic composite can be used as rigorous bounds for heavy-oil rocks. The viscoelastic bounds provide an effective tool for testing laboratory measurements and theoretical predictions for heavy-oil rocks.

It is important to note that these bounds are quasi-static and are designed to work at frequencies where the wavelength is much larger than the inhomogeneities.

Simplified parameterization used in the derivation can result in wider bounds. Alternatively, more restrictive bounds developed for a two-dimensional composite (Gibiansky et. al, 1999) can also be applied to rocks saturated with viscoelastic fluids.

CHAPTER 5 – A NEW SQUIRT MODEL FOR DISPERSION AND ATTENUATION IN FLUID-SATURATED GRANULAR ROCKS

5.1 BACKGROUND

A major cause of elastic wave attenuation in fluid saturated rocks is the flow of the pore fluid induced by the passing wave. When an elastic wave propagates through a fluid-saturated medium, it creates local pressure gradients within the fluid phase, resulting in fluid flow and corresponding internal friction until the pore pressure is equilibrated. The fluid flow can take place on various length scales.

Flow between mesoscopic (larger than the pore size but smaller than wavelength) patches of rock with different stiffness due to rock heterogeneity (White et al., 1975; Pride et al., 2003) or spatial variations in fluid saturation (White, 1975; Gist, 1994; Toms et al., 2007) is believed to be significant at seismic frequencies. At sonic and ultrasonic frequencies attenuation appears to be dominated by the local (pore-scale) flow between pores of different shapes and orientations (Mavko and Nur, 1975; Mavko and Nur, 1979; Jones, 1986). Mesoscopic flow can be treated using all the machinery of Biot's theory of poroelasticity (Biot, 1956a; Biot, 1956b; Biot, 1962; Bourbié et al., 1987) with spatially varying coefficients (Dutta and Ode, 1979a; Dutta and Ode, 1979b; Lopatnikov and Gurevich, 1988; Lopatnikov et al., 1990; Auriault and Boutin, 1994; Gurevich and Lopatnikov, 1995; Pride et al., 2004; Müller and Gurevich, 2005; Johnson, 2001).

Modelling local flow, also known as squirt, cannot be done in a similar manner, as local flow depends on variety of parameters describing pore shapes and orientations. Most theoretical models of squirt-flow attenuation are based on the analysis of aspect ratio distributions (Mavko and Nur, 1979; O'Connell and Budiansky, 1977; Palmer and Traviolia, 1980); a comprehensive review of these earlier studies is by Jones (1986). An alternative approach is based on the recognition

that the pore space of many rocks has a binary structure (Walsh, 1965; Mavko and Jizba, 1991; Shapiro, 2003): relatively stiff pores, which form the majority of the pore space, and relatively compliant (or soft) pores, which are responsible for the pressure dependency of the elastic moduli (Murphy et al., 1986; Dvorkin et al., 1995; Chapman et al., 2002). In particular, Dvorkin et al. (1995) model a rock as a granular aggregate in which the grains themselves are assumed porous. Inter-granular pores are stiff, while the intra-granular micro-pores are soft. This model was later reformulated and refined by Pride et al. (2004). The advantage of the porous grain model, particularly in the formulation of Pride et al. (2004), over all other squirt models, is in the fact that the medium can be treated as poroelastic on the sub-pore scale, and thus is amenable to treatment using Biot's equations of poroelasticity with spatially varying coefficients (Pride and Berryman, 2003). This model is also consistent with Mavko and Jizba (1991) predictions for the high-frequency limit of elastic moduli, which are known to be in good agreement with laboratory measurements (Mavko and Jizba, 1994; Wulff and Burkhardt, 1997; Endres and Knight, 1997). However, the concept of porous grains is somewhat abstract, and interpretation of parameters of this imaginary micro-porous grain in terms of rock properties is difficult. Furthermore, application of Biot's theory to micro-porous grains assumes that compliant pores are small compared to the grain size; this may not be the case for real rocks.

An appealing alternative is the approach of Murphy et al. (1986), who consider compliant pores as gaps at contacts between adjacent grains, see also Mayr and Burkhardt (2006). However, the model of Murphy et al. is not consistent with the well established high-frequency predictions of Mavko and Jizba (1991); in fact, its high-frequency prediction for the elastic moduli is unrealistically high. This inconsistency stems from the fact that the particular formulation of Murphy et al. (1986) is developed within the framework of Hertz-Mindlin grain contact theory (Digby, 1982; Winkler, 1983) where grains themselves are assumed rigid and the compliance of the rock is caused solely by weak grain contacts. In the high-frequency limit, fluid pressure cannot relax between the inter-granular gap and the

surrounding (stiff) pore, making its compliance vanishingly small and rock unrealistically stiff.

In this chapter, we propose a new model of squirt-flow attenuation which uses a pressure relaxation approach of Murphy et al. (1986) in conjunction with the discontinuity tensor formulation of Sayers and Kachanov (1995). The resulting model is consistent with the Gassmann's (1951) and Mavko-Jizba equations at low and high frequencies, respectively, and with the piezosensitivity model of Shapiro (2003). It can also naturally be incorporated into Biot's theory of poroelasticity to obtain velocity and attenuation prediction in a broad frequency range.

5.2 ASSUMPTIONS

The aim of this chapter is to derive expressions for frequency-dependent moduli of a rock when it is fully saturated by a single fluid with a bulk modulus K_f and dynamic viscosity η. Following Walsh (1965), Mavko and Jizba (1991) and Shapiro (2003), we assume that the pore space of the rock consists of stiff and compliant pores, which form fully interconnected pore space. We also assume that the dry rock frame (skeleton) is homogeneous, that is, consists of a single isotropic mineral with bulk modulus K_g and shear modulus μ_g. The frame is also assumed isotropic on both micro-scale (pore scale) and macro-scale (wavelength scale), and is characterised by stiff porosity ϕ_s, compliant porosity $\phi_c \ll \phi_s$, total porosity $\phi = \phi_s + \phi_c \approx \phi_s$, permeability κ, and dry bulk and shear moduli K_{dry} and μ_{dry} at a given confining pressure P. At pressure $P > P_h$, dry rock contains stiff pores only, and is a linearly elastic solid with a bulk modulus K_h. The frequency dependency (dispersion) in our rock can be caused by two principal mechanisms: (1) global flow dispersion due to the flow of fluid relative to the solid frame caused by the pressure gradients between peaks and troughs of the wave and (2) squirt flow between compliant pores and stiff pores. In this chapter, we are principally concerned with squirt flow. Therefore, to ensure that Biot's dispersion is negligible, we will, for the

time being, assume that the characteristic frequency f_{Biot} of Biot's dispersion is much higher than both the squirt characteristic frequency f_c, and the frequency of the propagating wave f. Both of these conditions will later be lifted.

5.3 LOW-FREQUENCY (RELAXED) MODULI

In the low-frequency limit, the bulk and shear moduli of our fluid-saturated rock are given by Gassmann's equations (Gassmann, 1951; White, 1983)

$$\frac{1}{K_{low}} = \frac{1}{K_g} + \frac{\phi\left(\frac{1}{K_f} - \frac{1}{K_g}\right)}{1 + \phi\left(\frac{1}{K_f} - \frac{1}{K_g}\right) \Big/ \left(\frac{1}{K_{dry}} - \frac{1}{K_g}\right)}, \tag{5.1}$$

and

$$\mu_{low} = \mu_{dry}. \tag{5.2}$$

Gassmann's equations 5.1 and 5.2 are valid when $f \ll f_c$. Physically, this means that the wave frequency is sufficiently low, so that fluid pressure has enough time to equilibrate between stiff and compliant pores during half wave cycle. Thus the moduli given by Gassmann's equations 5.1 and 5.2 can be called relaxed moduli.

5.4 HIGH-FREQUENCY (UNRELAXED) MODULI

When the frequency is higher than the squirt characteristic frequency, $f \gg f_c$, the fluid pressure doesn't have enough time to equilibrate between stiff and compliant pores during half wave cycle (so called unrelaxed state). Then, compliant pores at the grain contacts are effectively isolated from the stiff pores and hence become stiffer with respect to normal (but not tangential) deformation. To quantify this effect, Mavko and Jizba (1991) considered so called modified frame: the rock in which only compliant pores are filled with the fluid, while stiff pores are empty, and

showed that unrelaxed (high frequency) bulk and shear moduli K_{uf} and μ_{uf} of this modified frame are given by

$$\frac{1}{K_{uf}(P)} \approx \frac{1}{K_h} + \left(\frac{1}{K_f} - \frac{1}{K_g}\right)\phi_c(P) \tag{5.3}$$

and

$$\frac{1}{\mu_{uf}(P)} \approx \frac{1}{\mu_{dry}(P)} - \frac{4}{15}\left(\frac{1}{K_{dry}(P)} - \frac{1}{K_{uf}(P)}\right), \tag{5.4}$$

where K_h is the dry bulk modulus of a hypothetical rock without the compliant porosity; see also Berryman (2007). Note that for most rocks, $\phi_c(P)$ is on the order of 10^{-3} or smaller (Mavko and Jizba, 1991; Shapiro, 2003). For typical reservoir liquids (not gases!), the bulk modulus K_f is on the order 1/10 of the dry rock modulus and much smaller than the mineral modulus K_g. Therefore, the second term in the right hand side of equation 5.3 is at most on the order of 0.01 of the first term and hence is negligible for most liquids. This means that the bulk modulus of the modified frame is almost independent of the pressure. However, the shear modulus (and hence, both compressional and shear velocities) still depends on pressure through the pressure dependency of the dry bulk and shear moduli $K_{dry}(P)$ and $\mu_{dry}(P)$.

Equation 5.3 for the unrelaxed bulk modulus of the modified frame was derived by Mavko and Jizba (1991) as a first-order expansion in the powers of complaint porosity, and implies that $\phi_c\left(K_f^{-1} - K_g^{-1}\right) \ll K_h^{-1}$. Indeed, as discussed above, if the saturating fluid is liquid, this condition is usually satisfied. However, as will be seen later in our derivation, this condition is too restrictive for our purposes. Here we wish to obtain a more general expression for the unrelaxed frame moduli (without any restriction on the fluid compressibility) K_{uf} and μ_{uf} which represent the moduli of the rock whose interconnected stiff pores are drained (or dry) but the isolated soft pores can be either dry or filled with a fluid.

5.4.1 *ELASTIC MODULI IN TERMS OF DISPLACEMENT DISCONTINUITIES*

At a pressure $P < P_h$ the rock is weakened by the presence of compliant porosity. We represent the effect of compliant porosity on elastic properties by a system of isotropically distributed displacement discontinuities at grain boundaries. The effect of such discontinuities on elastic compliance of a rock S_{ijkl} can be quantified using the formulation of Sayers and Kachanov (1995)

$$S_{ijkl} = S^0_{ijkl} + \frac{1}{4}\left(\delta_{ik}\alpha_{jl} + \delta_{il}\alpha_{jk} + \delta_{jk}\alpha_{il} + \delta_{jl}\alpha_{ik}\right) + \beta_{ijkl}. \tag{5.5}$$

Here, α_{ij} and β_{ijkl} are second and fourth-rank tensors defined by

$$\alpha_{ij} = \frac{1}{V}\sum_r B_T^{(r)} n_i^{(r)} n_j^{(r)} A^{(r)}, \tag{5.6}$$

$$\beta_{ijkl} = \frac{1}{V}\sum_r \left(B_N^{(r)} - B_T^{(r)}\right) n_i^{(r)} n_j^{(r)} n_k^{(r)} n_l^{(r)} A^{(r)}, \tag{5.7}$$

where $B_N^{(r)}$ and $B_T^{(r)}$ are the normal and shear compliance of the r th discontinuity in volume V, $n_i^{(r)}$ is i th component of the normal to the discontinuity, and $A^{(r)}$ is the area of the discontinuity. $B_N^{(r)}$ characterizes the displacement jump normal to the discontinuity produced by a normal traction, while $B_T^{(r)}$ characterizes the shear displacement jump produced by a shear traction. The discontinuities are assumed to be rotationally symmetric, that is, $B_T^{(r)}$ is assumed to be independent of the direction of the shear traction within the plane of the discontinuity.

Sayers and Han (2002) showed that in the case of an isotropic distribution of discontinuities in an isotropic rock, equation 5.5 gives the following expressions for the isotropic bulk and shear compliances of the rock

$$\frac{1}{K_{uf}} = \frac{1}{K_h} + 3\alpha + 5\beta, \tag{5.8}$$

$$\frac{1}{\mu_{uf}} = \frac{1}{\mu_h} + 2\alpha + \frac{4}{3}\beta, \tag{5.9}$$

where $\alpha = \alpha_{11} = \alpha_{22} = \alpha_{33}$ and $\beta = \beta_{1111} = \beta_{2222} = \beta_{3333}$ are diagonal elements of the respective tensors. These tensor elements may be computed for an isotropic distribution of discontinuities by replacing the sums in equations 5.6 and 5.7 with integrals over all orientations and taking volume V to be a sphere of radius R,

$$\alpha = \alpha_{33} = \frac{1}{V}\int_S B_T \cos^2\theta \; dS = \frac{A}{3V} B_T, \tag{5.10}$$

$$\beta = \beta_{3333} = \frac{1}{V}\int_{S_v} \left(B_N - B_T\right)\cos^4\theta \; dS = \frac{A}{5V}\left(B_N - B_T\right) \tag{5.11}$$

where B_N and B_T are the normal and shear compliance of each individual plane discontinuity, S_v is the surface of all discontinuities in volume V, A is the total area of S_v and θ is angle between the normal to the surface area dS and the x_3 axis. Substituting these expressions into equations 5.8 and 5.9 gives

$$\frac{1}{K_{uf}} = \frac{1}{K_h} + sB_N, \tag{5.12}$$

$$\frac{1}{\mu_{uf}} = \frac{1}{\mu_h} + \frac{4}{15} sB_N + \frac{2}{5} sB_T, \tag{5.13}$$

where $s = A/V$ is volume to surface ratio of all discontinuities.

5.4.2 *EFFECT OF FLUID*

Equations 5.12 and 5.13 are valid for a rock in which compliant porosity is either dry of fluid saturated. For dry rocks we have

$$\frac{1}{K_{dry}} = \frac{1}{K_h} + sB_N^{dry}, \tag{5.14}$$

$$\frac{1}{\mu_{dry}} = \frac{1}{\mu_h} + \frac{4}{15} sB_N^{dry} + \frac{2}{5} sB_T^{dry}, \tag{5.15}$$

where B_N^{dry} and B_T^{dry} are the dry normal and shear compliances of an individual discontinuity (compliant pore). In turn, unrelaxed moduli of a rock in which compliant pores are fluid-filled can be expressed by equations 5.12 and 5.13, with B_N and B_T representing saturated fracture compliances. Because in Newtonian fluids the shear stresses are negligible (up to the characteristic frequency of viscous shear relaxation, [Mavko and Nur, 1975]), shear compliance B_T is independent of the fluid fill, so that $B_T = B_T^{dry}$ dry. Subtracting equation 5.12 from equation 5.14 and equation 5.13 from equation 5.15 then gives

$$\frac{1}{K_{dry}} - \frac{1}{K_{uf}} = s\left(B_N^{dry} - B_N\right), \tag{5.16}$$

$$\frac{1}{\mu_{dry}} - \frac{1}{\mu_{uf}} = \frac{4}{15} s\left(B_N^{dry} - B_N\right). \tag{5.17}$$

Combining these two equations we obtain equation 5.4, the original Mavko-Jizba equation.

To establish the dependency of K_{uf} and μ_{uf} on the fluid modulus, we need to know the fluid dependency of normal compliance B_N, which can be derived in a variety of ways. This dependency can be derived in a variety of ways. Perhaps the simplest and most general way is to use anisotropic Gassmann's equations (Gassmann, 1951; Brown and Korringa, 1975). The simplest, most general way is to use anisotropic Gassmann's equations (Gassmann, 1951; Brown and Korringa, 1975). In general, Gassmann's equations are not valid for an isotropic distribution of isolated compliant pores because pressure in individual pores differs depending on pore orientation. However, because all compliant pores are isolated, sB_N can be represented as a sum over all orientations of all soft pores aligned perpendicular to every direction:

$$sB_N = \int_{4\pi} B_N \frac{ds}{d\Omega} d\Omega, \tag{5.18}$$

where $d\Omega$ is the solid angle element around direction, and $ds/d\Omega$ is the total area of all soft pores normal to that direction. In equation 5.18, $Z_N = B_N ds/d\Omega$ is normal excess compliance caused by all soft pores aligned normal to any particular direction. For a dilute distribution of aligned compliant pores of the same shape, Gassmann's theory is approximately valid because all these pores will have approximately the same pressure induced by uniform deformation, even if they are isolated. Note that dilute concentration already is required by the use of noninteractive approximation of Sayers and Kachanov, equations 5.5–5.7. The anisotropic Gassmann's equation for aligned pores gives (Gurevich, 2003)

$$Z_N = \frac{Z_N^{dry}}{1+\dfrac{K_f Z_N^{dry}}{\phi_{cx}\left(1-\dfrac{K_f}{K_g}\right)}} = \frac{Z_N^{dry}}{1+\dfrac{Z_N^{dry}}{\phi_{cx}\left(\dfrac{1}{K_f}-\dfrac{1}{K_g}\right)}}, \tag{5.19}$$

where $\phi_{cx} = d\phi_c/d\Omega$ is the specific volume of compliant pores parallel to the plane normal to x axis (or any other single direction) and $Z_N^{dry} = \left(ds/d\Omega\right)B_N^{dry}$. Substituting these expressions into equation 5.19 gives

$$Z_N = \frac{\dfrac{ds}{d\Omega}B_N^{dry}}{1+\dfrac{\dfrac{ds}{d\Omega}B_N^{dry}}{\dfrac{d\phi_c}{d\Omega}\left(\dfrac{1}{K_f}-\dfrac{1}{K_g}\right)}}. \tag{5.20}$$

Noting that

$$\frac{\dfrac{ds}{d\Omega}}{\dfrac{d\phi_c}{d\Omega}} = \frac{s}{\phi_c}, \tag{5.21}$$

we obtain

$$Z_N = \frac{\frac{ds}{d\Omega} B_N^{dry}}{1 + \frac{sB_N^{dry}}{\phi_c \left(\frac{1}{K_f} - \frac{1}{K_g} \right)}}, \tag{5.22}$$

and thus

$$B_N = \frac{B_N^{dry}}{1 + \frac{sB_N^{dry}}{\phi_c \left(\frac{1}{K_f} - \frac{1}{K_g} \right)}}. \tag{5.23}$$

Equation 5.23 can also be derived from the first order (dilute) approximation for ellipsoidal cracks based on the Eshelby theorem (Küster and Toksöz, 1974; Berryman, 1980b; Thomsen, 1995). However, the derivation from anisotropic Gassmann's equation (Gurevich, 2003; Berryman, 2007) appears to be slightly more general, in that it does not assume any particular shape of the compliant pores in the plane of the discontinuity. All compliant pores must have approximately the same shape, though, or the pressure induced will be different! Also note that equation 5.23 differs from a similar expression in the theory of penny-shaped cracks (Hudson, 1981) by the presence of the small $1/K_g$ term. Hudson et al. (2001) discusses this minor discrepancy.

Substituting B_N as given by equation 5.23 into equation 5.12 yields the expression for the unrelaxed drained frame bulk modulus

$$\frac{1}{K_{uf}} = \frac{1}{K_h} + \frac{sB_N^{dry}}{1 + \frac{sB_N^{dry}}{\phi_c \left(\frac{1}{K_f} - \frac{1}{K_g} \right)}}. \tag{5.24}$$

The dry compliance can be obtained from the dry modulus using equation 5.14

$$sB_N^{dry} = \frac{1}{K_{dry}} - \frac{1}{K_h}, \tag{5.25}$$

which gives

$$\frac{1}{K_{uf}(P)} = \frac{1}{K_h} + \frac{1}{\dfrac{1}{\dfrac{1}{K_{dry}(P)} - \dfrac{1}{K_h}} + \dfrac{1}{\left(\dfrac{1}{K_f} - \dfrac{1}{K_g}\right)\phi_c(P)}}, \tag{5.26}$$

where as before, $K_h = K_{dry}(P_h)$ is the dry bulk modulus at the highest pressure available. Equation 5.26 is the main result of this section. Note that ϕ_c is usually very small (less than 1%, see Shapiro (2003)). Therefore, when the fluid is liquid, the term $\left(K_{dry}^{-1} - K_h^{-1}\right)^{-1}$ can be neglected compared to the term $\phi_c\left(K_f^{-1} - K_g^{-1}\right)^{-1}$ and equation 5.26 reduces to equation 5.3, the first of the Mavko-Jizba equations. However, unlike equation 5.3, equation 5.26 also is valid when the saturating fluid is gas. For a dry rock, $\phi_c\left(K_f^{-1} - K_g^{-1}\right)^{-1}$ vanishes and K_{uf} reduces to the dry modulus K_{dry}, as it should. Note that the second of Mavko-Jizba equations, equation 5.4, remains unchanged.

As mentioned earlier, the Mavko-Jizba equations are particularly useful because they are based entirely on measurable quantities and have no adjustable parameters. The same is true for more general equations 5.26 and 5.4. Indeed, compared with equation 5.3, the only new quantity in equation 5.26 is K_{dry}, which must be known as a function of pressure. However K_{dry} is already required by equation 5.4. Therefore, the combined equations 5.26 and 5.4 and the original Mavko-Jizba equations require knowledge of essentially the same information.

The unrelaxed frame moduli K_{uf} and μ_{uf} are obtained assuming that the stiff pores are dry. The saturated moduli then can be computed using Gassmann's and/or Biot's equations. Specifically, the saturated (undrained) bulk modulus can be obtained by substituting K_{uf} for the frame modulus in Gassmann's equation, while the saturated shear modulus will still be μ_{uf} :

$$\frac{1}{K_{high}(P)} = \frac{1}{K_g} + \frac{\phi_s\left(\frac{1}{K_f} - \frac{1}{K_g}\right)}{1 + \phi_s\left(\frac{1}{K_f} - \frac{1}{K_g}\right) \Big/ \left(\frac{1}{K_{uf}(P)} - \frac{1}{K_g}\right)}, \tag{5.27}$$

and

$$\mu_{high}(P) = \mu_{uf}(P). \tag{5.28}$$

The use of Gassmann's equations for high frequencies may raise some questions. Indeed, Gassmann's equations assume that fluid pressure is equalised within the representative volume (RV) of the pore space. Pressure equilibration can be achieved if (1) the pore space is interconnected and (2) the frequency is sufficiently low to allow enough time for pressure to equilibrate within wave's half-cycle. As previously discussed, higher frequency may prevent equilibration of pressure within half wave cycle, effectively making the pores hydraulically isolated. However, the condition of interconnected pore space is not a necessary condition for the validity of Gassmann's or Biot's equations. The key condition is the spatially uniform fluid pressure in the pores (within RV). In particular, Gassmann's equations are *exact* for a material with dilute concentration of randomly distributed isolated spherical pores, since the induced pressure is the same in all these pores (for any frequency below the characteristic frequency of scattering). Approximately, this is also true for all "equant" pores (pores with aspect ratio on the order O(1)) (Thomsen, 1985). Recently, Grechka (2009) showed numerically that Gassmann's equations are excellent approximations for isolated pores of aspect ratio larger than 0.1. Therefore, as suggested by Mavko and Jizba (1991), Gassmann's and Biot's equations are applicable to the *stiff* pores of our system, both at seismic and ultrasonic frequencies. This is also consistent with the well established observation that the squirt-flow dispersion between seismic and ultrasonic frequencies is caused mainly by compliant porosity, and is negligible at high effective stress, where compliant porosity is mostly closed and only stiff pores remain. Indeed, the characteristic frequency of squirt-flow dispersion is usually written as

$$f_c = \alpha^3 \frac{K}{\eta}, \tag{5.29}$$

where α is the mean aspect ratio of the pores, K is rock's bulk modulus (Jones, 1986). For stiff pores $\alpha = O(1)$ and thus the squirt frequency is much larger than 1 MHz even for fluids 1000 times more viscous than water.

To summarize, the high-frequency moduli of the fully saturated rock are given by Gassmann's equations 5.27 and 5.28 with the modified frame moduli given by equations 5.26 and 5.4. It should be also noted that a similar derivation of Mavko-Jizba equations was recently presented by Berryman (2007). However in Berryman's model, the rock did not contain stiff pores and therefore the parameter K_h was equal to the mineral modulus K_g.

5.4.3 EXAMPLE

To illustrate the applicability of our model, we use it to predict high-frequency unrelaxed velocities in a sample of Westerly granite (Coyner, 1984) saturated with three different fluids. Computation of unrelaxed bulk and shear moduli with equations 5.26 and 5.4 requires the knowledge of dry bulk and shear moduli $K_{dry}(P)$ and $\mu_{dry}(P)$, and of soft porosity $\phi_c(P)$ as a function of pressure P. In our calculations, the moduli $K_{dry}(P)$ and $\mu_{dry}(P)$ are obtained from measurements of dry compressional and shear velocities versus pressure at lab frequency 0.8 to 0.9 MHz. The soft porosity $\phi_c(P)$ is obtained using a recipe suggested by Mavko and Jizba (1991) as the difference between the measured total porosity $\phi(P)$ and the linear extrapolation of the pressure/porosity trend at high pressures. The Westerly granite sample has porosity of 0.7 to 0.8%, grain density of 2.64 g/cm^3, and a mineral bulk modulus of 56 GPa.

To compute the model predictions at each stress, first we calculate the unrelaxed frame bulk K_{uf} and shear μ_{uf} moduli using equations 5.26 and 5.4, assuming that only the soft pores are saturated (the stiff pores are dry). Then, to

[a]

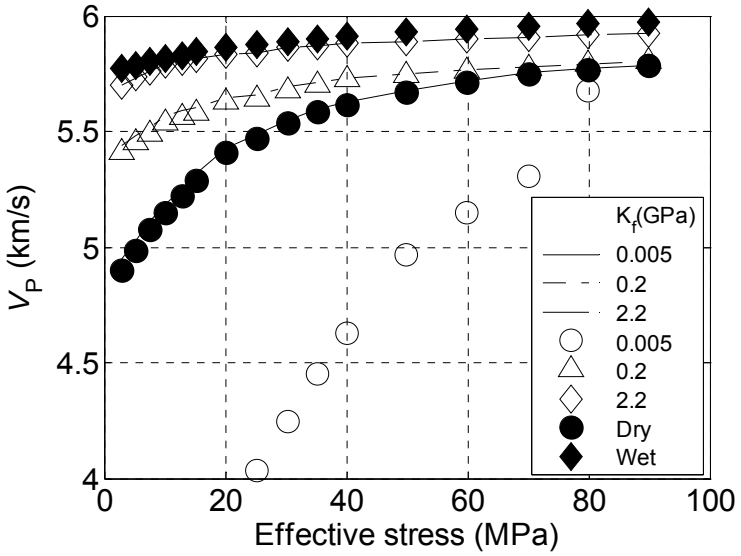

[b]

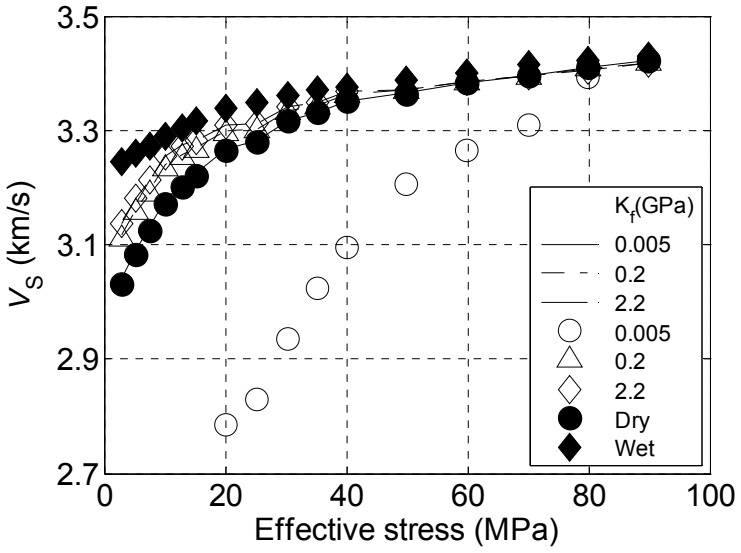

Figure 5.1 (a) Compressional and (b) shear-wave velocities in a Westerly granite sample as a function of effective stress: laboratory measurements on dry (solid circles) and water-saturated (solid diamonds) sample, predictions of the Mavko and Jizba (1991) model (open symbols), and predictions of the present model (lines) for three different fluids, with bulk moduli shown in the legend.

obtain the saturated compressional and shear velocities, K_{uf} and μ_{uf} must be substituted into Biot's dispersion equations. However, we note that for such a low-porosity rock ($\phi \approx 0.8\%$), the Biot and Gassmann predictions will be virtually identical.

Figure 5.1a,b compares Mavko-Jizba predictions (open symbols) and our model predictions (lines) of P-wave velocity versus pressure for the Westerly granite sample saturated with three different fluids having K_f ranging from 0.005 GPa to 2.2 GPa. Filled circles and diamonds indicate the dry and saturated laboratory measurements, respectively. For the liquid-saturated sample, the predictions of the Mavko-Jizba model (open diamonds) and our model (dashed lines) are identical, and they predict the measured wet velocities (filled diamonds) within 3% error. However, the two predictions differ substantially for the gas-saturated sample. In particular, for very low fluid modulus $K_f = 0.005$ GPa, our model's prediction (solid line) is very close to the dry measurements (solid circles), whereas the Mavko-Jizba model (open circles) predicts much smaller velocities. This is to be expected because for zero-fluid modulus, the Mavko-Jizba model, equation 5.3, yields zero unrelaxed bulk modulus, whereas our model, equation 5.26, yields the dry modulus. We can conclude that the new expressions are particularly convenient for computations because the same expressions can be used for dry, gas-saturated, and liquid-saturated rocks.

5.5 FREQUENCY-DEPENDENT (PARTIALLY RELAXED) MODULI

The aim of this section is to derive expressions for the moduli of the rock at intermediate frequencies, which represent some intermediate state between the low and high frequency limits.

5.5.1 MODIFIED FRAME

Since compliant porosity in rocks is usually much smaller than stiff porosity ($\phi_c << \phi_s$), we can consider stiff porosity approximately equal to total porosity

($\phi_s \approx \phi$). Therefore, saturated high-frequency moduli are given by the same Gassmann's equations 5.27 and 5.28 as the low frequency moduli (equations 5.1 and 5.2), except that for high-frequencies the dry moduli K_{dry} and μ_{dry} are replaced by the unrelaxed frame moduli K_{uf} and μ_{uf}. Furthermore, we note that the dry moduli K_{dry} and μ_{dry} can also be considered as the moduli of the modified frame (rock with empty stiff pores but fluid filled compliant pores), but in a *relaxed* state, that is, when compliant pores are in full pressure equilibrium with the stiff pores. Since in the modified frame stiff pores are empty, the pressure in compliant pores is zero. Thus, the relaxed moduli of the modified frame are equal to the rock's dry, or drained, moduli. In other words, the fully saturated (undrained) moduli of the rock in the low and high frequency limits are given by the same Gassmann's equations

$$\frac{1}{K_{sat}(P,\omega)} = \frac{1}{K_g} + \frac{\phi_s\left(\frac{1}{K_f} - \frac{1}{K_g}\right)}{1 + \phi_s\left(\frac{1}{K_f} - \frac{1}{K_g}\right) \Big/ \left(\frac{1}{K_{mf}(P,\omega)} - \frac{1}{K_g}\right)}, \tag{5.30}$$

and

$$\mu_{sat}(P,\omega) = \mu_{mf}(P,\omega), \tag{5.31}$$

where the modified frame moduli K_{mf} and μ_{mf} are to be taken at low and high frequency limits, respectively. Furthermore, it is logical to assume that moduli at the intermediate frequencies between these limits are also given by Gassmann's equations 5.30 and 5.31 with the modified K_{mf} and μ_{mf} taken at the corresponding frequency. Thus the problem of finding the frequency-dependent moduli of the fully saturated rock reduces to the problem of finding the frequency dependency of the moduli of the modified frame, where compliant pores are fluid filled and stiff pores are dry.

5.5.2 *FLUID RELAXATION IN THE AREA OF GRAIN CONTACT*

It is often the case with heterogeneity-related dispersion mechanisms that the low and high frequency limits of elastic moduli are independent of intricacies of geometry, but the shape of the frequency dependency of the moduli is defined by the particular geometrical configuration. A good example is a porous rock saturated with patches of two immiscible fluids (Johnson, 2001), where the low and high-frequency moduli are uniquely defined by the properties of the rock matrix, the properties of the two fluids, and their volume fractions. In contrast, the frequency dependency of the moduli (and attenuation) is controlled both by the size and shape of the patches.

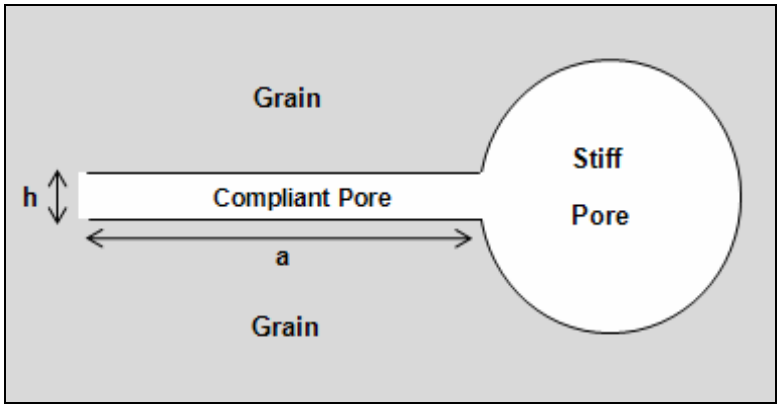

Figure 5.2. Sketch of the model configuration (Murphy et al., 1986). Soft pore forms a disc-shaped gap between two grains, and its edge opens into a toroidal stiff pore.

The squirt-flow dispersion has the same feature. The low frequency moduli are given by the exact Gassmann's equations, which involve only one explicit parameter of the pore space: total porosity. The high frequency limit (ignoring Biot's dispersion for a moment) as given by equations 5.26 and 5.4 requires, additionally, the knowledge of the compliant porosity. However, in order to model the frequency dependency of the moduli, we need to assume a particular geometrical configuration. Here we assume a particular geometry proposed by Murphy et al. (1986): a

compliant pore forms a disk-shaped gap between two adjacent grains, and its edge opens into a toroidal stiff pore (Figure 5.2). It is assumed that the gap also has asperities, and thus its stiffness is finite even when the gap is empty. However these asperities are assumed (somewhat arbitrarily) not to affect the geometry of the gap as far as the fluid movement is concerned. The gap has radius a and thickness h. The additional effective stiffness K^* of the gap due to the presence of fluid can be defined as a ratio of the force ΔF (acoustic force) exerted by the fluid onto the gap wall, to the uniaxial dynamic loading (displacement) $-\Delta h$

$$K^* = \frac{\Delta F}{-\Delta h}. \tag{5.32}$$

The force is essentially the integral of pressure over the surface S_g of the gap,

$$\Delta F = \int_{S_g} p(r) dS. \tag{5.33}$$

For sinusoidal loading $\Delta h \exp(i\omega t)$ with frequency $\omega = 2\pi f$, fluid pressure p can be obtained as a solution of the ordinary differential equation (Abramowitz and Stegun, 1964)

$$\frac{d^2 p}{dr^2} + \frac{1}{r}\frac{dp}{dr} + k^2 p = C, \tag{5.34}$$

where r is the radial coordinate,

$$k^2 = \frac{-i\omega h_0 D}{K_f}, \tag{5.35}$$

is the wavenumber of the pressure diffusion wave in the gap, $D = 12\eta / h_0^3$ is the viscous resistance and $C = i\omega D \Delta h$.

These equations have been presented by Murphy et al. (1986) in order to obtain an undrained saturated modulus. Thus, their boundary condition at the edge of the gap is the equation of fluid mass conservation between the gap and the annular pore. On the other hand, in the modified frame, only the inter-granular gap is fully

filled with the fluid, whereas the stiff (toroidal) pore is drained. Thus, in contrast to Murphy et al. (1986), our boundary condition (for equation 5.34) at the edge of the gap ($r = a$) is that the fluid pressure p is zero:

$$p\big|_{r=a} = 0\,. \tag{5.36}$$

Equation 5.34 is an inhomogeneous Bessel equation with a constant right-hand side. Substitution

$$p = q + \frac{C}{k^2}\,; \tag{5.37}$$

gives

$$\frac{d^2q}{dr^2} + \frac{1}{r}\frac{dq}{dr} + k^2 q = 0\,, \tag{5.38}$$

which is a homogeneous Bessel equation of zero order. The general solution of this equation is

$$q = C_1 J_0\left(kr\right), \tag{5.39}$$

which gives

$$p = C_1 J_0\left(kr\right) + \frac{C}{k^2}\,. \tag{5.40}$$

Substitution of this general solution into the boundary condition 5.36 gives

$$C_1 = -\frac{C}{k^2 J_0\left(ka\right)} \tag{5.41}$$

so that the pressure in the gap is given by

$$p = \frac{C}{k^2}\left[1 - \frac{J_0\left(kr\right)}{J_0\left(ka\right)}\right]. \tag{5.42}$$

Then the force ΔF is

$$\Delta F = 2\pi \int_0^a p(r) r dr = 2\pi \frac{C}{k^2} \left[\frac{a^2}{2} - \frac{1}{J_0(ka)} \int_0^a J_0(kr) r dr \right] \tag{5.43}$$

or

$$\Delta F = -\pi a^2 \left[1 - \frac{2J_1(ka)}{kaJ_0(ka)} \right] \frac{\Delta h K_f}{h_0}. \tag{5.44}$$

Substitution of this force into equation 5.32 gives the following expression for the fluid-related gap stiffness

$$K^* = \pi a^2 \left[1 - \frac{2J_1(ka)}{kaJ_0(ka)} \right] \frac{K_f}{h_0}. \tag{5.45}$$

5.5.3 *EFFECTIVE MODULUS OF PARTIALLY RELAXED FLUID*

In the low frequency limit $k \to 0$ and thus K^* vanishes. This corresponds to the fact that at the low frequencies the fluid poses no resistance to gap deformation. At sufficiently low frequencies, the pressure in the gap will be equilibrated, and thus will be zero throughout the gap. Conversely, in the limit of high frequency, equation 5.45 gives

$$K^* = \frac{\pi a^2}{h_0} K_f. \tag{5.46}$$

This is the gap resistance in the unrelaxed state, when fluid has no time to escape from the gap within the half-period of the wave. Comparison of equations 5.45 and 5.46 shows that, at any given frequency, the gap stiffness is the same as the unrelaxed stiffness computed for a modified fluid with a bulk modulus

$$K_f^*(P, \omega) = \left[1 - \frac{2J_1(ka)}{kaJ_0(ka)} \right] K_f. \tag{5.47}$$

[a]

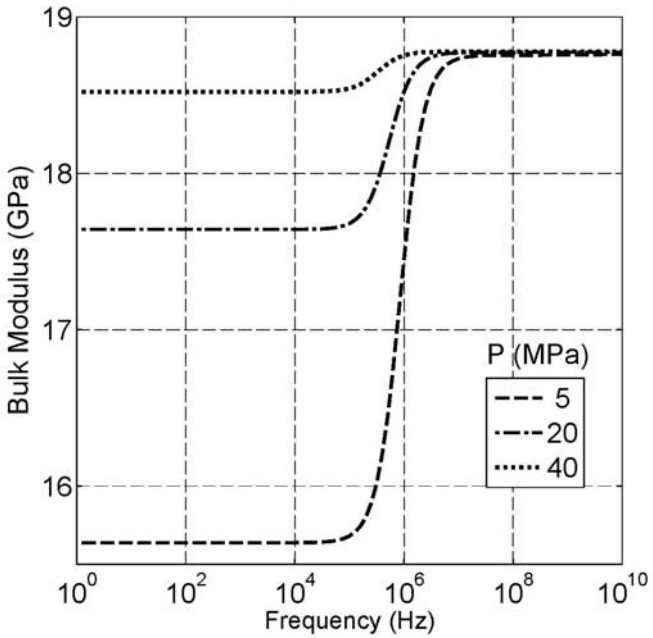

[b]

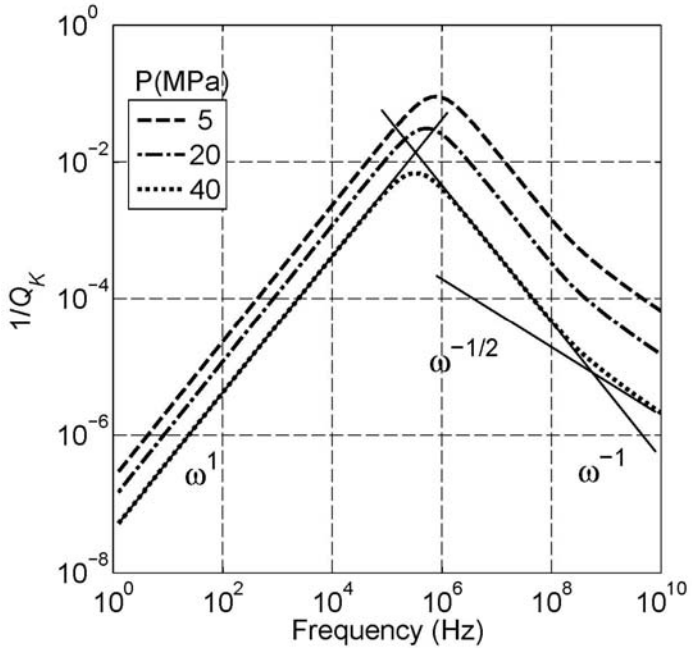

Figure 5.3. Predictions of (a) the bulk modulus (real part) and (b) attenuation for a range of frequencies and pressures (shown by different line patterns) for a water-saturated sample of Berea 5-600 sandstone. Solid lines show asymptotic frequency dependencies of attenuation: ω^1 at low frequencies , ω^{-1} at intermediate frequencies , $\omega^{-1/2}$ at high frequencies.

Substitution of K_f^* for the fluid modulus K_f in equation 5.26 gives the final expression for the partially relaxed modulus K_{mf} of the modified frame.

$$\frac{1}{K_{mf}(P,\omega)} = \frac{1}{K_h} + \frac{1}{\dfrac{1}{\dfrac{1}{K_{dry}(P)} - \dfrac{1}{K_h}} + \dfrac{1}{\left(\dfrac{1}{K_f^*(P,\omega)} - \dfrac{1}{K_g}\right)\phi_c(P)}}. \tag{5.48}$$

Then, the corresponding partially relaxed shear modulus μ_{mf} of the modified frame can be obtained by substituting K_{mf} for K_{uf} in equation 5.4

$$\frac{1}{\mu_{mf}(P,\omega)} = \frac{1}{\mu_{dry}(P)} - \frac{4}{15}\left[\frac{1}{K_{dry}(P)} - \frac{1}{K_{mf}(P,\omega)}\right]. \tag{5.49}$$

Note that the wavenumber k of the pressure wave, as given by equation 5.35, is complex and frequency dependent

$$k^2 = -\frac{12i\omega\eta}{h_0^2 K_f}, \tag{5.50}$$

and so are the effective fluid modulus K_f^* and partially relaxed frame moduli K_{mf} and μ_{mf}. This implies the presence of velocity dispersion and attenuation.

5.6 ASYMPTOTES

Frequency dependency of the partially relaxed modified frame moduli is controlled by the quantity

$$ka = \frac{1}{\alpha}\left(-\frac{3i\omega\eta}{K_f}\right)^{1/2}, \tag{5.51}$$

which depends on two new parameters: fluid viscosity η and aspect ratio of the gaps (or compliant pores) $\alpha = h_0 / 2a$. Its squared value $\Omega = |ka|^2$ is proportional to

[a]

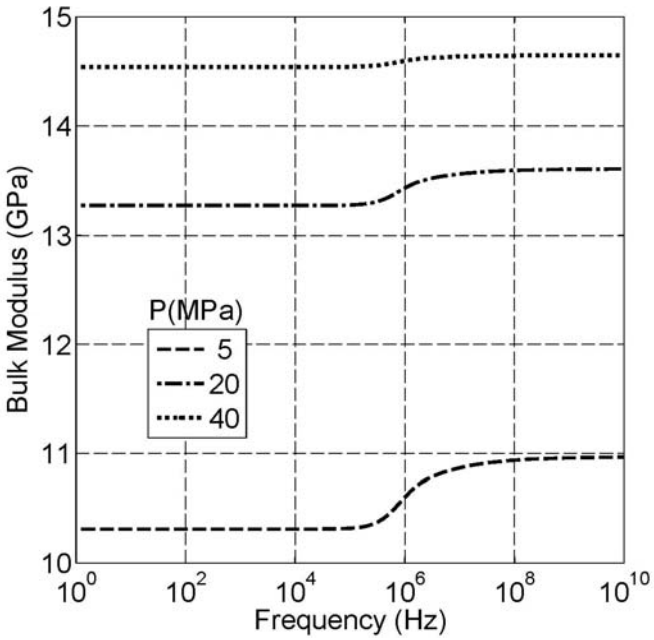

[b]

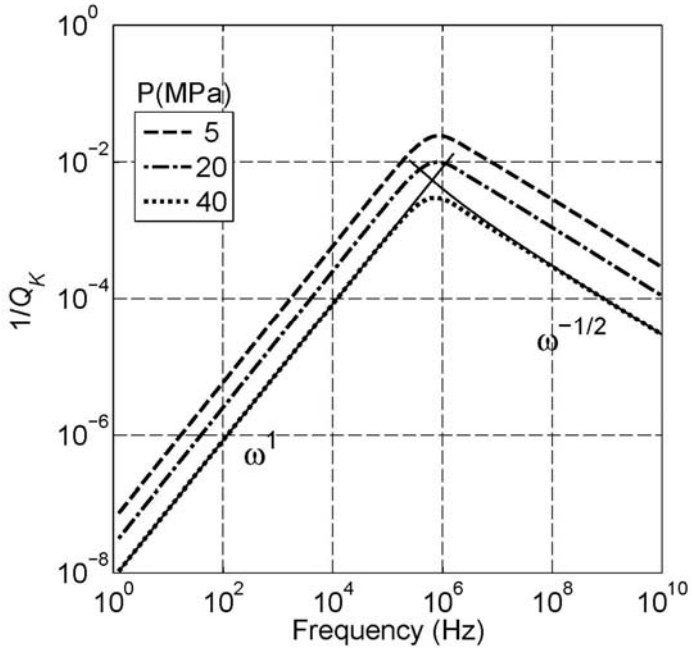

Figure 5.4. Predictions of (a) the bulk modulus (real part) and (b) attenuation for a range of frequencies and pressures (shown by different line patterns) for a gas-saturated sample of Berea 5-600 sandstone. Solid lines show asymptotic frequency dependencies of attenuation: ω^1 at low frequencies , ω^{-1} at intermediate frequencies , $\omega^{-1/2}$ at high frequencies.

frequency, and can be used as dimensionless frequency. Figure 5.3 shows the predictions of the model based on equation 5.48 for the bulk modulus $\mathrm{Re}\,K_{mf}$ and the bulk quality factor $Q^{-1} = \mathrm{Im}\,K_{mf} / \mathrm{Re}\,K_{mf}$ as functions of frequency at different pressure levels for the sample of Berea 5-600 sandstone (Han et al., 1986) fully saturated with water ($K_f = 2.2$ GPa, $\rho_f = 1031$ Kg/m3, $\eta = 10^{-3}$ Pa·s). Figure 5.4 shows the same dependencies for the same sample saturated with gas ($K_f = 0.0022$ GPa, $\rho_f = 10.8$ Kg/m3, $\eta = 11^{-5}$ Pa·s). The workflow for estimation of K_h and ϕ_c is described in Parameter estimation section.

For the water-saturated rock, the bulk modulus shows a smooth transition from the low to high frequency limit. Similar behaviour observed for the gas-saturated rock however, not surprisingly the dispersion appears to be much smaller in this case. Attenuation for the water-saturated rock shows slightly more complex behaviour, revealing existence of one additional asymptote at the intermediate frequencies ($10^6 - 10^8$ Hz), and one additional transition frequency (about 10^9 Hz).

To understand the behaviour of attenuation in the water-saturated case, consider first the case $|ka|^2 << 1$. Then, Taylor expansion of Bessel functions in equation 5.27 in powers of ka gives

$$K_f^* = -\frac{1}{8}(ka)^2 K_f . \tag{5.52}$$

Substitution of this expression into equation 5.48 gives

$$\frac{1}{K_{mf}(P,\omega)} = \frac{1}{K_h} + \frac{1}{\dfrac{1}{\dfrac{1}{K_{dry}(P)} - \dfrac{1}{K_h}} - \dfrac{(ka)^2 K_f}{8\phi_c(P)}} . \tag{5.53}$$

Here we can distinguish three limiting cases

1) Low frequencies:

$$|ka|^2 << \frac{8\phi_c(P)}{\left(\frac{1}{K_{dry}(P)} - \frac{1}{K_h}\right)K_f}. \tag{5.54}$$

In this case, Taylor expansion of equation 5.53 gives the following asymptote for the modified frame modulus

$$K_{mf}(P,\omega) = K_{dry}(P)\left[1 - \frac{(ka)^2}{8\phi_c(P)}\left(\frac{1}{K_{dry}(P)} - \frac{1}{K_h}\right)^2 K_f K_{dry}(P)\right], \tag{5.55}$$

showing that in the low frequency limit, the modified frame modulus tends to the dry modulus. Corresponding asymptotic expression for the dimensionless attenuation is

$$Q^{-1}(P,\omega) = \frac{1}{8}\left(\frac{1}{K_{dry}(P)} - \frac{1}{K_h}\right)^2 \frac{K_{dry}(P)K_f}{\phi_c(P)}|ka|^2 = \frac{3}{8}\left(\frac{1}{K_{dry}(P)} - \frac{1}{K_h}\right)^2 \frac{\omega\eta K_{dry}(P)}{\alpha^2\phi_c(P)} \tag{5.56}$$

This asymptote is shown in figures 5.3b and 5.4b.

2) Intermediate frequencies:

$$\frac{8\phi_c(P)}{\left(\frac{1}{K_{dry}(P)} - \frac{1}{K_h}\right)K_f} << |ka|^2 << 1. \tag{5.57}$$

In this case equation 5.53 yields

$$K_{mf}(P,\omega) = K_h\left[1 + \frac{8\phi_c(P)}{(ka)^2}\frac{K_h}{K_f}\right]. \tag{5.58}$$

Corresponding asymptotic expression for dimensionless attenuation is

$$Q^{-1}(P,\omega) = \frac{8\phi_c(P)}{|ka|^2}\frac{K_h}{K_f} = \frac{8\phi_c(P)\alpha^2 K_h}{3\omega\eta}. \tag{5.59}$$

Note that for this regime to exist we must have

$$\frac{8\phi_c(P)}{\left(\frac{1}{K_{dry}(P)}-\frac{1}{K_h}\right)} << K_f . \tag{5.60}$$

This means that the fluid modulus must not be too small ('liquid case'). This explains why this regime is not observed in the gas case (see Figure 5.4b). Note that in this intermediate regime, attenuation is proportional to $1/\omega$. This asymptote is shown in Figure 5.3b.

3) Finally, consider the case of high frequencies $|ka| >> 1$. In this case equation 5.47 gives

$$K_f^* = \left[1+\frac{2i}{ka}\right]K_f \tag{5.61}$$

and thus

$$K_{mf}(P,\omega) = K_{uf}(P) + \phi_c(P)\frac{K_h^2}{K_f}\left(\frac{2i}{ka}\right) \approx K_h\left[1+\frac{K_h}{K_f}\left(\frac{2i\phi_c(P)}{ka}\right)\right] \tag{5.62}$$

so that

$$Q^{-1}(P,\omega) = \frac{K_h}{K_f}\left(\frac{\sqrt{2}\phi_c(P)}{|ka|}\right) = \frac{\alpha\phi_c(P)K_h}{\left(3\omega\eta K_f/2\right)^{1/2}} . \tag{5.63}$$

Note that in this high-frequency limit, attenuation is proportional to $1/\sqrt{\omega}$. This asymptote is shown in Figure 5.3b.

5.7 SIMPLIFIED MODEL FOR THE LIQUID CASE

As we have seen in the previous section, for the most important case of liquid saturation, the attenuation exhibits three asymptotic regimes. However, only two regimes are visible in the velocity dispersion. This may look strange, but can be easily understood if we notice that the real parts of the modified frame moduli at

intermediate and high frequencies are K_h (high-pressure dry modulus) and K_{uf} (unrelaxed modulus), respectively, as given by equations 5.58 and 5.62. As discussed earlier, for liquid saturation the difference between these moduli is usually negligible (see equation 5.3 and corresponding discussion). Thus, the transition of the real parts of the modified frame moduli from the intermediate to high frequency regimes is unnoticeable and can be ignored. Moreover, the same can be said about attenuation. Indeed, attenuation corresponding to the high-frequency regime is negligibly small (this can be understood from the fact that in the intermediate regime the attenuation decays as $1/\omega$ and rapidly becomes very small). We thus can conclude that the transition from intermediate to high frequency regimes is unimportant, and for all practical purposes the behaviour described by equation 5.48 is accurately approximated by much simpler equation 5.53 describing a single dispersion transition. Equation 5.53 can also be rewritten in the form

$$\frac{1}{K_{mf}(P,\omega)} = \frac{1}{K_h} + \frac{1}{\dfrac{1}{\dfrac{1}{K_{dry}(P)} - \dfrac{1}{K_h}} + \dfrac{3i\omega\eta}{8\phi_c(P)\alpha^2}}, \tag{5.64}$$

with the shear modulus given by equation 5.49. It is interesting that dispersion and attenuation behaviour predicted by this model does not explicitly depend on fluid compressibility. However, we should keep in mind that the fluid compressibility must be sufficiently small (modulus large) to satisfy condition 5.60.

Equation 5.53 or 5.64 describes a simple transition of modified frame modulus from K_{dry} to K_h. The characteristic transition frequency can be obtained from the intersection of asymptotes given by equations 5.56 and 5.59. This gives

$$\Omega_t = |ka|^2 = \frac{8\phi_c(P)}{K_f}\left[\frac{1}{K_{dry}(P)} - \frac{1}{K_h}\right]^{-1}\left[\frac{K_h}{K_{dry}(P)}\right]^{1/2}. \tag{5.65}$$

This expression is slightly confusing, as both compliant porosity ϕ_c and dry modulus K_{dry} are functions of pressure. Equation 5.65 can be simplified by noting that pressure variation of dry modulus is caused by progressive closure of compliant

porosity. Indeed, according to Shapiro (2003), the difference between dry and high-stress compressibilities $K_{dry}^{-1} - K_h^{-1}$ is proportional to the compliant porosity ϕ_c

$$\frac{1}{K_{dry}(P)} - \frac{1}{K_h} = \frac{\phi_c(P)}{K_h}\theta_c \tag{5.66}$$

where θ_c is parameter of stress sensitivity related to the compliance of compliant pores (or their effective aspect ratio). This gives

$$\Omega_t = |ka|^2 = \frac{8K_h}{\theta_c K_f}\left[\frac{K_h}{K_{dry}(P)}\right]^{1/2} \tag{5.67}$$

or

$$\omega_t = \frac{8\alpha^2 K_h}{3\eta\theta_c}\left[\frac{K_h}{K_{dry}(P)}\right]^{1/2} \tag{5.68}$$

For small concentration of randomly oriented penny shaped cracks, parameter θ_c can be related to their aspect ratio α by (see e.g., Mavko et al., 1998)

$$\theta_c = \frac{K_g(3K_g + 4\mu_g)}{\pi\alpha\mu_g(3K_g + \mu_g)}. \tag{5.69}$$

Using equation 5.69, expression 5.68 for squirt characteristic frequency can be written as

$$\omega_t = \alpha^3 \frac{B}{\eta}, \tag{5.70}$$

where

$$B = \frac{8\pi\mu_h(3K_h + \mu_h)}{3(3K_h + 4\mu_h)}\left[\frac{K_h}{K_{dry}(P)}\right]^{1/2} \tag{5.71}$$

is a combination of the dry moduli of the rock, which has dimensions of elastic moduli and is weakly dependent on pressure (in equation 5.71, μ_h is dry shear modulus of the rock without compliant pores).

Note that in bi-logarithmic scale asymptotes 5.56 and 5.59 have identical slopes. Thus, the attenuation peak given by equation 5.53 is symmetric about the transition frequency Ω_t, and maximum attenuation occurs exactly at Ω_t (or ω_t). This maximum attenuation value can be obtained by substituting equation 5.67 into 5.53, and taking imaginary and real parts (note that $(ka)^2 = -i|ka|^2$). This yields

$$Q^{-1}(P,\omega_t) = \frac{K_h - K_{dry}(P)}{K_h + K_{dry}(P)}\left[\frac{K_h}{K_{dry}(P)}\right]^{1/2}. \tag{5.72}$$

Recall that K_h is nothing more than K_{dry} in the limit of high pressure. If the variation of dry bulk modulus with pressure is moderate, then $(K_h / K_{dry})^{1/2} = O(1)$ and thus the peak attenuation is equal half the fractional variation of the dry bulk modulus with pressure. For example, if the difference between K_{dry} and K_h is 20%, then Q will be about 10.

5.8 EXAMPLE

5.8.1 ESTIMATION OF MODEL PARAMETERS

Our model given by equations 5.64 and 5.49 predicts modified frame moduli and, when combined with Gassmann's or Biot's theory, compressional and shear wave moduli, velocities and attenuation coefficients of a saturated rock as a function of frequency and material properties (of the rock frame and pore fluid). Since the model contains a number of parameters, it is always possible to fit it to data sufficiently well by varying the unknown parameters. It is therefore critical to measure or estimate independently as many parameters as possible, that is, to perform a controlled experiment.

Dry moduli

In a typical laboratory set-up, compressional and shear ultrasonic velocities are measured on dry and fluid saturated rock samples as a function of pressure. Thus,

parameters K_{dry} and μ_{dry} as functions of pressure can be obtained from the ultrasonic measurements using standard equations $K_{dry} = \left[V_P^2 - (4/3)V_S^2\right]\rho$ and $\mu_{dry} = V_S^2\rho$.

High-pressure modulus

High-pressure modulus K_h can be taken as K_{dry} at the highest pressure available. Note that this approach assumes that at this pressure all the compliant porosity is closed, and corresponds to the fact that K_{dry} as function of pressure has levelled off at this pressure value.

Compliant porosity.

Compliant porosity ϕ_c cannot be directly measured; however it can be estimated from the variation of total porosity with pressure (Schmitt and Li, 1995). This variation can be estimated, for instance, by measuring volumetric strain as a function of pressure using strain gauges. Once the total porosity variation is known, stiff porosity can be

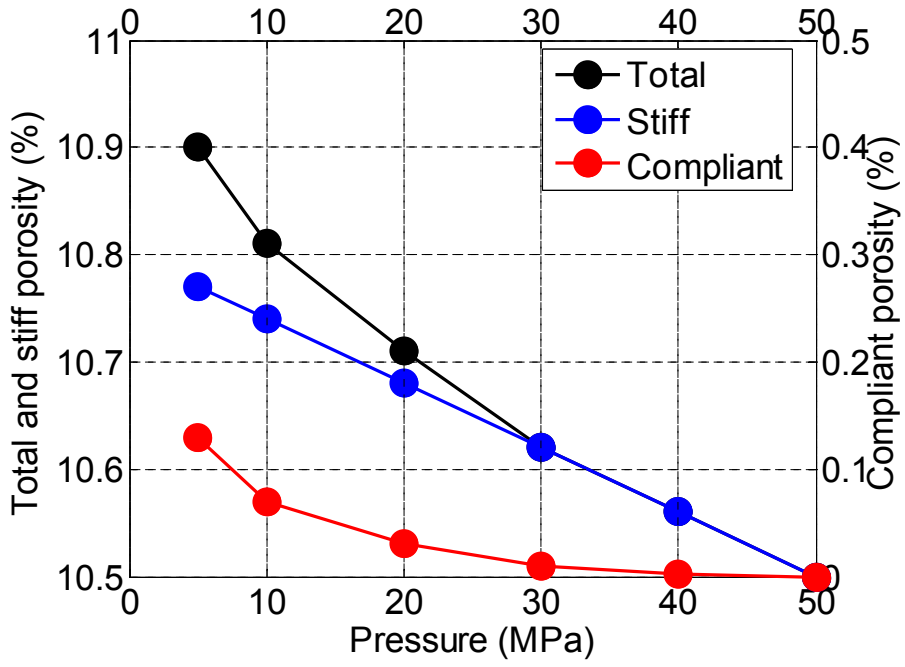

Figure 5.5. Schematic plot of dry rock porosity versus pressure. The volume of the soft porosity at any pressure is estimated as the difference between the total porosity and the extrapolation of the high-pressure porosity versus pressure trend.

estimated by fitting a linear trend to total porosity in the high pressure range where compliant porosity is assumed closed (and thus total porosity equals stiff porosity) (Figure 5.5). Compliant porosity can be obtained as a difference between total porosity and the linear trend of stiff porosity extrapolated to the lower pressures (Walsh, 1965; Mavko and Jizba, 1991; Pervukhina et al., 2010). Note, however, that since compliant porosities are usually 0.001 or smaller, high accuracy measurements of total porosity variations with pressure are required. If such precise porosity measurements are not available, compliant porosity can be estimated from the stress dependency of dry elastic moduli obtained from ultrasonic measurements as suggested by Pervukhina et al. (2010). Stress dependency of the dry bulk modulus can be approximated as follows (Shapiro, 2003)

$$1/K_{dry}(P) - 1/K_h = (\phi_{c0}/P_h)\exp(-P/P_h), \tag{5.73}$$

where ϕ_{c0} is compliant porosity at zero pressure and P_h is a characteristic pressure at which compliant porosity closes. The parameters ϕ_{c0}/P_h and P_h can be obtained by fitting of stress dependency of bulk moduli using equation 5.73 and ϕ_{c0} can be estimated as a ratio of these fitting parameters. Then the pressure variation of compliant porosity can be written as

$$\phi_c(P) = \phi_{c0}\exp[P/P_h]. \tag{5.74}$$

Note that neither of the two compliant porosity estimation approaches utilises the velocity or attenuation measurements on saturated samples. Therefore, these estimates are independent of dispersion/attenuation data.

Aspect ratio of the contact gap

Like compliant porosity, aspect ratio α of the grain contact gap cannot be directly measured. It is tempting to estimate the gap aspect ratio from the variation of, say, dry moduli with compliant porosity, e.g., using elastic effective medium

[a]

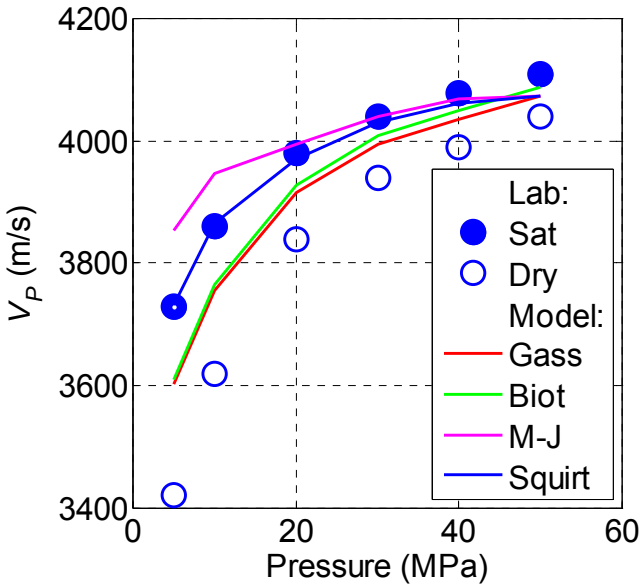

[b]

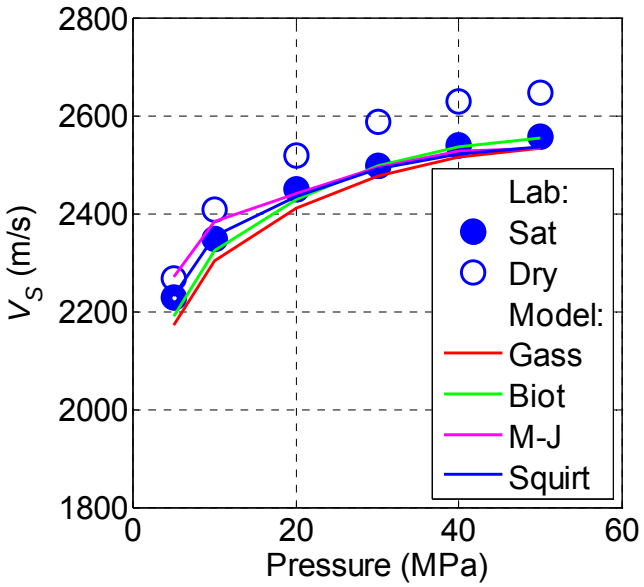

Figure 5.6. Velocities of (a) compressional and (b) shear-wave in a sample of Berea 5-600 sandstone as a function of pressure: ultrasonic laboratory measurements on dry (empty circles) and saturated (blue circles) sample, predictions of the Mavko-Jizba (1991) model (magenta line), Gassmann's (red line) and Biot's (green line) theories, and predictions of the present model (blue line).

[a]

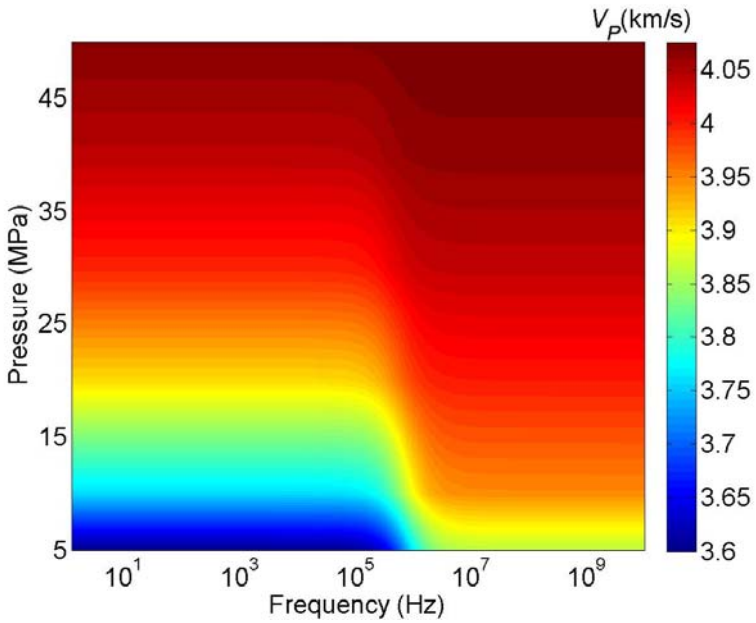

[b]

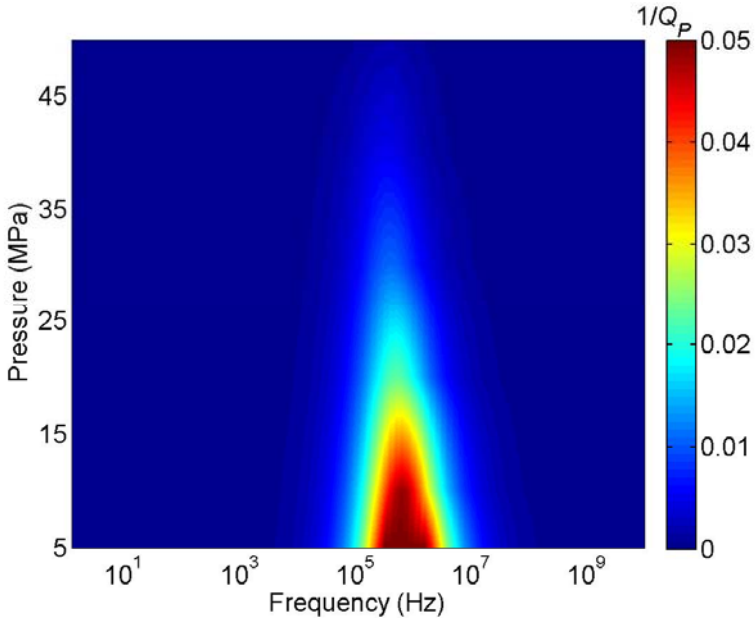

Figure 5.7. Predictions of (a) Velocity and (b) attenuation of P-wave in a water saturated sample of Berea 5-600 sandstone as a function of frequency and pressure.

[a]

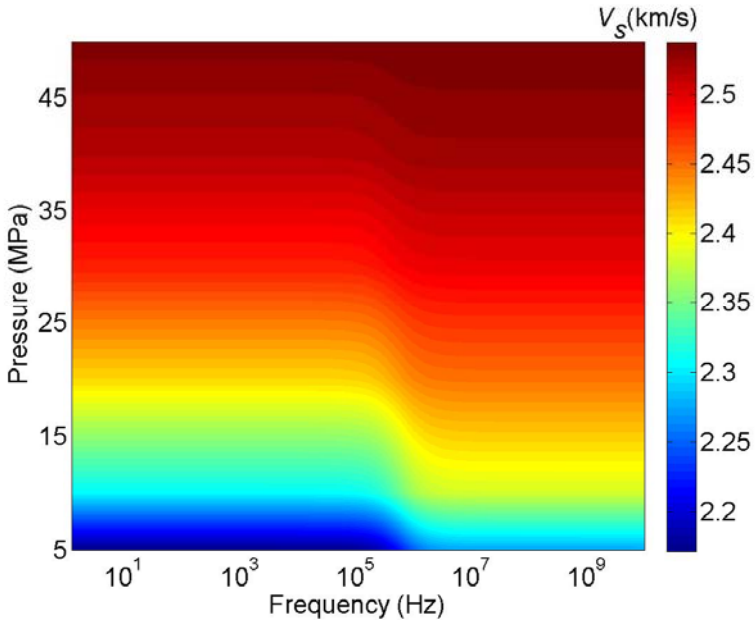

[b]

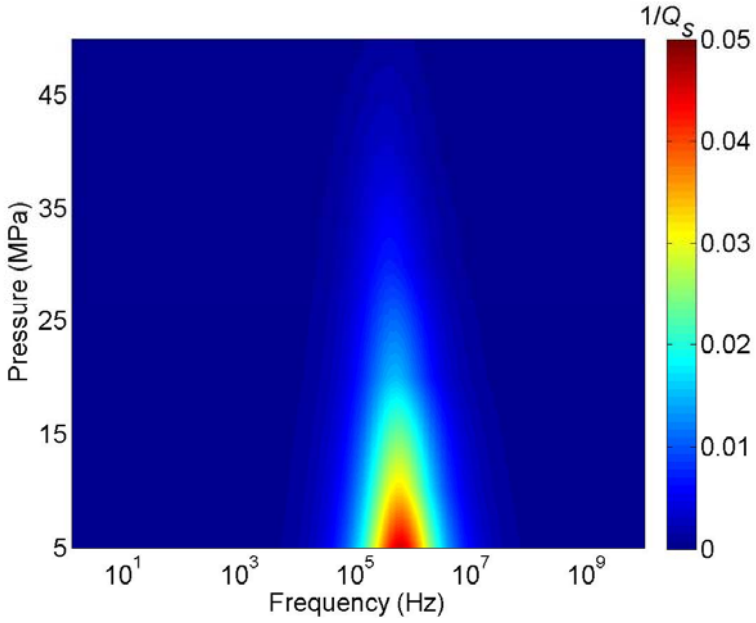

Figure 5.8. Predictions of (a) Velocity and (b) attenuation of S-wave in a gas saturated sample of Berea 5-600 sandstone as a function of frequency and pressure.

theory (Küster and Toksöz, 1974; Berryman, 1980a; Berryman, 1980b). However, the aspect ratio that controls fluid pressure relaxation in the flat inter-granular gap may not be related to the aspect ratio of penny-shaped cracks that control the pressure variation of the effective elastic moduli of the dry rock. In this study we use gap aspect ratio α as a free fitting parameter and estimate it as the value that provides the best fit for modulus - pressure dependency on saturated samples (Figures 5.6, 5.9).

5.8.2 *LABORATORY DATA EXAMPLES*

In this section, we illustrate predictions of our squirt model on a number of rocks and compare these predictions with laboratory measurements. Our aim is to illustrate the behaviour of the model on a few samples.

Figure 5.6 shows a comparison between measured (blue circles) and predicted by our model (blue lines) compressional and shear velocities as functions of pressure for a water-saturated sample of Berea 5-600 sandstone (Han et al., 1986). We also plot the measurements carried out on a dry sample (empty circles) as well as the predictions by Mavko-Jizba model (magenta lines), and Gassmann's (red lines) and Biot's equations (green lines). The parameters of the grain material are taken to be: density $\rho_g = 2653\,\mathrm{Kg/m^3}$ and the grain bulk modulus $K_g = 39\,\mathrm{GPa}$, which is estimated by assuming that at the highest pressures the saturated bulk modulus is given by Gassmann's equation. The compliant porosity is obtained from velocity in the dry sample using the theory of Shapiro (2003). The estimated compliant porosity ranges from 0.0002 to 0.000003 depending on pressure. The aspect ratio of the grain contact $\alpha = 0.01$ is obtained by the best fit of the predictions to the experimental data (see the details of parameter estimation). Figures 5.7 and 5.8 show the dispersion and attenuation of compressional and shear velocities, respectively, as functions of pressure and frequency. We observe the decrease of both dispersion and attenuation with increasing pressure. This is logical, as pressure increase causes closure of compliant porosity.

Figure 5.9 shows a comparison between measured and predicted velocities as functions of pressure for a water-saturated carbonate sample S1 (Agersborg et al.,

2008). The model parameters for the carbonate sample are taken to be: $\rho_g = 2670\ \text{Kg/m}^3$, $K_g = 82\ \text{GPa}$, $\alpha = 0.01$. The estimated compliant porosity ranges from 0.0003 to 0.00002 depending on pressure. We see that for both the sandstone and carbonate samples our model describes the observed shape of the pressure dependency reasonably well.

5.9 DISCUSSION

In this chapter, we have generalized Mavko-Jizba expressions for high-frequency bulk and shear moduli to gas-saturated rocks. We have also developed a simple model of elastic wave attenuation and dispersion due to squirt flow between stiff and soft pores in a granular rock. The model applicability is shown on a couple of illustrative examples. By construction, the model is exactly consistent with Gassmann's theory in the low frequency limit, and with Mavko-Jizba model in the high-frequency limit. The expression for the characteristic frequency ω_t, equation 5.70, is the same as the commonly used expression for squirt frequency (Jones, 1986), except that in our model the bulk modulus of the rock is replaced by a combination of bulk and shear moduli. Furthermore, for liquid-saturated rocks the attenuation and dispersion curves are symmetric about ω_t in log-log scale. Attenuation $1/Q$ is proportional to ω at low frequencies, and to $1/\omega$ at high frequencies. The magnitude of attenuation and dispersion is directly related to the variation of dry bulk modulus with pressure. All these features are also characteristic of the double-porosity model of Pride et al. (2004). The present model is designed to describe the same physical processes as the double-porosity model but uses a very different theoretical approach and is much simpler. An important advantage of our model is that it gives closed form expressions for velocity and attenuation as functions of frequency and pressure.

The model contains one adjustable parameter: aspect ratio of compliant pores. All other parameters can be measured or estimated from measurements of ultrasonic

velocities and strains versus confining pressure on dry samples. One assumption in this workflow is that all compliant pores are closed at the upper limit of the pressure

[a]

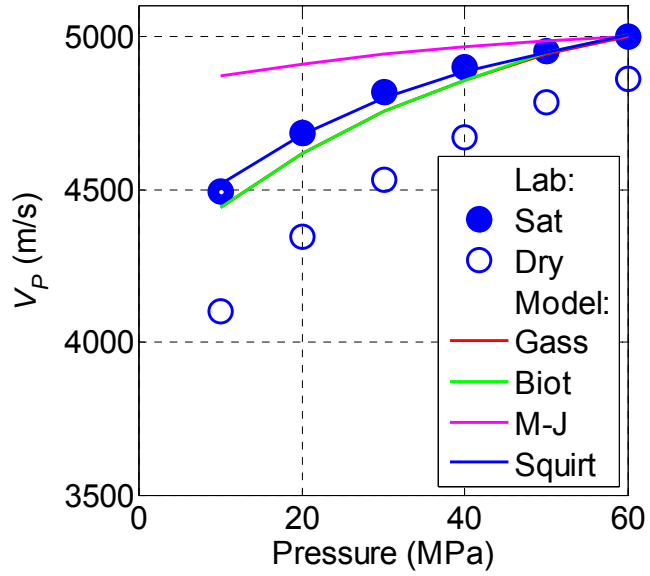

[b]

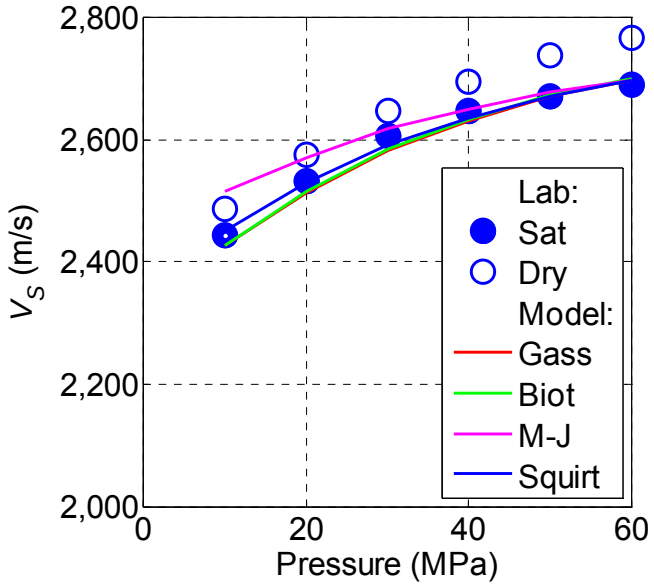

Figure 5.9. Velocities of (a) compressional and (b) shear-wave in a sample of S1 carbonate as a function of pressure: ultrasonic laboratory measurements on dry (empty circles) and saturated (blue circles) sample, predictions of the Mavko-Jizba (1991) model (magenta line), Gassmann's (red line) and Biot's (green line) theories, and predictions of the present model (blue line).

range of the measurements and hence ultrasonic velocities become independent of pressure. Therefore, there is no squirt at these pressures and the saturated and dry velocities should approximately satisfy Gassmann's (or Biot's) equations. This is the case in the example given in Figures 5.7. However, in many other cases the compliant pores will not be completely closed at the pressure of 50 or even 100 MPa. This can be seen by the fact that in many cases the dry velocities at these pressures continue to increase with the pressure increase. This closure of remaining compliant porosity gives a significant linear term in the velocity-pressure relationship of Eberhart-Phillips et al. (1989), which is based on the analysis of measurements on a large set of sandstone samples from different areas of the world (Han et al., 1986). If the compliant pores close at higher pressures than the available range of experimental data, then the modulus K_h cannot be estimated directly from the measurements. Instead, K_h should be estimated by using some effective medium theory assuming a typical aspect ratio of stiff pores in a particular rock (see, e.g., Xu and White, 1995).

Experimental validation of our model requires a comparison of its predictions against measurements of fluid saturated velocities and attenuation factors versus frequency and pressure. The frequency range of ultrasonic measurements is usually quite narrow (say, 0.25 – 1 MHz) which makes it difficult to observe the velocity dispersion. One way to overcome this difficulty is to look at variations of velocity (and attenuation) with fluid viscosity. This can be done by saturating the same sample with a number of different fluids (e.g., Best and McCann, 1995; Adam et al, 2009), or by using a fluid (say, glycerol) whose viscosity can be varied by changing temperature (Jones, 1986). Alternatively, frequency dependency can be obtained from resonant bar (Born, 1941; Gardner, 1962; Wyllie et al., 1962; McCann and Sothcott, 2009) or forced-oscillation measurements (Batzle et al., 2006; Adam et al., 2009). A comprehensive comparison of model predictions with laboratory data will be a subject of a separate study.

5.10 CHAPTER CONCLUSIONS

We present a new and concise derivation of expressions for high-frequency bulk and shear moduli of fluid-saturated rocks from pressure dependency of dry moduli and compliant porosity. The derivation is based on the Sayers-Kachanov plane-discontinuity formalism applied to an isotropic distribution of discontinuities. The derived expressions generalize the established Mavko-Jizba relations to gas-saturated rocks. The new expressions are particularly convenient for computations because the same expressions can be used for dry, gas-saturated, and liquid-saturated rocks.

We also develop a new simple model of squirt-flow dispersion and attenuation in granular fluid-saturated media for a wide range of frequencies. The results are exactly consistent with Gassmann's theory in the low frequency limit, and with Mavko-Jizba unrelaxed moduli in the high-frequency limit. For liquid-saturated rocks the attenuation and dispersion curves are symmetric about ω_t in log-log scale. Attenuation $1/Q$ is proportional to ω at low frequencies, and to $1/\omega$ at high frequencies. The magnitude of attenuation and dispersion is directly related to the variation of dry bulk modulus with pressure, and is relatively independent of fluid properties. The model contains one adjustable parameter: aspect ratio of compliant pores (grain contacts). All other parameters can be measured or estimated from measurements of ultrasonic velocities and strains versus confining pressure on dry samples.

CHAPTER 6 – ARE PENNY-SHAPED CRACKS A GOOD MODEL FOR COMPLIANT POROSITY?

6.1 BACKGROUND

Understanding and modelling of the effect of pressure and stress on elastic properties of rocks is important for such diverse applications as lithology and fluid identification in presence of mechanical compaction, pore pressure prediction, and analysis of time-lapse response to fluid injection and depletion. Laboratory measurements on porous rocks show that increase of pressure from zero to typical reservoir pressures causes substantial (up to 50%) increase of bulk and shear moduli, but only small (below 1%) reduction in overall porosity. This suggests that pressure dependency of elastic properties is caused by preferential closure of very compliant pores with small overall volume but large specific surface area. Perhaps the simplest shape that captures such properties is a so-called penny-shaped crack: an oblate spheroid (ellipsoid of revolution) whose aspect ratio (ratio of smaller to larger semi-axis) is a small parameter (say, from 10^{-4} to 10^{-2}). In granular rocks these compliant pores (cracks) most likely occur at grain contacts or as intra-granular micro-fractures.

Pores are modelled by ellipsoids not because anyone believes pore space consists of ellipsoids, but because they (1) appear to capture some essential properties of subsurface voids, (2) provide intuitively simple parameterization of enormous complexity of the real pore space, and (3) are relatively easily amenable to theoretical analysis. For a given porosity, the smaller is the (mean) aspect ratio of the pores, the stronger is the effect of these pores on the overall rock stiffness. For this reason, aspect ratios or their distributions are often used as lithology indicators. However, aspect ratio is also a function of (effective) pressure, as pores of small aspect ratio are more compliant and thus close preferentially under pressure – one more reason to study compliant pores in more detail.

The model of spheroidal pores is intuitively appealing (with obvious reservations), but is it quantitatively adequate? As mentioned above, complaint pores cause a reduction in bulk and shear moduli. This reduction occurs because each crack adds a little extra compliance to the rock – reducing both resistance to compression in the direction normal to its surface (normal compliance) and resistance to shear in the same plane (shear or tangential compliance). Since we can only measure the overall effect of these cracks, we cannot compute the normal or shear compliances for an individual crack, but we can compute the ratio of normal to shear compliances from measurements. Expressions for both normal and tangential compliances caused by an ellipsoidal crack are well known, and their ratio can be easily computed. In this chapter, we will assess the adequacy of the penny-shaped crack model by comparing the compliance ratio obtained from measurements against the theoretical expression for penny-shaped cracks.

6.2 METHOD

Our first objective is to obtain the ratio of normal to tangential compliance from ultrasonic measurements. For simplicity, we will only consider isotropic rocks. Similar analysis for anisotropic rocks is also possible if full elastic tensor measurements are available (Verdon et al., 2008). For isotropic materials, Sayers and Han (2002) proposed an elegant approach to computing normal to shear compliance ratio from measured bulk and shear moduli. They assumed that a rock at the highest available confining pressure has no compliant porosity, and that reduction of the moduli at lower pressures occurs due to the presence of isotropically distributed compliant cracks. As mentioned in chapter 5, the general additive compliance equations of Sayers and Kachanov (1995) for the isotropic case are given by equations 5.14-5.15.

If for a given sample, the bulk K_h and shear μ_h moduli of a rock at the highest pressure P_h (no compliant porosity!) and the dry moduli K_{dry} and μ_{dry} at a given pressure $P < P_h$ are measured, equations 5.14-5.15 can be easily solved for

sB_N^{dry} and sB_T^{dry} (s is the total area of the cracks). Sayers and Han (2002) used this approach to obtain the ratio of the normal and shear compliances of an individual crack $B = B_N / B_T$ from dry and saturated sandstone ultrasonic velocities measured by Han et al. (1986). Their results show that for dry rocks, most values of B lie between 0.25 and 1.5, with a few values between 1.5 and 3. Similar results for dry anisotropic rocks were obtained by Verdon et al. (2008).

According to Sayers and Kachanov (1995) the ratio B for dry penny-shaped cracks is

$$B = 1 - \nu / 2, \tag{6.1}$$

where ν is Poisson's ratio. The results of Sayers and Han (2002) appear to be inconsistent with the penny-shape prediction. However there is still uncertainty about the validity about experimental B values due to the following factors.

Some of the samples studied by Han (1986) show the moduli still increasing with pressure even when they approach the highest pressure (50 MPa). This suggests that either not all compliant pores are closed at the highest pressure, or reduction of stiff porosity contributes to the increase of the moduli.

The propagation of measurement errors causes large relative errors of B values in the upper part of the pressure range, where both normal and shear compliances are small.

In an attempt to attain compliance ratios with higher degree of confidence, we use the theory of Shapiro (2003), who recently proposed an alternative approach to modelling stress sensitivity. Shapiro showed that well known exponential dependency of elastic moduli on pressure can be written in the form

$$\frac{1}{K_{dry}} = \frac{1}{K_h} + \frac{\theta_s P}{K_h} + \frac{1}{K_h}\theta_c \phi_c, \tag{6.2}$$

and

$$\frac{1}{\mu_{dry}} = \frac{1}{\mu_h} + \frac{\theta_{s\mu} P}{\mu_h} + \frac{1}{\mu_h}\theta_\mu \phi_c, \tag{6.3}$$

where θ_c and θ_μ are bulk and shear stress sensitivity parameters due to compliant porosity, θ_s and $\theta_{s\mu}$ are corresponding parameters due to (weak) compression of stiff porosity, and $\phi_c(P)$ is compliant porosity given by

$$\phi_c = \phi_{c0} \exp\left(-\theta_c P / K_h\right). \tag{6.4}$$

The consistency of Shapiro's (2003) theory with experiment was recently demonstrated by Pervukhina et al. (2010) who compared the values of compliant porosity obtained from fitting equations 6.2 and 6.3 to data against direct porosity data obtained from measured strain.

Comparing Shapiro's equations 6.2 and 6.3 with equations 5.14 and 5.15, we can see that they are mutually consistent. In essence, ignoring the stiff porosity effect for a moment, we can view Shapiro's equations as a particular variant of Sayers-Kachanov (1995) equations with normal and tangential compliances defined as

$$sB_N^{dry} = \frac{\theta_c}{K_h}\phi_{c0} \exp\left(-\theta_c P / K_h\right) \tag{6.5}$$

and

$$sB_T^{dry} = \left(\frac{5}{2}\frac{\theta_\mu}{\mu_h} - \frac{2}{3}\frac{\theta_c}{K_h}\right)\phi_{c0} \exp\left(-\theta_c P / K_h\right), \tag{6.6}$$

so that

$$B = \frac{B_N^{dry}}{B_T^{dry}} = \frac{1}{\dfrac{5K_h\theta_\mu}{2\mu_h\theta_c} - \dfrac{2}{3}} \tag{6.7}$$

or

$$B = \frac{B_N^{dry}}{B_T^{dry}} = \frac{3}{\dfrac{5\left(1+\nu_h\right)\theta_\mu}{\left(1-2\nu_h\right)\theta_c} - 2}, \tag{6.8}$$

where ν_h is Poisson's ratio of the rock in high-pressure limit, where all compliant porosity is closed. Note that ϕ_c / s is some effective thickness of compliant pores. Shapiro (2003) showed that linear terms in equations 6.2 and 6.3 are often small compared with the exponential terms. Thus the compliance ratio can be obtained by

fitting equations 6.2 and 6.3 to measured elastic moduli functions of pressure, computing the ratio of stress sensitivity parameters $q = \theta_\mu / \theta_c$, and then computing compliance ratio B using equation 6.8. Note that in the theory of Shapiro (2003), the compliance ratio B is independent of pressure. The consistency of this conclusion with experimental data was analysed by Pervukhina et al. (2010) and Verdon et al. (2008).

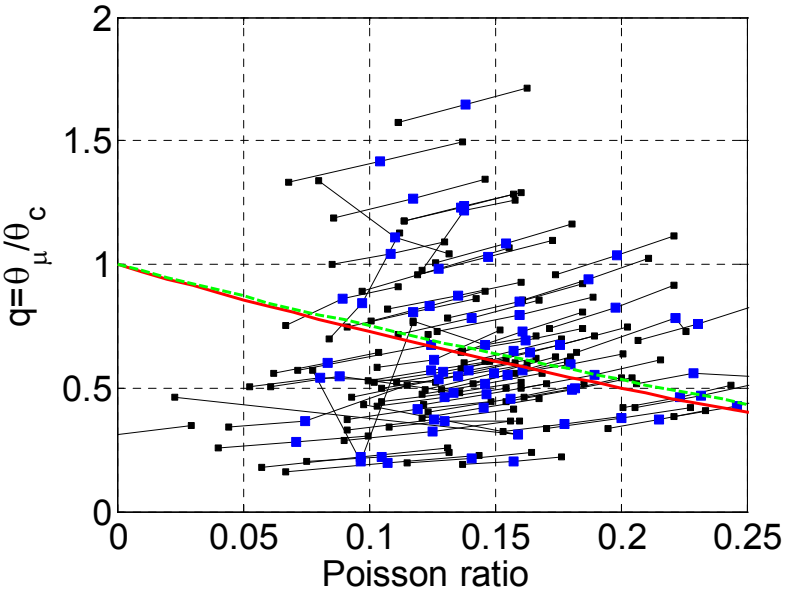

Figure 6.1. Stress sensitivity ratio q estimated from ultrasonic velocity measurements on 76 dry samples (blue squares), errobars due to systematic errors in shear velocities (black lines and squares), scalar cracks (green line), and spheroidal cracks (red line).

6.3 APPLICATION TO SANDSTONE DATA

Stress sensitivity coefficients and corresponding values of compliance ratio have been computed for ultrasonic measurements on 76 dry sandstone samples as reported in Han et al. (1986) and in Grochau and Gurevich (2008). Figure 6.1 shows q ratios computed for all samples as a function of Poisson's ratio ν_h in the limit of large pressure (blue squares). The line passing through each circle shows confidence limits for q ratio and Poisson's ratio as discussed below. Green dashed line shows the dependency of $q(\nu_h)$ as predicted by Shapiro and Kaselow (2005) for the special

case of an isotropic rock with porosity tensor of special symmetry (scalar cracks). Solid red line shows the ratio of stress sensitivities as predicted by non-interactive approximation for spheroidal cracks. From the first glance at Figure 6.1 we can see that compliance ratios predicted by Shapiro and Kaselow are almost identical to that for spheroidal cracks. We also see that ultrasonic data on stress sensitivity ratio show large scatter and do not show much correlation with Poisson's ratio.

As mentioned earlier, the aim of this chapter is to analyse what values of stress sensitivity ratio and compliance ratio are realistic. To this end we perform extensive error and sensitivity analysis. Influence of the following factors has been analysed.

Effect of the linear (stiff porosity) term in equations 6.2 and 6.3 was analysed by comparing quality of the fit to data with and without these terms. To our surprise, in all but 5% of samples, inclusion of the linear term reduces the misfit to much larger extent than expected due to the increase of the number of degrees of freedom. Thus we conclude that the deformation of stiff porosity plays significant role in defining stress dependency of elastic properties of rocks.

We also analysed the sensitivity of the results to systematic errors in velocity picking. This was done by assuming that all shear wave velocities were misestimated by ±50 m/s, and re-computing all the results. These results are shown in Figure 6.1 as the end points of the error bars. As expected, the relative error introduced is much larger for Poisson ratios than for stress sensitivity ratios.

We also analysed the effect of random errors, computed using standard error propagation analysis and χ^2 criterion. Random errors create a thin confidence tube-shaped area around the systematic error bar. For all but a handful of really bad samples, the influence of these random errors turns out to be negligibly small compared to model errors and systematic errors discussed above.

The stress sensitivity estimates shown in Figure 6.1 were used to compute compliance ratios using equation 6.8. The resulting estimates of B ratio are shown in

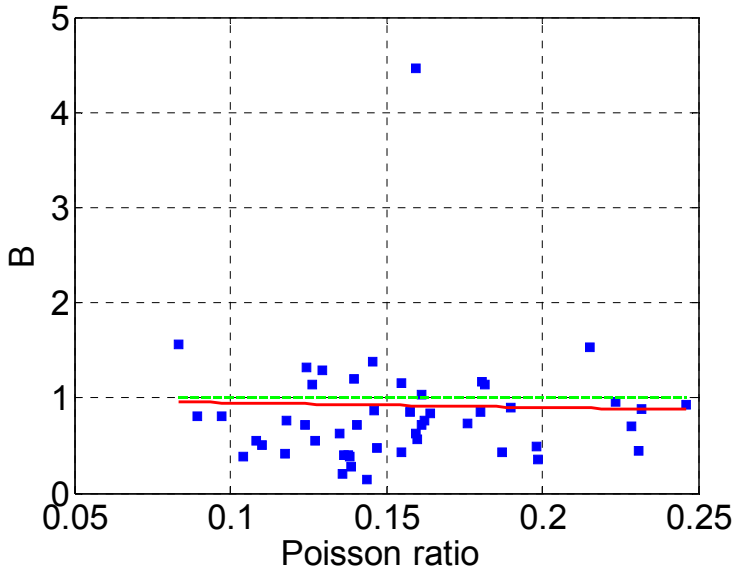

Figure 6.2. Compliance ratio B from ultrasonic velocity measurements on 64 dry samples with systematic errors less than 100% (blue squares), theory for scalar cracks (green line), and spheroidal cracks (red line).

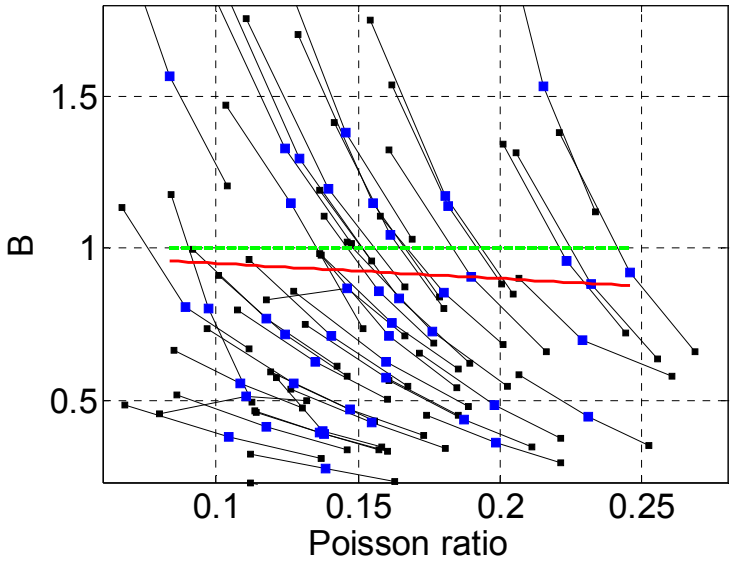

Figure 6.3. Compliance ratio B estimated from ultrasonic velocity measurements on 49 dry samples (blue squares) with systematic errors less than 40% (black lines and squares), scalar cracks (green line), and spheroidal cracks (red line).

Figure 6.2. Since B ratios show much larger scatter than q ratios, in Figure 6.2 we only show the results for samples where the relative error in B caused by systematic shear velocity errors is less than 100% per cent (64 out of 76 samples; error bars are not shown to avoid clutter). The dashed green line $B=1$ corresponds to stress-sensitivity ratio as suggested by Shapiro and Kaselow (2005), and earlier by Sayers and Kachanov (1991) (so-called scalar cracks). The solid line corresponds to non-interaction approximation for spheroidal cracks. We see that the B ratios are mostly scattered between 0 and 2, with no visible correlation with Poisson's ratios.

In Figure 6.3 we show the error bars for those samples with systematic (relative) errors in B ratio below 50% (49 samples). We see that errors in B (vertical spread of the error bar) are much larger than for q ratio. This is understandable, as errors in Poisson's ratio propagate into B when the latter is computed using

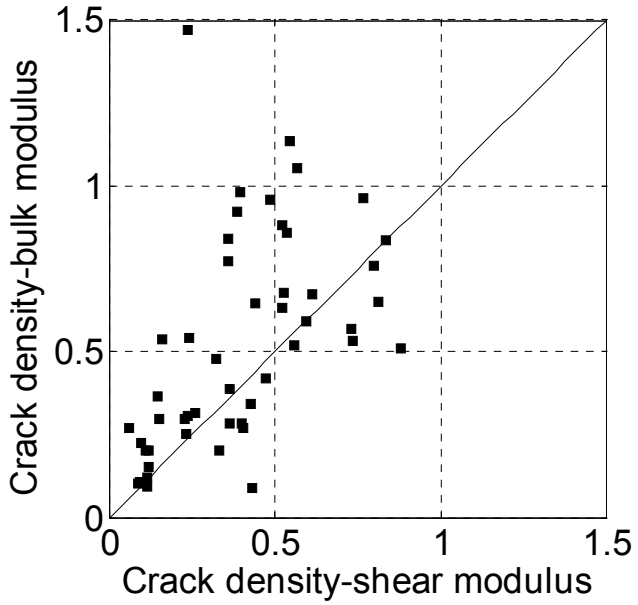

Figure 6.4. Crack density extracted from shear modulus against crack density extracted from bulk modulus.

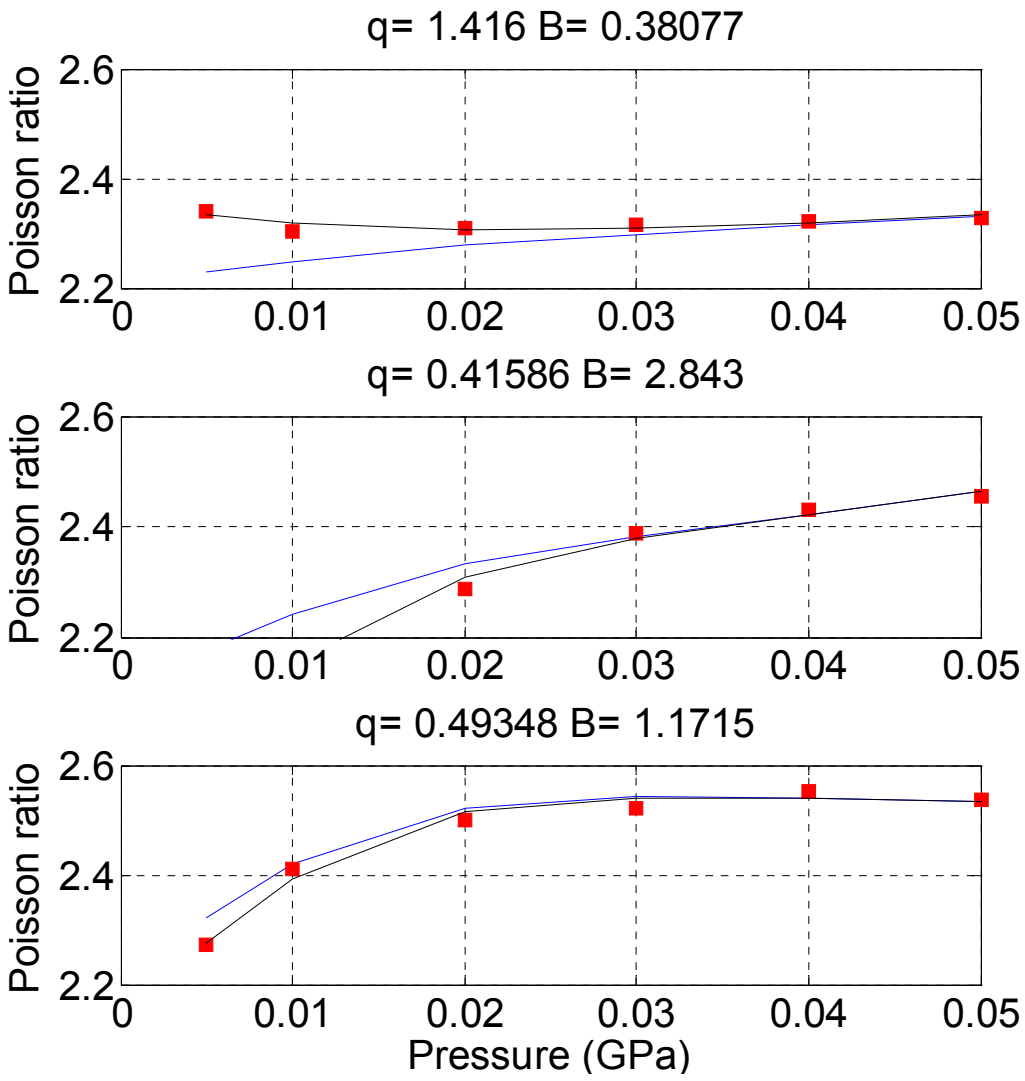

Figure 6.5. Pressure variation of Poisson's ratio for a number of samples computed from measured velocities (symbols), predicted by combining Sayers-Kachanov (1995) and Shapiro (2003) theories (black line) and by spheroidal crack theory (blue line).

equation 6.8. For most samples the vertical spread of the error bar far exceeds the difference between B values for spheroidal cracks, equation 6.1, and for 'scalar' cracks ($B=1$). Where $B>1$, one or both ends of the error bar appears to cross or approach the line $B=1$.

To check this last observation, we select only those samples for which the error bar corresponding to systematic shear velocity errors does not enter the band $0.9<B<1.1$. This leaves 19 samples (40% out of those with errors below 50%). Importantly, all but one of these selected samples have values $B<1$. This allows us to make an important conclusion: where B can be confidently said to be significantly different from 1, it is always smaller than 1.

What is the effect of compliance ratio B being smaller than predicted by spheroidal crack theory? One effect is that if we estimate crack density from bulk or shear modulus, the results will be different. These estimates are plotted in Figure 6.4 against one another for those samples with relative errors below 50%. We see that for roughly half of these samples, the crack density predicted from shear compliance is significantly higher than that from the bulk modulus. This graphically illustrates that the measured data on sandstones is inconsistent with spheroidal crack theory.

To show the meaning of various B values, in Figure 6.5 a-c we show stress dependency of Poisson's ratio obtained from measurements (symbols) against that predicted by spheroidal crack theory. We see that when compliance ratio is significantly different from 1, the prediction of the spheroidal crack theory deviates from measured data.

6.4 CHAPTER CONCLUSIONS

The ratio of shear to bulk stress sensitivities shows large scatter and, for a large number of dry sandstone samples, is not consistent with either the "scalar" crack approximation or spheroidal crack theory.

The ratio of normal to tangential compliance shows large scatter, with most values between 0 and 2. Values over 1 have higher relative errors. Data with relative systematic errors below 50% show compliance ratios close to or below 1. About half

of those are inconsistent with the spheroidal crack theory. This can be attributed to the fact that crack geometries of real rocks are very complicated and cannot be adequately represented by spheroids. Further research needs to be undertaken to better understand the limitations of the spheroidal crack theory.

CONCLUDING REMARKS

Pore fluids strongly influence elastic properties of rocks. In this thesis, the effect of viscous and viscoelastic fluids on elastic properties of porous rocks has been investigated using theoretical and numerical approaches. Various research aspects covered in this thesis include (1) digital rock physics modelling of the effect of partial saturation on seismic velocities and developing a test scenario for grid-based numerical methods, (2) investigating the sensitivity of Gassmann's equations to microheterogeneity, (3) developing an alternative fluid substitution scheme for rocks saturated with heavy oils, (4) examining rigorous viscoelastic bounds for heavy-oil rocks, (5) theoretical modelling of squirt dispersion of elastic wave velocity, (6) analysing the validity of using spheroids as idealization of real crack geometry to model pressure dependencies of rock properties. Given the diversity of rock physics problems considered in this study and independence of various chapters, results from each chapter are summarized separately.

- Chapter 1. Finite element model (FEM) (Arns, 2002) has been used to predict the linear effective elastic properties of three dimensional rocks saturated with mixture of gas and water for the first time. A test scenario for grid-based numerical methods has been developed. It has been shown that the accuracy of FEM simulations is dependent upon the area of an interface between pore fluids and the size of pore channels (or how a digital image is resolved). The optimal size of the individual pore channels needs to be relatively large (>4 voxels in diameter) to ensure accurate simulations.

- Chapter 2. The effect of microheterogeneity on Gassmann's fluid substitution in its traditional and generalized forms has been investigated for different idealized porous quartz/clay structures using numerical approach. It has been demonstrated that for highly porous structures such as periodic spheres models with different clay distributions, the accuracy of Gassmann predictions of P-wave velocity remains sufficient (error 16 m/s) despite the

large contrasts between the moduli of solid phases (factor 5 for K_g, and 38 for μ_g). This suggests that Gassman's equations are adequate for multiphase highly porous rocks with large contrasts between elastic properties of minerals composing the rock frame.

- Chapter 3. Traditional rock physics based on Gassmann theory becomes inapplicable to rocks saturated with viscoelastic fluids such as heavy oils. An alternative fluid substitution scheme for rocks saturated with viscoelastic fluids has been proposed in this thesis. The scheme is based on a self-consistent mixing method known as coherent potential approximation. Comparison of the model predictions with low-frequency measurements carried out on an Uvalde heavy-oil rock sample shows that our scheme reproduces frequency- and temperature-dependent behaviour of the shear modulus and attenuation. This confirms that the proposed scheme provides realistic estimates of the properties of heavy-oil rocks and can be used as an approximate fluid substitution approach for rocks saturated with viscoelastic fluids.

- Chapter 4. Commonly used Hashin-Shtrikman elastic bounds are not rigorous if one of the rock constituents is viscoelastic. In this doctorate, it has been demonstrated that the viscoelastic bounds of Milton and Berryman (1997) for the effective shear modulus of a two phase three-dimensional isotropic composite can be used as rigorous bounds for dispersion and attenuation of S-waves in heavy-oil rocks.

- Chapter 5. (1) Established Mavko-Jizba quantitative high-frequency model of squirt dispersion of elastic-wave velocities is limited to liquid-saturated rocks. In this thesis, generalization of Mavko-Jizba model to gas-saturated rocks has been presented. The new expressions are particularly convenient for computations because the same expressions can be used for dry, gas-

saturated, and liquid-saturated rocks. (2) A new model of squirt-flow dispersion and attenuation for a wide range of frequencies in granular fluid-saturated media has been presented and analysed. The results are exactly consistent with Gassmann's theory in the low frequency limit, and with Mavko-Jizba unrelaxed moduli in the high-frequency limit. The magnitude of attenuation and dispersion is directly related to the variation of dry bulk modulus with pressure, and is relatively independent of fluid properties. The model contains one adjustable parameter: aspect ratio of compliant pores (grain contacts). All other parameters can be measured or estimated from measurements of ultrasonic velocities and strains versus confining pressure on dry samples.

- Chapter 6. The validity of penny-shaped or spheroidal approximation to model real crack/pore geometry has been investigated using ratios of shear to bulk stress sensitivity coefficients and normal to tangential compliances extracted from ultrasonic measurements on 76 dry sandstone samples. The obtained ratios show large scatter and, for a large number of dry sandstone samples, are not consistent with either the "scalar" crack approximation or spheroidal crack theory.

REFERENCES

Abramowitz, M., and I. A. Stegun, 1964, Handbook of mathematical functions: National Bureau of Standards Applied Mathematics Series.

Adam, L., M. L. Batzle, K. T. Lewallen, and K. van Wijk, 2009, Seismic wave attenuation in carbonates: Journal of Geophysical Research, **114**, B06208.

Adler, P., C. Jacquin, and J.-F. Thovert, 1992, The formation factor of reconstructed porous media: Water Resources Research **28**, 1571.

Agersborg, R., T. A. Johansen, M. Jakobsen, J. Sothcott, and A. Best, 2008, Effects of fluids and dual-pore systems on pressure-dependent velocities and attenuations in carbonates: Geophysics, **73**, no. 5, N35–N47.

Anstey, N. A., 1991, Velocity in thin section, First break, **10**, 449-457.

Arns, C. H., 2002, The influence of morphology on physical properties of reservoir rocks: Ph.D. Dissertation, University of New South Wales, Sydney, Australia.

Arns, C. H., M. A. Knackstedt, W. V. Pincewski, and E. J. Garboczi, 2001, Accurate estimation of transport properties from microtomographic images: Geophysical Research Letters, **28**, 3361–3364.

Arns, C. H., M. A. Knackstedt, W. V. Pincewski, and E. J. Garboczi, 2002, Computation of linear elastic properties from microtomographic images: methodology and agreement between theory and experiment: Geophysics, **67**, 1396–1405.

Arns, C. H., M. A. Knackstedt, W. V. Pincewski, and N. S. Martys, 2004, Virtual permeametry on microtomographic images: Journal of Petroleum Science and Engineering, **45**, 41–46.

Artola, F. A. V., and V. Alvarado, 2003, Sensitivity analysis of Gassmann's fluid substitution equations: Some implications in feasibility studies of time-lapse seismic reservoir monitoring: Journal of Applied Geophysics, **59**, 47– 62.

Auriault, J.-L., and C. Boutin, 1994, Deformable porous media with double porosity III: Acoustics: Transport in Porous Media, **14**, 143-162.

Auzerais, F. M., J. Dunsmuir, B. B. Ferreol, N. S. Martys, J. Olson, T. S. Ramakrishnan, D. H. Rothman, and L. M. Schwartz, 1996, Transport in sandstone: a study based on three dimensional microtomography: Geophysical Research Letters, **23**, 705–708.

Batzle, M. L., D.-H. Han, and R. Hofmann, 2006, Fluid mobility and frequency-dependent seismic velocity — Direct measurements: Geophysics, **71**, no. 1, N1-N9.

Batzle, M., R. Hofmann, and D.-H. Han, 2006, Heavy oils - seismic properties: The Leading Edge, **25**, 750-757.

Bayuk, I. O., M. Ammerman, and E. M. Chesnokov, 2007, Elastic moduli of anisotropic clay: Geophysics, **72**, no. 5, D107-D117.

Bear, J., 1988, Dynamics of Fluids in Porous Media: Dover.

Beggs, H. D., and J. R. Robinson, 1975, Estimation of the Viscosity of Crude Oil Systems: Journal of Petroleum Technology, **27**, 1140-1141.

Behura, J., M. Batzle, R. Hofmann, and J. Dorgan, 2007, Heavy oils: Their shear story: Geophysics, **72**, no. 5, E175-E183.

Berryman, J. G., 1980a, Long-wavelength propagation in composite elastic media—I. Spherical Inclusions: Journal of the Acoustical Society of America, **68**, 1809–1831.

Berryman, J. G., 1980b, Long-wavelength propagation in composite elastic media II. Ellipsoidal inclusions: Journal of the Acoustical Society of America, **68**, 1980-1831.

Berryman, J. G., 1992a, Effective stress for transport properties of inhomogeneous porous rocks: Journal of Geophysical Research, **97**, 17409-17424.

Berryman, J. G., 1992b, Single-scattering approximations for coefficients in Biot's equations of poroelasticity: Journal of the Acoustical Society of America, **91**, 551-571.

Berryman, J. G., 2006, Estimates and rigorous bounds on pore-fluid enhanced shear modulus in poroelastic media with hard and soft anisotropy: International Journal of Damage Mechanics, **15**, 133–167.

Berryman, J. G., 2007, Seismic waves in rocks with fluids and fractures: Geophysical Journal International, **171**, 954–974.

Berryman, J. G., and G. W. Milton, 1991, Exact results for generalized Gassmann's porous media with two constituents: Geophysics, **56**, 1950-1960.

Berryman, J. G., S. R. Pride, and H. F. Wang, 2002, A differential scheme for elastic properties of rocks with dry or saturated cracks: Geophysical Journal International, **151**, 597–611.

Best, A, and C. McCann, 1995, Seismic attenuation and pore-fluid viscosity in clay-rich reservoir sandstones: Geophysics, **60**, 1386-1397.

Biot, M. A., 1956a, Theory of propagation of elastic waves in a fluid-saturated porous solid. I. Low-frequency range: Journal of the Acoustical Society of America, **28**, 168-178.

Biot, M. A., 1956b, Theory of propagation of elastic waves in a fluid-saturated porous solid. II. Higher frequency range: Journal of the Acoustical Society of America, **28**, 179-191.

Biot, M. A., 1962, Mechanics of deformation and acoustic propagation in porous media: Journal of Applied Physics, **33**, 1482-1498.

Biot, M. A., and D. G. Willis, 1957, The elastic coefficients of the theory of consolidation: Journal of Applied Mechanics, **24**, 594–601.

Born, W. T., 1941, The attenuation constant of earth materials: Geophysics, **6**, 132-148.

Bourbié, T., O. Coussy, and B. Zinszner, 1987, Acoustics of Porous Media: Technip.

Brown, R. J. S., and J Korringa, 1975, On the dependence of the elastic properties of a porous rock on the compressibility of the pore fluid: Geophysics, **40**, 608-616.

Budiansky, B., 1965, On the elastic moduli of some heterogeneous materials: Journal of the Mechanics Physics of Solids, **13**, 223-227.

Chapman, M., S. V. Zatsepin, and S. Crampin, 2002, Derivation of a microstructural poroelastic model: Geophysical Journal International, **151**, 427-451.

Ciz, R., and S. A. Shapiro, 2007, Generalization of Gassmanns equations for porous media saturated with a solid material: Geophysics, **72**, no. 6, A75-A79.

Ciz, R., B. Gurevich, A. Siggins, and J. Dvorkin, 2006, Effect of microhomogeneity on the effective stress coefficient for elastic properties of rocks: 67th Annual International Meeting, EAGE, Expanded Abstracts, P045.

Cole, K.S., and R. H. Cole, 1941, Dispersion and absorption in dielectrics I. Alternating current characteristics: Journal of Chemical Physics, **9**, 341-351.

Coyner, K. B., 1984, Effects of stress, pore pressure, and pore fluids on bulk strain, velocity, and permeability in rocks: Ph.D. thesis, Massachusetts Institute of Technology.

Das A., and M. Batzle, 2008, Modeling studies of heavy oil-in between solid and fluid properties: The Leading Edge, **27**, 1116-1123.

Digby, P. J., 1982, The effective elastic moduli of porous granular rocks: Journal of Applied Mechanics ASME, **48**, 803-808.

Dunsmuir, J. H., S. R. Ferguson, K. L. D'Amico, 1991, Design and operation of an imaging X-ray detector for microtomography: Institute of Physics: Conference Series, **121**, 257–261.

Dutta, N. C., and H. Ode, 1979a, Attenuation and dispersion of compressional waves in fluid-filled porous rocks with partial gas saturation (White model)-Part I: Biot theory: Geophysics, **44**, 1777-1788.

Dutta, N. C., and H. Ode, 1979b, Attenuation and dispersion of compressional waves in fluid-filled porous rocks with partial gas saturation (White model) Part II: Results: Geophysics, **44**, 1789-1805.

Dvorkin, J., G. Mavko, and A. Nur, 1995, Squirt flow in fully saturated rocks: Geophysics, **60**, 97–107.

Dvorkin, J., D. Moos, J. L. Packwood, and A. M. Nur, 1999, Identifying patchy saturation from well logs: Geophysics, **64**, 1756–1759.

Dvorkin, J., G. Mavko, and B. Gurevich, 2007, Fluid substitution in shaley sediment using effective porosity: Geophysics, **72**, no.3, O1-O8.

Eastwood, J., 1993, Temperature-dependent propagation of P-waves and S-waves in Cold Lake oil sands: Comparison of theory and experiment: Geophysics, **58**, 863-872.

Eberhart-Phillips, D., D.-H. Han, and M. D. Zoback, 1989, Empirical relationships among seismic velocity, effective pressure, porosity and clay content in sandstone: Geophysics, **54**, 82–89.

Endres, A. L., and R. J. Knight, 1997, Incorporating pore geometry and fluid pressure communication into modeling the elastic behavior of porous rocks: Geophysics, **62**, 106-117.

Ferry, J. D., 1980, Viscoelastic properties of polymers: John Wiley & Sons, Inc.

Flannery, B. P., H. W. Deckman, W. G. Roberge, K. L. D'Amico, 1987, Three-dimensional X-ray microtomography: Science, **237**, 1439–1444.

Fredrich, J., B. Menendez, T. F. Wong, 1995, Imaging the pore structure of geomaterials: Science, **268**, 276–279.

Garboczi, E. J., 1998, Finite element and finite difference programs for computing the linear electric and linear elastic properties of digital images of random materials: National Institute of Standards and Technology, Internal Report 6269, USA, /http://ciks.cbt.nist.gov/monograph.

Garboczi, E. J., and A. R. Day, 1995, An algorithm for computing the effective linear elastic properties of heterogeneous materials: three-dimensional results for composites with equal phase Poisson ratios: Journal of Mech. Phys. Solids, **43**, 9, 1349-1362.

Gardner, G. H. F., 1962, Extensional waves in fluidsaturated porous cylinders: Journal of the Acoustical Society of America, **34**, 36-40.

Gassmann, F., 1951, Über die Elastizität poröser Medien (Elasticity of porous media): Vierteljahrsschrift der Naturforschenden Gesselschaft in Zürich, **96**, 1-23.

Gibiansky, L. V., and G. W. Milton, 1993, On the effective viscoelastic moduli of two-phase media. I. Rigorous bounds on the complex bulk modulus: Proceedings of the Royal Society of London A, **440**, 163-188.

Gibiansky, L. V., G. W. Milton, and J. G. Berryman, 1999, On the effective viscoelastic moduli of two-phase media. III. Rigorous bounds on the complex shear modulus in two dimensions: Proceedings of the Royal Society of London A, **455**, 2117-2149.

Gist, G. A., 1994, Interpreting laboratory velocity measurements in partially gas-saturated rocks: Geophysics, **59**, 1100-1109.

Goldberg, I., and B. Gurevich, 1997, A semi-empirical velocity-porosity-clay model for petrophysical interpretation of P- and S-velocities: Geophysical Prospecting, **46**, 271-285.

Grechka, V., 2003, Effective media: a forward modeling view: Geophysics **68**, 2055–2062.

Grochau, M. H., and B. Gurevich, 2008, Investigation of core data reliability to support time-lapse interpretation in Campos Basin, Brazil: Geophysics, **73**, no. 2, E59-E65.

Grechka, V., 2009, Fluid-solid substitution in rocks with disconnected and partially connected porosity: Geophysics, **74**, no. 5, WB89–WB95.

Gurevich, B., 2002, Effect of fluid viscosity on elastic wave attenuation in porous rocks: Geophysics, **67**, 264-270.

Gurevich, B., 2003, Elastic properties of saturated porous rocks with aligned fractures: Journal of Applied Geophysics, **54**, 203–218.

Gurevich, B., 2004, A simple derivation of the effective stress coefficient for seismic velocities in porous rocks: Geophysics, **69**, no.2, 393-397.

Gurevich, B., and J. Carcione, 2000, Gassmann modeling of acoustic properties of sand-clay mixtures: Pure and Applied Geophysics, **157**, 811-827.

Gurevich, B., and S. L. Lopatnikov, 1995, Velocity and attenuation of elastic waves in finely layered porous rocks: Geophysical Journal International, **121**, 933-947.

Gurevich, B., K. Osypov, R. Ciz, and D. Makarynska, 2008, Modeling elastic wave velocities and attenuation in rocks saturated with heavy oil: Geophysics, **73**, no. 4, E115-E122.

Gurevich, B., E. H. Saenger, R. Ciz, 2005, Poroelastic effect on the shear wave in the systems of alternating solid and viscous fluid layers: theory vs. numerical modeling: 75th Annual International Meeting, SEG, Expanded Abstracts, 1601–1605.

Haddad, Y. M., 1995, Viscoelasticity of engineering materials: Springer.

Halbert, M. K., 2006, Rock physics models for unconsolidated sands and shales: BSc (Hons) Thesis, Curtin University, Perth, Australia.

Han, D-H., 1986, Effects of porosity and clay content on acoustic properties of sandstones and unconsolidated sediments: PhD thesis, Stanford University.

Han, D-H., A. Nur, and D. Morgan, 1986, Effects of velocity and clay content on wave velocities in sandstones: Geophysics, **51**, 2093-2010.

Han, D.-H., Q. Yao, and H.-Z. Zhao, 2007a, Complex properties of heavy oil sand: 77th Annual International Meeting, SEG, Expanded Abstracts, 1609-1613.

Han, D.-H., H.-Z. Zhao, and Q. Yao, 2007b, Velocity of heavy oil sand: 77th Annual International Meeting, SEG, Expanded Abstracts, 1619-1623.

Han, D.-H., J. Liu, and M. Batzle, 2008, Seismic properties of heavy oils-measured data: The Leading Edge, **27**, 1108-1115.

Hashin Z., and S. Shtrikman, 1963, A variational approach to the theory of the elastic behaviour of multiphase materials: Journal of the Mechanics and Physics of Solids, **11**, 127-140.

Hashin, Z., 1970, Complex moduli of viscoelastic composites-I. General theory and application to particulate composites: International Journal of Solids and Structures, **6**, 539-552.

Hill, R., 1952, The elastic behaviour of crystalline aggregate: Proceedings of Physical Society of London A, **65**, 349-354.

Hill, R., 1961. Elastic properties of reinforced solids: some theoretical principles. Journal of the Mechanics and Physics of Solids **11**, 357–372.

Hill, R., 1965, A self-consistent mechanics of composite materials: Journal of the Mechanics and Physics of Solids, **13**, 213-222.

Hudson, J. A., 1981, Wave speeds and attenuation of elastic waves in material containing cracks.: Geophysical Journal International, **64**, 133–150.

Hudson, J. A., T. Pointer, and E. Liu, 2001, Effective-medium theories for fluid-saturated materials with aligned cracks: Geophysical Prospecting, **49**, 509–522.

Johnson, D. L., 2001, Theory of frequency dependent acoustics in patchy-saturated porous media: Journal of the Acoustical Society of America, **110**, 682-694.

Jones, T. D., 1986, Pore fluids and frequency dependent wave propagation in rocks: Geophysics, **51**, 1939–1953.

Katahara, K. W., 1996, Clay minerals elastic properties: 66th Annual International Meeting, SEG, Expanded Abstracts, 1691–1694.

Katahara, K. W., 2004, Fluid substitution in laminated shaley sands: 74th Annual International Meeting, SEG, Expanded Abstracts, 1718-1721.

Keehm, Y., T. Mukerji, and A. Nur, 2004, Permeability prediction from thin sections: 3D reconstruction and lattice-Boltzmann flow simulation: Geophysical Research Letters, **31**, L04606.

Knackstedt, M. A., C. H., Arns, W. V. Pinczewski, 2003, I. Accurate velocity model for clean consolidated sandstones: Geophysics **68**, 1822–1834.

Knackstedt, M. A., C. H. Arns, and W. V. Pinczewski, 2005, Velocity-porosity relationships: Predictive velocity model for cemented sands composed of multiple mineral phases: Geophysical Prospecting, **53**, 349-372.

Knight, R., J. Dvorkin, and A. Nur, 1998, Acoustic signatures of partial saturation: Geophysics, **63**, 132–138.

Krief, M., J. Garat, J. Stellingwerff, and J. Ventre, 1990, A petrophysical interpretation using the velocities of P and S waves (full-waveform sonic): The Log Analyst, **31**, 355-369.

Küster, G. T., and M. N. Toksöz, 1974, Velocity and attenuation of seismic waves in two-phase media: Part I. Theoretical formulations: Geophysics, **39**, 587–606.

Lebedev, M., J. Toms-Stewart, B. Clennell, M. Pervukhina, V. Shulakova, L. Paterson, T. M. Müller, B. Gurevich, B., and F. Wenzlau, 2009, Direct laboratory observation of patchy saturation and its effects on ultrasonic velocities: The Leading Edge, January 2009, 24-27.

Leurer, K. C., and J. Dvorkin, 2006, Viscoelasticity of precompacted unconsolidated sand with viscous cement: Geophysics, **71**, no. 2, T31-T40.

Lopatnikov, S. L., and B. Gurevich, 1988, Transformational mechanism of elastic wave attenuation in saturated porous media: Izvestija Academy of Sciences USSR, Physics of the Solid Earth, **24**, 151-154.

Lopatnikov, S. L., P. Y. Gorbachev, and B. Gurevich, 1990, Acoustic wave propagation in a porous medium with randomly non-homogeneous gas distribution: Izvestija Academy of Sciences USSR, Physics of the Solid Earth, **26**, 468-471.

Marion, D., and A. Nur, 1991, Pore-filling material and its effect on velocity in rocks: Geophysics, **56**, 225-230.

Mavko, G., and A. Nur, 1975, Melt squirt in the aesthenosphere: Journal of Geophysical Research, **80**, 1444–1448.

Mavko, G., and A. Nur, 1979, Wave attenuation in partially saturated rocks: Geophysics, **44,** 161-178.

Mavko, G., and D. Jizba, 1991, Estimating grain-scale fluid effects on velocity dispersion in rocks: Geophysics, **56**, 1940–1949.

Mavko, G., and D. Jizba, 1994, The relation between seismic P- and S-wave velocity dispersion in saturated rocks: Geophysics, **59**, 87–92.

Mavko, G., and T. Mukerji, 1998, Bounds on low-frequency seismic velocities in partially saturated rocks: Geophysics, **63**, 918–924.

Mavko, G., T. Mukerji, and J. Dvorkin, 1998, The rock physics handbook: Tools for seismic analysis in porous media: Cambridge University Press.

Mayr, S. I., and H. Burkhardt, 2006, Ultrasonic properties of sedimentary rocks: effect of pressure, saturation, frequency and microcracks: Geophysical Journal International, **164**, 246-258.

McCann, C., and J. Sothcott, 2009, Sonic to ultrasonic Q of sandstones and limestones: Laboratory measurements at in situ pressures: Geophysics, **74**, no.2, WA93–WA101.

Milton, G. W., 1985, The coherent potential approximation is a realizable effective medium scheme: Communications in Mathematical Physics, **99**, 463-500.

Milton, G. W., and J. G. Berryman, 1997, On the effective viscoelastic moduli of two-phase media. II. Rigorous bounds on the complex shear modulus in three dimensions: Proceedings of the Royal Society of London A, **453**, 1849-1880.

Mukerji, T., J. G. Berryman, G. Mavko, and P. A. Berge, 1995, Differential effective modeling of rock elastic moduli with critical porosity constraints: Geophysical Research Letters, **22**, 555-558.

Müller, T. M., and B. Gurevich, 2005, Wave-induced fluid flow in random porous media: Attenuation and dispersion of elastic waves: Journal of the Acoustical Society of America, **117**, 2732-2741.

Murphy, W. F., K. W. Winkler, and R. L. Kleinberg, 1986, Acoustic relaxation in sedimentary rocks: Dependence on grain contacts and fluid saturation: Geophysics, **51**, 757–766.

Nur, A., C. Tosaya, and D. V. Thanh, 1984, Seismic monitoring of thermal enhanced oil recovery processes: 54th Annual International Meeting, SEG, Expanded Abstracts, 118-121.

Nur, A., G. Mavko, J. Dvorkin, and D. Gal, 1995, Critical porosity: The key to relating physical properties to porosity in rocks: 65th Annual International Meeting, SEG, Expanded abstracts, 878-881.

O'Connell, R., and B. Budiansky, 1977, Viscoelastic properties of fluid-saturated cracked solids: Journal of Geophysical Research, **82**, 5719–5735.

Ogushwitz, P. R., 1985, Applicability of the Biot theory. I Low porosity materials: Journal of the Acoustical Society of America, **77**, 429-440.

Palmer, I. D., and M. L. Traviolia, 1980, Attenuation by squirt flow in undersaturated gas sands: Geophysics, **45**, 1780-1792.

Pervukhina M., D. N. Dewhurst, B. Gurevich, U. Kuila, T. Siggins, M. Raven, and H. M. Nordgård Bolås, 2008, Stress-dependent elastic properties of shales: measurement and modelling: The Leading Edge, **27**; 772-779.

Pervukhina, M., B. Gurevich, D. N. Dewhurst, and A. F. Siggins, 2010, Experimental verification of the physical nature of velocity-stress relationship for isotropic porous rocks: Geophysical Journal International, **181**, 3, 1473-1479.

Plona, T. J., 1980, Observation of a second bulk compressional wave in a porous medium at ultrasonic frequencies: Applied Physics Letters, **36**, 259–261.

Prasad, M., M. Kopycinska, U. Rabe, and W. Arnold, 2002, Measurements of Young's modulus of clay minerals using atomic force acoustic microscopy: Geophysical Research Letters, **29**, 1172–1175.

Pride S. R., A. F. Gangi, and F. D. Morgan, 1992, Deriving the equations of motion for porous isotropic media: Journal of the Acoustical Society of America, **92**, 3278- 3290.

Pride, S. R., and J. G. Berryman, 2003, Linear dynamics of double-porosity dual-permeability materials. I. Governing equations and acoustic attenuation: Physical Review E., **68,** 036603.

Pride, S. R., J. G. Berryman, and J. M. Harris, 2004, Seismic attenuation due to wave-induced flow: Journal of Geophysical Research, **109**, B01201.

Pride, S. R., J. M. Harris, D. L. Johnson, A. Mateeva, K. T. Nihel, R. L. Nowack, J. W. Rector, H. Spetzler, R. Wu, T. Yamomoto, J. G. Berryman, and M. Fehler, 2003, Permeability dependence of seismic amplitudes: The Leading Edge, **22**, 518-525.

Roberts, A. P., and E. J. Garboczi, 2000, Elastic properties of modelporous ceramics: Journal of the American Ceramic Society, **83**, 3041–3048.

Roberts, A. P., and E. J. Garboczi, 2002, Computation of the linear elastic properties of random porous materials with a wide variety of microstructure: Proceedings of the Royal Society of London A, **458**, 1033–1054.

Saenger, E. H., O. S Krüger, and S. A. Shapiro, 2004, Numerical considerations of fluid effects on wave propagation: Influence of the tortuosity: Geophysical Research Letters, **31**, L21613.

Sayers, C. M., and M. Kachanov, 1991, A simple technique for finding effective elastic constants of cracked solids for arbitrary crack orientation statistics: International Journal of Solids and Structures, **27**, 671–680.

Sayers, C. M., and M. Kachanov, 1995, Microcrack-induced elastic wave anisotropy of brittle rocks: Journal of Geophysical Research, **100**, 4149–4156.

Sayers, C. M., and D.-H. Han, 2002, The effect of pore fluid on the stress-dependent elastic wave velocities in sandstones: 72nd Annual International Meeting, SEG, Expanded Abstracts, 1842–1845.

Schmitt, D. R., 1999, Seismic attributes for monitoring of a shallow heated heavy oil reservoir: A case study: Geophysics, **64**, 368–377.

Schmitt, D. R., and Y. Y. Li, 1995, A high-pressure technique for determining the microcrack porosities of damaged brittle materials: Canadian Journal of Physics, **73**, 330–337.

Schwartz, L. M., F. M. Auzerais, J. Dunsmuir, N. Martys, D. P. Bentz, and S. Torquato, 1994, Transport and diffusion in three-dimensional composite media: Physica A, **207**, 28–36.

Shapiro, S. A., 2003, Elastic piezosensitivity of porous and fractured rocks: Geophysics, **68**, 482–486.

Shapiro, S. A., and A. Kaselow, 2005, Porosity and elastic anisotropy of rocks under tectonic stress and pore-pressure changes: Geophysics, **70**, no. 5, N27-N38.

Smith, T. M., C. H. Sondergeld, and C. S. Rai, 2003, Gassmann fluid substitutions: A tutorial: Geophysics, **68**, 430-440.

Spanne, P., J. Thovert, J. Jacquin, W.B. Lindquist, K. Jones, and D. Coker, 1994, Synchrotron computed microtomography of porous media: topology and transports: Physical Review Letters, **73**, 2001–2004.

Thomsen, L., 1985, Biot-consistent elastic moduli of porous rocks: Low-frequency limit: Geophysics, **50**, 2797-2807.

Thomsen, L., 1995, Elastic anisotropy due to aligned cracks in porous rock: Geophysical Prospecting, **43**, 805–829.

Toms, J., T. M. Muller, R. Ciz, and B. Gurevich, 2006, Comparative review of theoretical models for elastic wave attenuation and dispersion in partially saturated rocks: Soil Dynamics and Earthquake Engineering, **26**, 548–565.

Toms, J., T. M. Müller, and B. Gurevich, 2007, Seismic attenuation in porous rocks with random patchy saturation: Geophysical Prospecting, **55,** 671U678.

Tosaya, C., A. Nur, D. Vo-Thanh, and G. Da Prat, 1987, Laboratory seismic methods for remote monitoring of thermal EOR: SPE Reservoir Evaluation and Engineering, **2**, 235-242.

Tsiklauri, D., and I. Beresnev, 2003, Properties of elastic waves in a non-Newtonian (Maxwell) fluid-saturated porous medium: Transport in Porous Media, **53**, 39–50.

Vanorio, T., M. Prasad, and A. Nur, 2003, Elastic properties of dry clay mineral aggregates, suspensions and sandstones: Geophysical Journal International, **155**, 319–326.

Verdon, J. P., D. A. Angus, J. M. Kendall, and S. A. Hall, 2008, The effect of microstructure and nonlinear stress on anisotropic seismic velocities: Geophysics, **73**, no. 4, D41-D51.

Walsh, J. B., 1965, The effect of cracks on the compressibility of rock: Journal of Geophysical Research, **70,** 381–389.

Wang, Z., 2000, The Gassmann Equation revisited: comparing laboratory data with Gassmann's predictions, Seismic and Acoustic velocities in reservoir rocks, vol. 3: Recent developments, 8-23, Reprint series, SEG.

White, J. E., 1975, Computed seismic speeds and attenuation in rocks with partial gas saturation: Geophysics, **40**, 224-232.

White, J. E., 1983, Underground sound: Application of seismic waves: Elsevier Science Publ. Co., Inc.

White, J. E., N. G. Mikhaylova, and F. M. Lyakhovitsky, 1975, Low frequency seismic waves in fluid saturated layered rocks: Izvestija Academy of Sciences USSR, Physics of the Solid Earth, **11**, 654–659.

Williams, M. L., R. F. Landel, and J. D. Ferry, 1955, The temperature dependence of relaxation mechanisms in amorphous polymers and other glass-forming liquids: The Journal of the American Chemical Society, **77**, 3701–3706.

Winkler, K. W., 1983, Contact stiffness in granular porous materials: comparison between theory and experiment: Geophysical Research Letters, **10**, 1073-1076.

Wood, A.B., 1955. A Textbook of Sound: G. Bell and Sons Ltd.

Wu, T. T., 1966, The effect of inclusion shape on the elastic moduli of a two-phase material: International Journal of Solids and Structures, **2**, 1–8.

Wulff, A.-M., and H. Burkhardt, 1997, Mechanisms affecting ultrasonic wave propagation in fluid-containing sandstones under high hydrostatic pressure: Journal of Geophysical Research, **102**, 3043–3050.

Wyllie, M. R., G. H. F. Gardner, and A. R. Gregory, 1962, Studies of elastic wave attenuation in porous media: Geophysics, **27**, 569-589.

Xu, S., and R. E. White, 1995, A new velocity model for clay-sand mixtures: Geophysical Prospecting, **43**, 91-118.

Yeong, C. L. Y., S. Torquato, 1998, Reconstructing random media: Physical Review E, **57**, 495–506.

Every reasonable effort has been made to acknowledge the owners of copyright material. I would be pleased to hear from any copyright owner who has been omitted or incorrectly acknowledged. Appendix 1 contains permission statements from the copyright owners of the material presented in this thesis which was published as journal articles or conference extended abstracts.

APPENDIX 1

Some material from Chapter 1 was published in Computers&Geosciences. (http://libraryconnect.elsevier.com/lcp/0403/lcp040302.html). Elsevier pamphlet #4 states:

"Authors publishing in Elsevier journals retain wide rights to continue to use their works to support scientific advancement, teaching and scholarly communication.

An author can, without asking permission, do the following after publication of the author's article in an Elsevier-published journal:

Make copies (print or electronic) of the author's article for personal use or the author's own classroom teaching.

Make copies of the article and distribute them (including via email) to known research colleagues for their personal use but not for commercial purposes as described in this pamphlet.

Present the article at a meeting or conference and distribute copies of the article to attendees.

Allow the author's employer to use the article in full or in part for other intracompany use (e.g., training).

Retain patent and trademark rights and rights to any process or procedure described in the article.

Include the article in full or in part in a thesis or dissertation.

Use the article in full or in part in a printed compilation of the author's works, such as collected writings and lecture notes.

Use the article in full or in part to prepare other derivative works, including expanding the article to book-length form, with each such work to include full acknowledgment of the article's original publication in the Elsevier journal.

Post, as described further down on this page, the article to certain websites or servers. "

Some material presented in Chapter 2 and Chapter 4 was published as EAGE abstracts. Please see below my correspondence with the EAGE Senior Publications Coordinator.

From: Linda Molenaar on behalf of EAGE Publications
To: Dina Makarynska
Subject: RE: re-publishing EAGE abstract in thesis
Date: Tuesday, 22 June 2010 5:50:59 PM

Hi Dina,

All copyright on EAGE conference extended abstracts fall back to the authors a year after the conference has taken place. You could therefore best ask them for permission.

Kind regards, Linda

Ms. Linda Molenaar
Senior Publications Coordinator
EAGE Publications BV PO Box 59 3990 DB Houten The Netherlands
Tel.: +31 88 9955011 Fax: +31 30 6343524 E-mail: lm@eage.org
www.eage.org

****

From: Dina Makarynska [mailto:D.Makarynska@exchange.curtin.edu.au] **Sent:** 16 June 2010 08:12 **To:** EAGE Publications **Subject:** re-publishing EAGE abstract in thesis

Dear Sirs/Madams,

I am a PhD student at Curtin University of Technology (Perth, Western Australia). I am planning to include EAGE conference extended abstracts in my thesis. Do I need to get permission to republish this work in my thesis?

Thank you.

Dina Makarynska PhD candidate

Some material presented in Chapter 3, Chapter 5 and Chapter 6 was published as papers in Geophysics and as an SEG extended abstract. SEG Transfer of Copyright Agreement
(see http://www.seg.org/resources/publications/geophysics/forms) states:

"Authors shall retain the following royalty-free rights: (1) the right to reproduce the Work, including figures, drawings, tables, and abstracts of the Work, with proper copyright acknowledgment, for any purpose; (2) the nonexclusive right, after publication by SEG, to authorize third parties to republish the Work or translations or portions thereof, provided the SEG-formatted version is not used (SEG permission is required if the SEG-formatted version is used)."